CONTROLLING THE TRIBOELECTRIC CHARGES ON CELLULOSE-BASED FABRIC TRIBOELECTRIC NANOGENERATOR WITH THE INORGANIC DYES

RAWIWAN KHWANMING

Graduate School Srinakharinwirot University

2023

การควบคุมประจุไทรโบอิเล็กทริกบนอุปกรณ์กำเนิดพลังงานไฟฟ้าขนาดเล็กไทรโบอิเล็กทริกที่ใช้ผ้าในกลุ่มเซลลูโลสด้วยสีย้อมสังเคราะห์

ระวิวัลย์ ขวัญมิ่ง

ปริญญานิพนธ์นี้เป็นส่วนหนึ่งของการศึกษาตามหลักสูตร
วิทยาศาสตรมหาบัณฑิต สาขาวิชาวัสดุศาสตร์
คณะวิทยาศาสตร์ มหาวิทยาลัยศรีนครินทรวิโรฒ
ปีการศึกษา 2566

CONTROLLING THE TRIBOELECTRIC CHARGES ON CELLULOSE-BASED FABRIC TRIBOELECTRIC NANOGENERATOR WITH THE INORGANIC DYES

RAWIWAN KHWANMING

A Thesis Submitted in Partial Fulfillment of the Requirements

for the Degree of MASTER OF SCIENCE

(Materials Science)

Faculty of Science, Srinakharinwirot University

2023

THE THESIS TITLED

CONTROLLING THE TRIBOELECTRIC CHARGES ON CELLULOSE-BASED FABRIC TRIBOELECTRIC NANOGENERATOR WITH THE INORGANIC DYES

BY

RAWIWAN KHWANMING

HAS BEEN APPROVED BY THE GRADUATE SCHOOL IN PARTIAL FULFILLMENT OF THE REQUIREMENTS FOR THE MASTER OF SCIENCE IN MATERIALS SCIENCE AT SRINAKHARINWIROT UNIVERSITY

(Assoc. Prof. Dr. Chatchai Ekpanyaskul, MD.)

Dean of Graduate School

ORAL DEFENSE COMMITTEE

..... Major-advisor

(Dr.Thitirat Charoonsuk)

..... Chair

(Prof.Naratip Vittayakorn)

..... Committee

(Assoc. Prof. Dr.Natthapong Phinichka)

Title	CONTROLLING THE TRIBOELECTRIC CHARGES ON CELLULOSE-BASED FABRIC TRIBOELECTRIC NANOGENERATOR WITH THE INORGANIC DYES
Author	RAWIWAN KHWANMING
Degree	MASTER OF SCIENCE
Academic Year	2023
Thesis Advisor	Dr. Thitirat Charoonsuk

Nowadays, the application of wearable and portable electronic industries for electronic textiles (E-textiles) has seen unprecedented growth with rising new functionalities. However, the electronic components of E-textiles need appropriate energy to work. The most mechanical energy harvesting devices, the triboelectric nanogenerator (TENG) that provide the highest electrical efficiency that have been widely researched and documented. In this work, textile-based TENG was fabricated using four different cellulose fabrics (cotton, linen, rayon, and Tencel) as the primary friction material and modified its functional group with inorganic dyes. Three types of dyes included reactive, direct, and basic dyes are studied. All functional groups of cellulose-based fabric and dyes are identified. Fabric morphologies, fabric properties, and the effect of the functional group of dyes on the electrical output are studied. The results showed that all fabrics contained hydroxyl group from cellulose structure. All inorganic dyes contained an amine group that could react with the fabric to generate different electrical outputs after dyeing. Moreover, all dyed cellulose-based fabric showed higher electrical output than pristine cellulose-based fabric. The findings of this research could be applied to various wearable sensors in the textile-TENG and textile industries in the future.

Keyword : Cellulose-based fabric, Triboelectric nanogenerator, Inorganic dye, Textiles

ACKNOWLEDGEMENTS

I would like to express my sincere thanks to my thesis advisor DR. Thitirat Charoonsuk for her invaluable help and constant encouragement throughout this research. In addition, I am grateful for the teacher of physical science. Asst. Prof. Dr. Suwan Plaipichit for suggestions and all his help. This work was financially supported by the Fundamental Research Funds for the Srinakharinwirot University (No. 214/2566) and the National Research Council of Thailand (NRCT) under Grant Number N42A650220. Finally, I most gratefully acknowledge my parents and friends for all their support throughout this research.

RAWIWAN KHWANMING

TABLE OF CONTENTS

Page

List of tatle

Page

List of figures

Page

CHAPTER 1
INTRODUCTION

Background and significance of the research

Nowadays, the application of electronic textiles (E-textiles), the combination of fabric technologies and small electronic devices, has seen an unprecedented growth with rising new functionalities (1). The global E-textile market is expected to grow with a compound annual growth rate (CAGR) of 28.74% during the 2022-2026 period (2). Supporting this, wearable and portable electronic industries for E-textiles are consolidating R&D efforts around the devices while offering the proposition of highest value. However, all electronic components need appropriate energy power for working. Using batteries as a power source still have some limitations, such as the rapid falloff in charge-storage capacity, deterioration after cyclic recharging, and toxicity in case of leakage or after the end of life (3, 4). In addition, smaller, flexible and lightweight batteries are still needed for comfortable using, which require the advanced and expensive technology to produce. Introducing a wearable self-charging system by the energy harvester that can convert renewable energy sources, for examples; sunlight, wind and thermal, into electricity, becomes the effective way to directly provide electricity from surrounding (5). Nevertheless, the limitation of specific external conditions as well as the uncontrollable environmental change is still the problem of those renewable energy sources (6) and it needs to be overcome. Therefore, this work aims to merge the field of energy harvester with E-textiles by paying attention to mechanical energy source that can be acquired anytime even from the human activities including breathing, walking, body shaking, and hand touching (7), (8). Among the mechanical energy harvesting devices, triboelectric nanogenerator (TENG) can provide the highest electrical output and energy conversion efficiency.

After being discovered by Prof. Z. L. Wang and et. al., in 2012 (9), TENG is the most promising candidate for the mechanical energy harvesting technology owning to their light weight and low cost with easy fabrication and no restriction of materials

(10). The electric generation mechanism of TENG is based on the coupling effects between triboelectrification and electrostatic induction of two materials with a significant electronegativity difference. The positive and negative charges generated on the surfaces during the friction process of two materials will induce the opposite charges on the electrode of each side causing a flow of electrons to the external electrical circuit (11). The electricity from TENG is sufficient to drive the small electronic devices without necessary connection to the external power sources. The most common fabrics used in TENG are synthetic polymers, *i.e.,* Nylon, Polyester, Polyethylene terephthalate (PET), Polypropylene (PP), etc. (12-15) owning to their high flexibility and ease of fabrication into a device with a reasonable price. Currently, according to the concern about environmental friendliness and electronic waste, natural-based fabric becomes attention. Cellulose is the major player in this category, mostly due to its abundant quantity. It is also easily formed into yarns or fibers due to its intrinsic flexible structure. Cellulose is a polysaccharide natural polymer that composed of glucan chains linked by 1,4-β-glycosidic bond with general formula of $(C_6H_{10}O_5)_n$ (16). The molecule of cellulose contains plentiful hydroxyl (-OH) groups(17), that exhibit a high tendency of losing electrons and thus become positively charged when in contact with most of the materials in the triboelectric series (18, 19). Among various kinds of cellulose-based fabric (20), cotton is now focused because of its widespread production with tremendous volumes such that it can be bought easily with reasonably priced (21).

In 2019, J. Jeong and co-workers used cotton as positive triboelectric layer for TENG. The output efficiency of 1.59 V could be provided (22). In the same year, Mule and co-workers reported that the electrical output of the TENG device with bare cotton was very low. The open circuit output voltage (V_{OC}) and short circuit current (I_{SC}) values were almost zero (23). Even though the pristine cotton fabric generates non-impressive output signal, its efficiency could possibly be improved. According to literature, several modifying techniques, for examples; coating, making composites and chemical functionalization have been successful for many types of polymers based TENG. Among those kinds of technologies, chemical functionalization is a highly efficient method and

suitable for the development of fiber and fabric-based materials. Therefore, it has become an interesting topic at present. Yao et al. employed a chemical reaction approach to introduce nitro groups and methyl groups to tune the triboelectric polarity of –OH groups for TENG. Nitro- and methyl- TENG exhibited a surface charge density of -85.8 and 62.5 μC/m^2, which is larger than -13.3 μC/m^2 from non-modifying TENG (24). In 2019, Zhang et al. explored friction material modification of cellulose nanofiber (CNF) by the glutaraldehyde crosslinked polyethyleneimine (PEI), which is a highly branched polymer rich in amino groups. The results show that the open-circuit voltage of the modified amino groups of CNF TENG is increased from 68 to 100 V, and the short-circuit current is increased from 0.6 to 1.1 μA (25). Sunanda et al. modified CNF with natural sulfur compound, allicin, to amplify its triboelectric property. Allicin was grafted onto CNF using a 'thiol-ene' click chemistry. The V_{OC} and I_{SC} were increased from 1.23 V and 0.80 μA to 7.9 V, and 5.13 μA, which was ~6.5 times greater than the pristine cellulose based TENG (26). In 2020, Nie and a co-worker grafted 3-(2-amino ethyl amino)-propyl dimethoxy methyl silane (AEAPDMS) onto the surface of CNF. The output performance of the CNF film based TENG were significantly enhanced after AEAPDMS functionalization. The transfer charge was increased from 37 to 65 nC with 10% AEAPDMS. The voltage was enhanced from 159 to 195 V, and the current was increased from 7.0 to 13.4 μA (27). Nie and co-workers modified the surface polarizability of cellulose molecules with triethoxy-1H, 1H, 2H, 2H-tridecafluoro-n-octylsilane (PFOTES). The open-circuit voltage and short-circuit current of the PFOTES-CNF-based TENG increased from 10 V to 28.5 V and from 5 μA to 9.3 μA, which is about twice that of CNF-based TENG before modification (28). In 2022, Boonchai and co-workers functionalized the cellulose film through phosphorylation and sulfonation processes. After functionalization, TENG output performance of phosphorylated samples was 76.7 V and 6.35 μA, which 2 times higher than that of non-modified ones. The sulfonated samples also showed the improvement of output voltage and current in the same way (29). From all previous research, it has been proved that functional groups are the crucial part for controlling and improving the charge accumulation of

friction materials. However, most of the above methods are prepared by chemical process with complicated steps and difficult to control the environmental parameters. This research, therefore, is interested in modifying the functional group of the cellulose-based fabric with a simple method by fabric dyeing. The dye is a colored substance that chemically bonds to the substrate to which it is being applied. The molecules of dyes contain a variety of functional groups with different withdrawn and donated electrons that depend on the relative electronegativity of the atoms (30). Therefore, controlling the functional groups presented in the cellulose-based fabric by dyeing has high possibility for improving the charge accumulation and output efficiency of TENG (31) and no such improvement has been reported before.

In this work, the textile TENG was fabricated by using cellulose-based fabric as the primary friction material and modified its functional group with inorganic dyes. Three types of dyes including reactive, direct, and basic dyes each with six different colors are studied. All functional groups of cellulose-based fabric and dyes are identified by infrared spectroscopy (IR). Fabric morphology before and after dying is studied by scanning electron microscope (SEM). The effect of the dye's functional group on the electrical output, including the output voltage (*V*), output current (*I*) and maximum output power (*P*) is studied by using oscilloscope and digital multimeter (DMM).

Objectives of the study

1. To prepare cellulose-based fabrics and modify their functional group with fabric dyeing.

2. To study the characteristics of cellulose-based fabrics before and after dyeing.

3. To study the fabric properties of cellulose-based fabrics before and after dyeing.

4. To fabricate cellulose-based fabrics triboelectric nanogenerator (CF-TENG).

5. To study the effect of dyes on the electrical output performance of cellulose-based fabric triboelectric nanogenerator (CF-TENG).

Scope of the study

1. Prepare cellulose-based fabrics and modify their functional group with three type of dyes including reactive, direct, and basic dyes.

2. Study the characteristics, including the functional groups and fabric morphology of cellulose-based fabrics before and after dyeing.

3. Study the fabric properties of cellulose-based fabrics before and after dyeing, including color fastness and dry friction test.

4. Fabricate cellulose-based fabrics triboelectric nanogenerator (CF-TENG) with vertical contact-separation mode and single electrode mode.

5. Study the effect of the dyes on the electrical output performance, including the output voltage, output current and maximum output power of cellulose-based fabric triboelectric nanogenerator (CF-TENG).

Conceptual Framework

The conceptual framework of this work is shown in Figure 1.

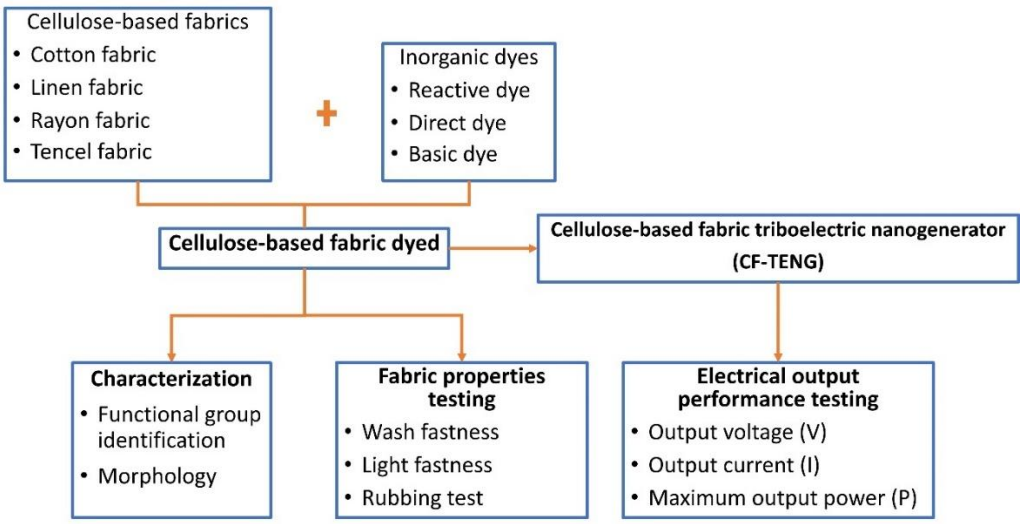

Figure 1 Conceptual framework

Expected Outcome

The outcomes from this research are as follow:

1. Cellulose-based fabrics with three different types of dye, including reactive, direct, and basic dyes.

2. Knowledge of the characteristics, including the functional groups and fabric morphology of cellulose-based fabrics before and after dyeing.

3. Knowledge of the fabric properties of cellulose-based fabrics before and after dyeing, including colorfastness and dry friction test.

4. Cellulose-based fabrics triboelectric nanogenerator (CF-TENG) with vertical contact-separation mode and single electrode mode

5. Knowledge of the effect of dyes on the electrical output performance and find the optimum condition of cellulose-based fabric triboelectric nanogenerator (CF-TENG).

CHAPTER 2
LITERATURE REVIEW

2.1 Textiles

Textiles are fibers, yarns, fabrics, or products made from fibers, yarns, or fabrics from the use of natural or synthetic materials to weave or weave until homogeneous, such as cotton, silk, nylon, etc. Textiles are one of the important factors for human life that always allow the textile industry to expand forward. The global textile market size was expected to grow with a compound annual growth rate (CAGR) of 4.4% from 2021 to 2028 with its demand growth rate of 3.7% (2), according to Figure 2. Textiles are used for many purposes, such as sewing into garments with various fabric appliances. Textiles can be categorized into two categories of conventional textiles and technical textiles.

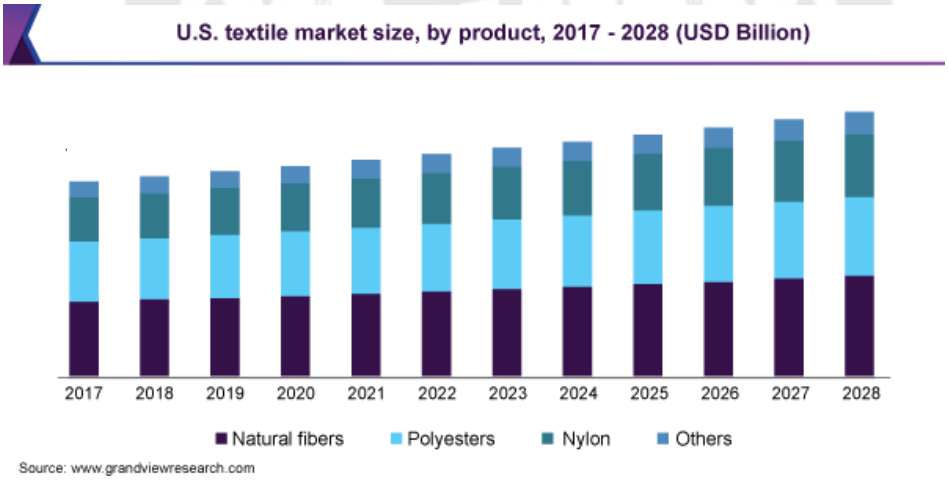

Figure 2 Textile market size

Source: https://www.asdreports.com/market-research-report-575237/textile-market-size-share-trends-analysis-report-raw-material-wool.

2.1.1 Conventional Textiles

Conventional Textiles is the forming of fibers into yarns to form into fabrics. The appearance of the product depends on the application. Most of the products are in

the form of clothing. Conventional textiles are used to protect the body from surroundings. It is used to show wealth and status. It is used for psychological comfort and modesty. The primary reason for making textiles is to cover up people's embarrassment.

2.1.2 Technical Textiles

Technical Textiles are textiles and products made to qualify and technical utilization rather than aesthetic or decorative features or in specialized industrial sectors rather than general apparel production. Technical textile has chemical functions such as mechanical resistance, reinforcement and elasticity by also having exchange functions such as insulation, filtration, fire resistance, thermal resistance, conductivity and so on (32).

The demand for technical textiles is likely to grow steadily due to the demand for specialized textiles in various industries. One of the technical textiles that gain much attention nowadays is electronic textiles.

2.2 Electronics textile

Electronic textiles (E-textiles) are one of the textiles industries that have been extensively interested. E-textiles are the combinations of industrial technologies from textiles and electronics that have been developed to add functionality in addition to wearing for use conveniently and safely (33). E-textiles are textile structures with electrical functions of electronics and physically behaving as a textile simultaneously. In general, the evolution of E-textiles has encouraged the concept of wearable computing or electronic devices in garment designs on the style and functionality of the product. The general components of E-textile are shown in Figure 3, which includes the 4 main electronic components of sensor, control unit, actuator, and power supply.

Figure 3 The components of the E-textile system

Source: https://www.mdpi.com/1424-8220/20/23/6910

2.2.1 Sensor

Sensors are electronic components that are responsible for detecting a signal or measuring physical properties to track, record, or otherwise respond to it. The most common types of sensors incorporating textiles are ECG sensors, sensors for humidity, temperature, pressure and more.

2.2.2 Control unit

A control unit is an electrical panel that controls the operation of all devices in the system, especially in the processor to run properly. The control unit is used to control the signal output from the sensor to the actuator for further responding and instructing the communication device to correctly transmit the messages.

2.2.3 Actuator

An actuator is a machine component that operates depending on the environment, such as air, wind, heat, and electricity. it is responsible working for the movement or control of mechanisms and systems by converting the energy source into motion. Examples of textile actuators include organic light-emitting diodes, phase-changing materials, temperature regulating textiles, and more.

2.2.4 Power supply

A power supply is an essential device for providing power to a system for driving the various components of the system to work. The power supply for E-textiles typically uses lithium polymer batteries (34, 35).

At present, battery technology is a large-scale technology with a wide range of applications and still has some limitations in development, for example, the rapid falloff in charge-storage capacity, deterioration after cyclic recharging, and toxicity in case of leakage or after the end of life. For use in textiles, the battery is moderately heavy and uncomfortable to use and sew. The smaller or thinner battery also requires advanced and expensive technology to produce (36). As a result, a wearable self-charging system by the energy harvester that can convert renewable energy sources into electricity becomes an effective way to directly provide electricity from the surroundings.

2.3 Renewable energy

Renewable energy refers to the clean energy derived from natural sources such as sunlight, wind, rain, waves, biomass and geothermal heat (37) as shown in Figure 4 that can be replenished, renewed or recycled at a higher rate than that of consumption. In the field of E-textile technology, renewable energy sources are used for the electricity generation to drive their electrical components. Most of the renewable energy sources utilized in the E-textiles are the solar energy, wind energy, and thermal energy conversion from thermoelectric materials that can be harvested and transformed into electricity by passing through the energy harvesting devices.

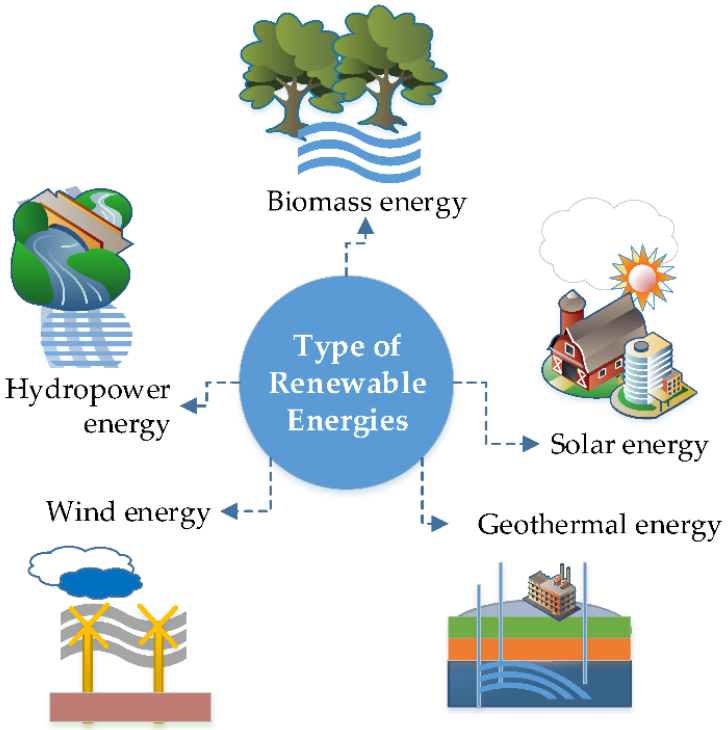

Figure 4 Renewable energy sources

Source: https://www.mdpi.com/2079-9276/8/3/149

2.3.1 The energy harvesting technology for E-textiles

2.3.1.1 Solar energy harvesting

Solar energy is an environmentally friendly energy source with a large and unlimited supply of renewability. Solar energy can be used to generate electricity through electronic devices, which is called “Solar cells”. It is responsible for converting solar energy into electrical energy immediately when exposed to light by the phenomenon of the p-n junction. The generated electricity can be used immediately at the moment of harvesting time and/or stored in batteries for later use (38). Therefore, to drive their electrical component, the electronic devices can do it work properly or harvest the electricity after carrying the E-textile during sunlight (Figure 5).

Figure 5 Solar-powered jacket

Source: https://www.allaboutcircuits.com/news/embedding-solar-technology-into-fabric/

2.3.1.2 Wind energy harvesting

The wind is a natural phenomenon that is caused by differences in atmospheric pressure and the force of the Earth's rotation. Wind energy is the utilization of wind through the technology of converting kinetic energy from the movement of the wind into mechanical energy to generate electrical energy and distribute electricity through an electrical control system. The amount of electricity produced depends on the wind speed, the length of the devices, and the installation location (39).

In 2020, Wang and co-workers were inspired by a toy windmill with constructed hybrid harvesting devices of mechanical energy and wind as shown in Figure 6. The device can operate using wind-driven in free-standing mode. At a wind speed of 10 m/s, the electrical output voltage and current of 530 V and 10.5 μA, with 1.5 mW of maximum power can be generated (40).

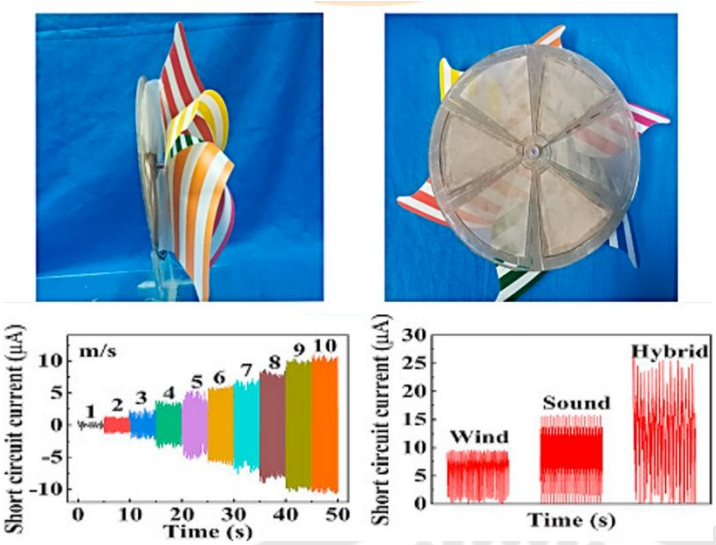

Figure 6 Structure schematic of the hybrid TENG with P(VDF-TrFE) membrane and electrical output current.

Source: Wang (2020). Nano Energy p. 105244.

2.3.1.5 Thermoelectric energy harvesting

Thermoelectric energy is the transformation of an energy between electrical energy and heat energy through a thermoelectric material. The conversion of heat energy into electrical energy or the conversion of electrical energy into heat energy is based on the electron movement within the material structure, connecting to p-n junction. When thermoelectric materials are subjected to different temperatures, there is a temperature transfer from high temperature to low temperature, and it will produce electrical energy (41). Figure 7 shows the thermoregulation device that uses the optical properties of graphene to develop an adaptive graphene optical textile. The material is a t-shirt with elements of graphene/polyester film stuck on cotton and stainless-steel mesh. The microcontroller was used to transmit signals in Morse code and show infrared images with high and low radiation.

Figure 7 Thermoelectric textiles

Source: https://prog.world/smart-clothing-graphene-based-temperature-modulation-device/

Even though many renewable energy sources can be harvest through the devices and produce the electricity, nevertheless, some energy sources remain limited by the surrounding environment, such as temperature and weather, which are sometimes difficult to control (42). To reduce this limitation, other renewable energy sources, namely, mechanical energy is interested in this work.

2.4 Mechanical energy harvesting

Mechanical energy harvesting is an energy harvesting technology derived from various natural sources and can harvest energy from activities within our daily lives including walking, breathing, exercising, body shaking, hand touching, and other activities. With using this kind of technology, the electricity can be produced at any time (43). Among mechanical energy harvesting devices, piezoelectric nanogenerator (PENG) and triboelectric nanogenerator (TENG) are being developed and interesting as detailed below.

2.4.1 Piezoelectric Nanogenerator (PENG)

Piezoelectric nanogenerator (PENG) is a technology that generates electricity from the impact on material by using mechanical force, known as the direct piezoelectric effect. Piezoelectric can measure mechanical forces such as pressure, vibration, or other forces acting on an object and convert this mechanical energy into electrical energy (44). According to Figure 8, the working principle of piezoelectric relies on the piezoelectric effects of materials. In the state of no mechanical load, the positive and negative charge centers are random. The dipole moment is zero (0). The intensity of spontaneous polarization is constant and there are no piezoelectric output signals. When the material is subject to external force, materials are deformed leading to the electric output between two electrodes. Meanwhile, the material in the c-axis direction occurs the strains of piezoelectric crystals, resulting in the center of charges being orientated. In the state of pressing, electrons flow from the lower electrode to the upper electrode until balance forms in the hold state. When materials regained orientation, the electrons reversed to flow from the upper electrode to the lower electrode. During the process of pressing and releasing, the material is capable of converting the external force into electric signals. The electricity generated has essential applications for self-powered devices (45).

.

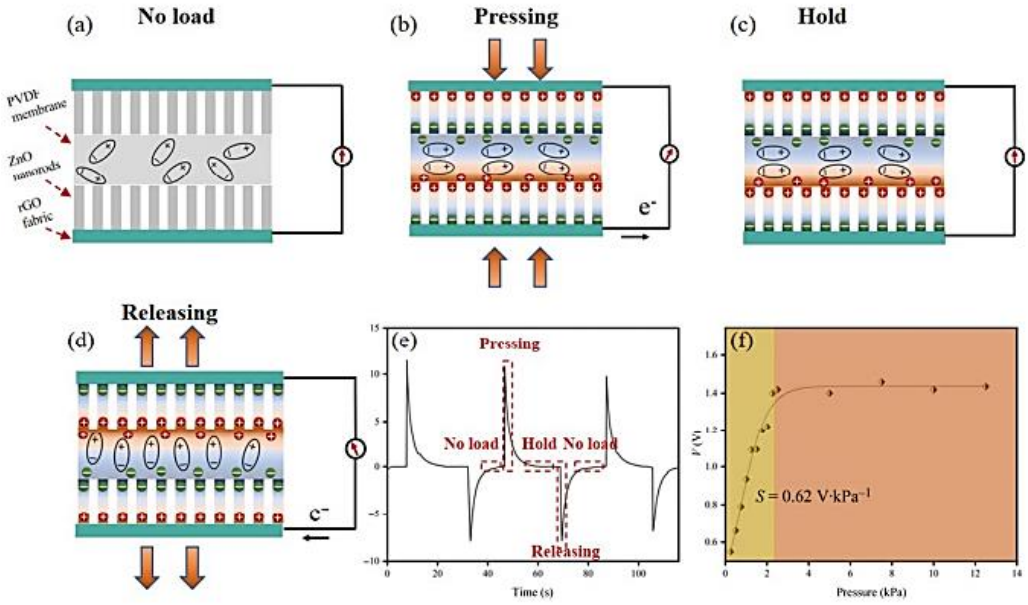

Figure 8 The piezoelectric sensing mechanism of the textile piezoelectric pressure sensor. (a) No load. (b) Pressing. (c) Hold. (d) Releasing. (e,f) Output voltage under different states and different pressure.

Source: Tan (2021). Nano Research p. 3969–3976.

In 2019, Zhang and co-workers developed zinc oxide (ZnO) nanorods patterned textile-based PENG by a screen-printing method. PENG consists of vertically arranged ZnO nanorod arrays sandwiched between two layers of silver-coated nylon fabrics (Figure 9). The electrical output performances of this PENG are 4 V, 0.8 V, and 20 nA, 5 nA for palm clapping and finger bending. This kind of textile-based PENG exhibit can develop into wearable electronics (46).

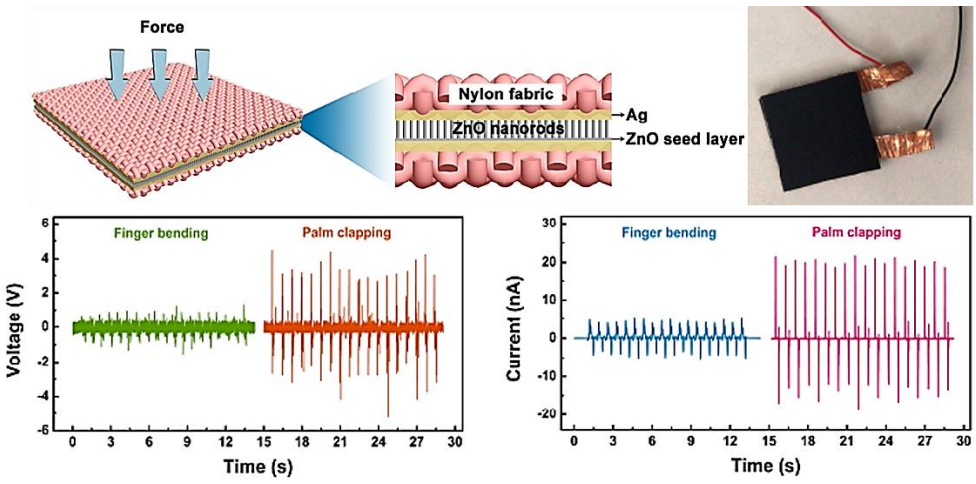

Figure 9 The structure and diagram of the sandwich structured PENG. The output performances of PENG by finger bending and palm clapping.

Source: Zhang (2019). Physica E: Low-dimensional Systems and Nanostructures p. 212-218.

As can be seen in the literatures, the combination of PENG in E-textile is a compelling advantage in realizing electronic devices that do not require the batteries. Nevertheless, the specific piezoelectric materials are still limited. Also, there is still the competition about the efficiency of power generation. Among the mechanical energy harvesting devices, the triboelectric nanogenerator (TENG) can provide the highest electrical output and energy conversion efficiency that will be the interesting of this work. According to literature, the comparative efficiency of 5 technical promising energy harvesting technologies is shown in Figure 10. It can be seen that the power density of the TENG device has reached 100 mW/cm^2 with the maximum energy conversion efficiency achieved at 85% (47).

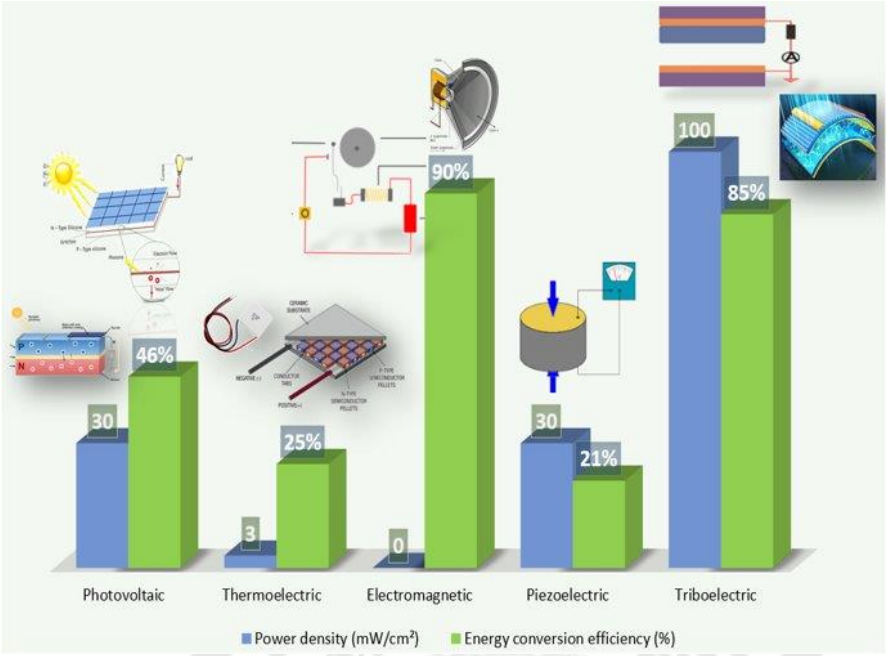

Figure 10 Summary of 5 technical promising methods for harvesting energy from the environment.

Source: Su (2019). In Flexible and Stretchable Triboelectric Nanogenerator Devices p. 113.

2.5 Triboelectric Nanogenerator (TENG)

Triboelectric Nanogenerator (TENG) generates electricity from mechanical energy based on the coupling effects between triboelectrification and electrostatic induction of material when it comes into frictional contact with a different material (9, 11). The composition of the TENG device consists of at least two materials, one material as an electron acceptor called tribo-negative and the other material as an electron donor called tribo-positive. The two materials are sandwiched by electrodes and assembled. Then, the device is connected to an external load.

Figure 11 shows the working principle of the TENG device. When two electrically neutral materials come into contact, materials that already contain the difference in electronegativities (EN) value will provide the electrification by following their electrostatic phenomenon. Materials with low EN values donate electrons and then

create positive charges on the material surface. Materials with higher EN values accept electrons and create negative charges also on the material surface. This charge exchanging process occurs without electrons and current flows because the two materials remain in contact with charge balancing. When the material is separated, each material carries the generated charge with it. The negatively charged material induces positive charges and the positively charged material induces negative charges on their electrode. In this induction process, a charge imbalance causes electrons to flow from the negative to the positively charged electrode. So, the electricity can be provided through the external load. While the material is still separate, the electrons will completely flow until the charges are back to balance again. When the two materials come into contact again, an inductive charge causes electrons to flow through the load from the opposite direction. Then, the full signal of alternative current can be obtained.

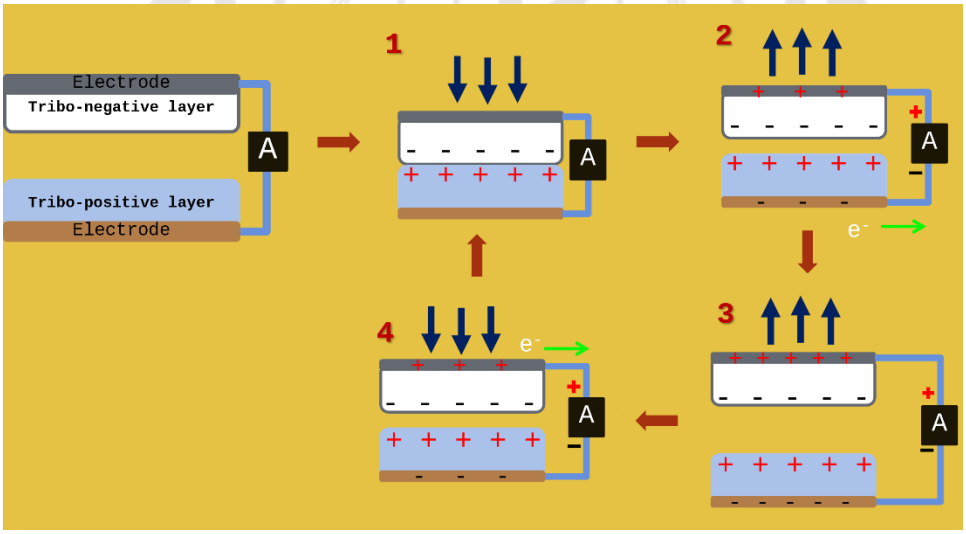

Figure 11 The working principle of the TENG device

Source: Yang Wang et al (2017). Triboelectric nanogenerators as flexible power sources. Nature.

In general, four types of working modes have been put forward for TENG as shown in Figure 12 (48):

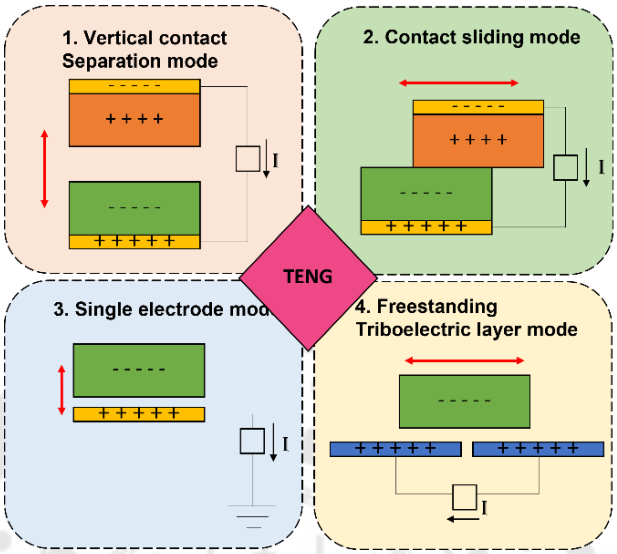

Figure 12 TENG modes (1.) vertical contact separation mode (2.) in-plane contact sliding mode (3.) single electrode mode and (4.) freestanding triboelectric layer mode.

Source: Khushboo (2017). Triboelectric nanogenerator is based on vertical contact separation mode for energy harvesting. Computer Science.

2.5.1 The vertical contact-separation mode

The vertical contact-separation mode is the simplest structural design and high peak output current of the TENG device as shown in Figure 13. The structure of this mode contains two triboelectric layers. The electrode is attached to the back side of the triboelectric layer. The contact pattern is vertical contact of triboelectric layers. When the vertical force is applied, the device touches. And when the force is released, the device separates. The output performance can be enhanced by multilayer structures (49).

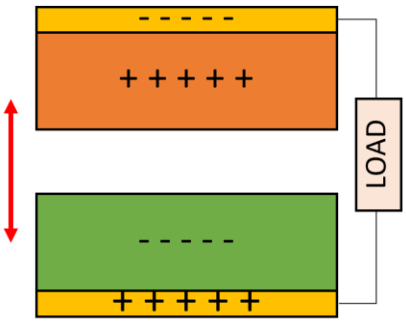

Figure 13 The vertical contact-separation mode

2.5.2 The lateral-sliding mode

The lateral-sliding mode is developed to reduce the frequency limitation of the vertical contact-separation mode. The device structure is the same as the vertical contact-separation mode, as shown in Figure 14. When two materials touch and move parallel on the material surface. This causes the inductance of charges on the surface of both materials. Electrons from the top and bottom of the electrodes flow into the material surface to balance the charge. The lateral-sliding mode is suitable for high-frequency applications and generates a continuous output current. but, the surface of the material is not durable (49).

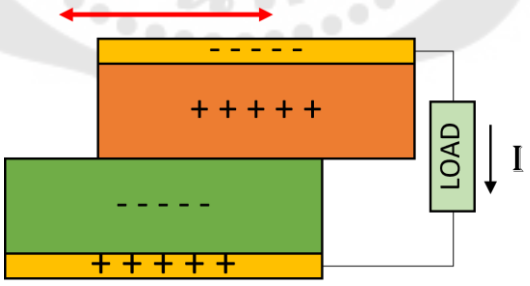

Figure 14 The contact sliding mode

2.5.3 The single-electrode mode

The single electrode mode is the removal of one triboelectric layer and electrode on the back side of this layer to form a single electrode mode as shown in

Figure 15. When one freely moving material is in contact with material attached to electrodes. Electrostatic induction occurs on the surface of the material. When the material is separated, the electrons on the surface of the material attached to the electrode flow along the external load and generate an output current (49).

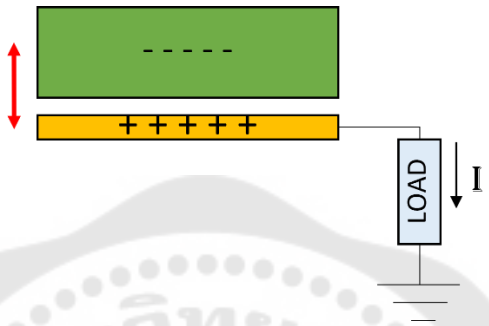

Figure 15 The single electrode mode

2.5.4 The freestanding triboelectric-layer mode

The freestanding triboelectric-layer mode can be operated with a free-moving triboelectric layer between two electrodes, as shown in Figure 16. When two base materials are placed in parallel. The base material has electrodes attached and connected to an external load. When the shear force is applied to the material, the top material moves past the first base material to the second base material. Charges of the upper material are exchanged with the two base materials and static electricity is generated on the surface of the material. When the top material is separated from the base material, the electrons on the surface of the base material flow through the electrodes to an external load and generate an output current (49).

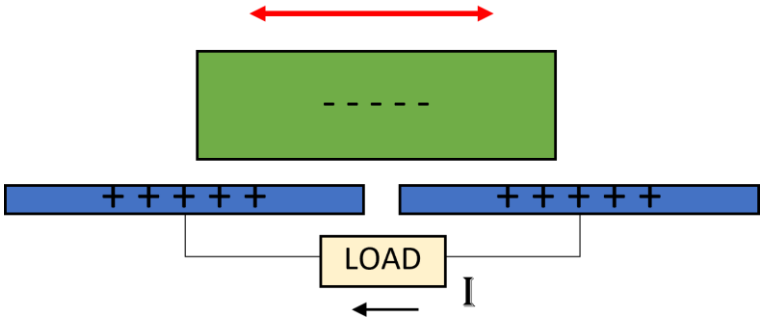

Figure 16 The freestanding triboelectric-layer mode

The electrical output performance is highly dependent on the material pairs. Thus, the triboelectric series was invented to provide a guideline for material selection.

2.5.5 Triboelectric series

The triboelectric series is a ranking of various materials according to the tendency to gain or lose electrons which reflects the properties of the material. The position of the materials in the triboelectric series determines the efficiency of charge exchange. Figure 17 shows the first triboelectric series that have been established. The material at the top tends to give electrons, and the material at the bottom tends to gain electrons. For the selection of the right triboelectric materials, highly negative charge materials should be paired with highly positive charge materials from the triboelectric The suitable pair material selection makes to increase the efficiency of the triboelectric effect (50).

Figure 17 A triboelectric series of materials (51)

Source: Kim (2017). RSC Advances p. 49368-49373.

As shown in Figure 17, several textile materials can be developed as Textile-TENG such as nylon, polyester, and polyethylene. These materials are synthetic. At present, there is a campaign to reduce the use of synthetic materials, especially in electronic devices, according to the concern about environmental friendliness and electronic waste. Cellulose-based textiles, one of natural material, is therefore interested in this work.

Cellulose fabric is a natural fiber with a chemical structure that composed of C, H, and O with the molecular formula $(C_6H_{10}O_5)_n$ (18, 52). Cellulose has a hydroxyl functional group as the main functional group with large quantities in one molecule (Figure 18). In the field of TENG fabrication, cellulose has classified as a high electron donor class and used as a tribo-positive layer of triboelectric material (19, 53). Among several king of cellulose-based fabric. Cotton is an interesting derivative and becomes the main materials of this work.

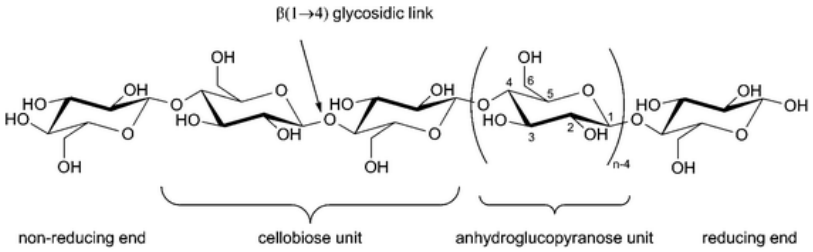

Figure 18 Cellulose chain showing the anhydro glucose unit in the chair conformation along with atom numbering, the glycosidic link, and both reducing and non-reducing ends of the polymer.

2.6 Cotton

Cotton is a type of cellulose fiber that weaves into fabrics. Cotton is the most produced fiber because it is readily available and cheap. The production of cotton fabrics begins by spinning cotton threads into yarns and weaving yarns into fabrics.

Generally, cotton is used in the production of apparel, clothing, home textiles, medical textiles, and more as shown in Figure 19. In addition, the properties of cotton fabric are soft, have good flexibility, good breathability, and are comfortable to wear. This makes cotton a preferred option used in driving electronic components in textiles into wearable electronics today (17).

Figure 19 Application of cotton in textile.

Source: https://sewport.com/fabrics-directory/cotton-fabric

Cotton is a cellulose-based fabric that is a polysaccharide natural polymer composed of glucan chains linked by a 1,4-β-glycosidic bond with the general formula of $(C_6H_{10}O_5)_n$ as the same as cellulose. In addition, the cotton molecule contains constituents of wax and pectin, as shown in Figure 20. When cotton fibers are produced into fabrics can be good breathable and has soft touch (54).

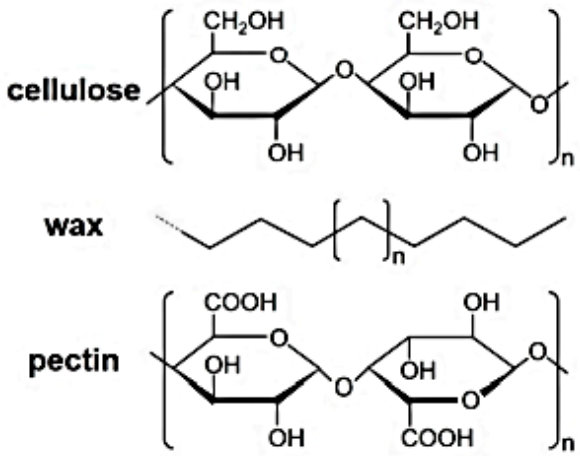

Figure 20 The molecular structures of cellulose, wax, and pectin in cotton fiber.

2.6.2 Cotton-based fabric TENG

According to properties of cotton fabric that are mentioned above, cotton fabrics are therefore an option to apply to TENGs in much research to study their electrical output performance and to develop into wearable devices. In 2019, Jeong and co-workers (22) fabricated a cotton-based TENG device with different patterns to study the effect of the contact area on electrical output efficiency. The output efficiency of 1.59 V could be provided, as shown in Figure 21.

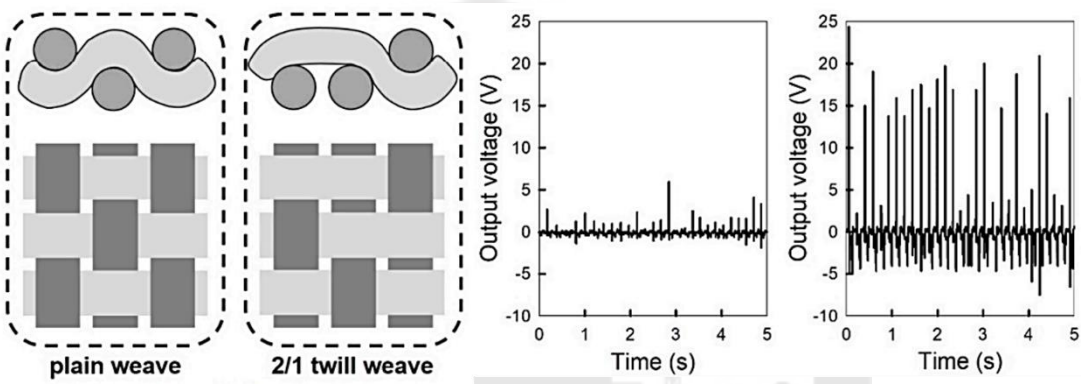

Figure 21 Output efficiency of cotton based TENG with different patterns.

Source: Jeong (2019). Polymers p. 1443.

In the same year, Mule and co-workers reported that the electrical output of the TENG device with bare cotton was very low. Figure 22 shows the open-circuit output voltage (V_{OC}) and short circuit current (I_{SC}) values were almost zero (23).

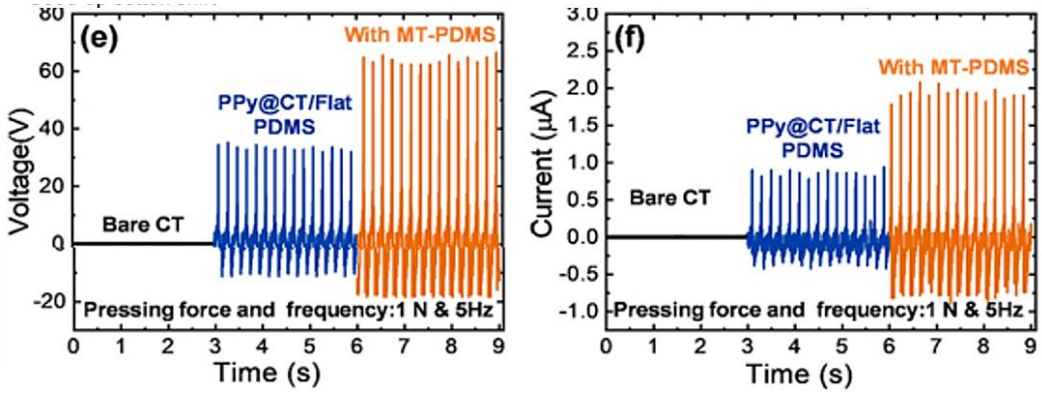

Figure 22 The outputs voltage and current curves of cotton based TENG.

Source: Mule (2019). ACS Sustainable Chemistry & Engineering p. 16450-8.

In addition, Zhang and co-workers report approaches to creating wearable textile-TENGs by sewing with conductive yarn to modify their electrical conductivity (Figure 23). The V_{oc}, I_{sc}, and transferred charge of the textile TENG with pure cotton are 1.5 V, 0.3 μA/cm^2, and 10 μQ/m^2 (55).

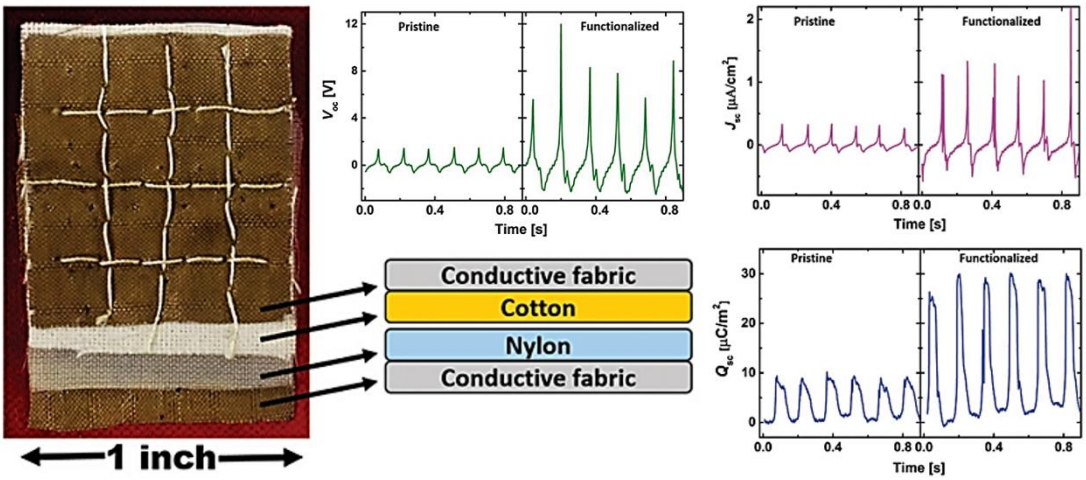

Figure 23 The image of a textile-TENG is included a cotton/ conductive fabric and nylon/ conductive fabric. The electric output measurements of V_{OC} and I_{SC} for a textile TENG.

Source: Zhang (2016). Advanced Materials Technologies p. 1600147.

All the mentioned research shows that the use of cotton based TENG devices is low performance to be energy harvester. However, there are still opportunities to improve cotton for better electrical performance. According to the literature based on the improvement of the electrical performance of cellulose can be improved with a variety of techniques. Several modifying techniques have been successful for many types of polymers based TENG. Details are as follows:

1. Surface modification by improving the surface of cellulose with knitted, woven, or polymer-coated surfaces for better performance.

2. Composite materials by doping or adding various conductor materials onto cellulose.

3. Chemical functionalization by adding or replacing the cellulose functional group with another functional group in the original functional group for the desired applications (56, 57).

From the three processes above, chemical functionalization was the suitable method because it does not damage the surface of the fabric material. It only improves the functional groups within the molecule. Unlikely, the process of surface modification and the composite material changes the texture or reduces the surface area of the material. Therefore, this research aims to study chemical functionalization method for TENG application in textile. There are examples of research on chemical functionalization as follows.

2.7 Chemical functionalization for TENG

Yao et al. developed cellulose nanofibrils (CNF) applied in TENG with two functional group modifications: hydroxyl group replacement with the nitro group and the replacement of hydroxyl groups with methyl groups. As shown in the diagram in Figure 24, it appears that replacing functional groups with nitro groups makes electric signal of cellulose less than methyl group replacement. The methyl group gives cellulose an increased electron donor charge and is used as a positive layer material. The nitro group gives cellulose the ability to accept electrons and is used as a negative layer material. When CNF treated with nitro and methyl groups were coupled, the resulted in

higher electrical output than untreated CNF. Nitro-CNF and methyl-CNF show additional output to average voltage and current of 8 V and 9 μA, respectively (24).

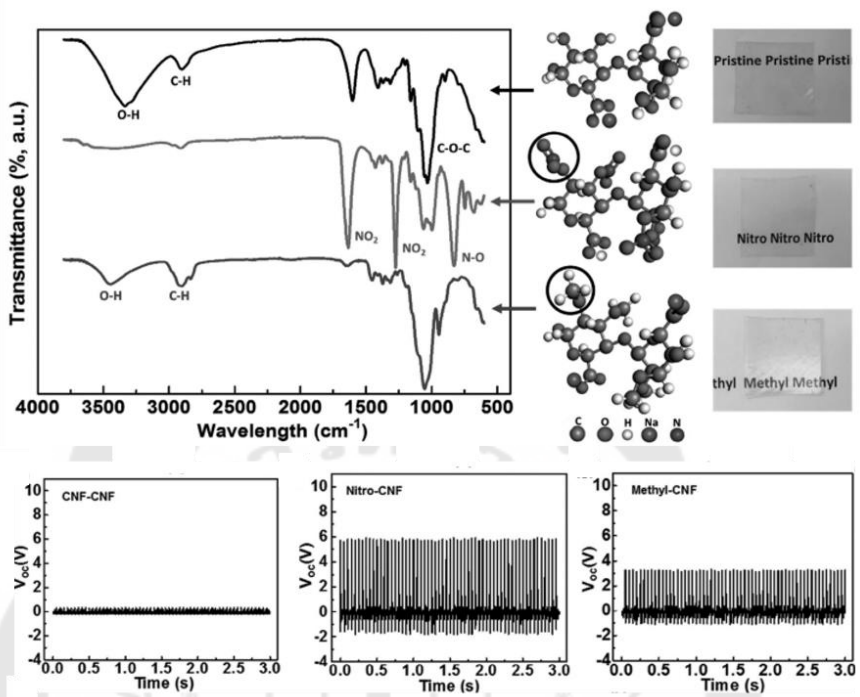

Figure 24 FTIR spectrum and molecular structure of pure CNF (top row), nitro-CNF (middle row), and methyl-CNF (bottom row). Photos show the transparent films fabricated from three CNF materials and the output efficiency of CNF-CNF, nitro-CNF, and methyl-CNF.

Source: Yao (2017). Advanced Functional Materials p. 1700794.

In subsequent research, Roy et al. also modified CNF by grafting a sulfoxide group in allicin onto the hydroxyl group to increase the electron donor capacity of the CNF as shown in Figure 25. The results of the hydroxyl functional group improvement by sulfoxide can show a high electrical output efficiency is ~ 6.5 times of normal cellulose (26). This work confirms that the type of functional group affects the electrical output efficiency of cellulose-based TENG.

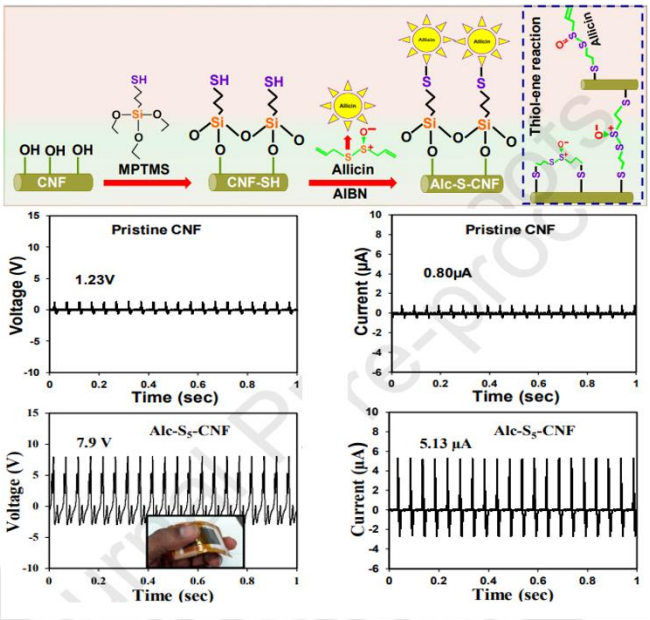

Figure 25 Synthesis and mechanism of allicin grafting onto CNF and output voltage and output current of TENG before and after modification.

Source: Roy (2020). Chemical Engineering Journal p. 123723.

In 2020, Nie and co-workers modified cellulose functional groups by grafting amino groups from 3-(2-aminoethylamino) -propyldimethoxymethylsilane (AEAPDMS) onto the hydroxyl group as shown in Figure 26 and coupled with FEP. The amino functional group leads to higher electrical output and greater than pure cellulose when paired with the same material. Chemical functionalization with amino groups increased the electron donor capacity of cellulose. The transfer charge was increased from 37 to 65 nC. The voltage was enhanced from 159 to 195 V, and the current was increased from 7.0 to 13.4 μA (27).

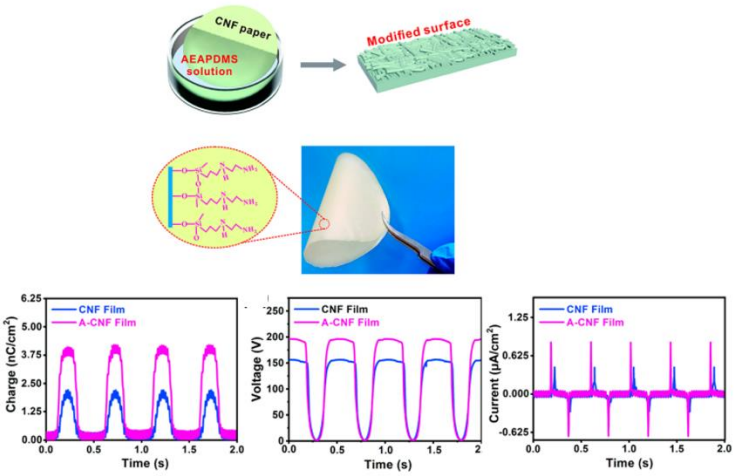

Figure 26 Chemical functionalization on a CNF paper and the A-CNF-based TENG and output performances of the CNF-based TENG: transfer charge, voltage, and current.

Source: Nie (2020). ACS Sustainable Chemistry & Engineering p. 18678-85.

Moreover, Nie and co-workers have modified cellulose functional groups to electron acceptors or to be negative with trimethoxy 1H,1H,2H,2H-tridecafluoro-n-octylsilane (PFOTES), and fluorine-bearing silane chains are grafted to the surface of CNF as shown in Figure 27. The presence of fluorine functional groups on cellulose can increase electron acceptability until can use cellulose as a negatively charged contact layer. The modified TENG short-circuit current and open-circuit voltage was increased to 28.5 V and 9.3 μA as observed before the modification (28).

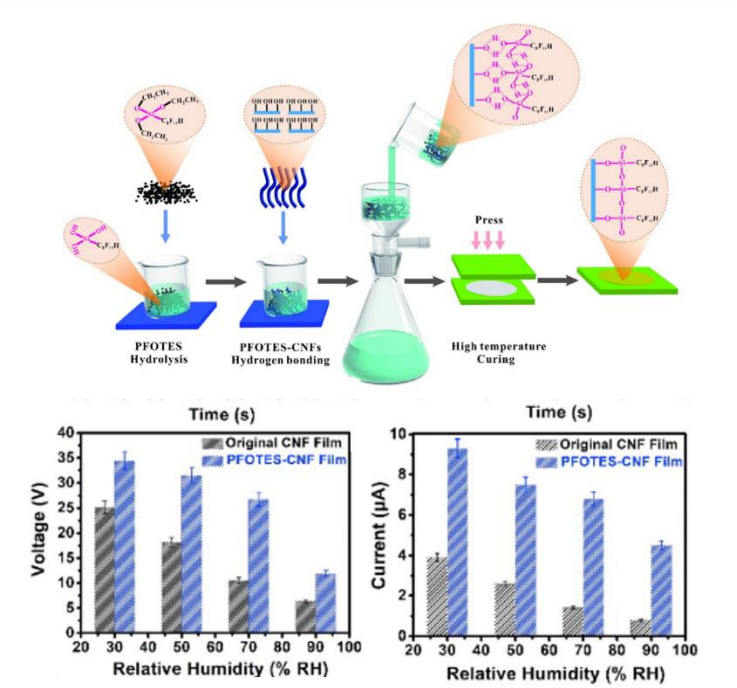

Figure 27 Preparation of the PFOTES grafting CNF film and V_{OC} and I_{SC} of the TENG.

Source: Nie (2021). Chemical Engineering Journal p. 126512.

In addition, Boonchai and co-workers performed surface functionalization of BC using phosphorylation and sulfonation, as shown in Figure 28. Both processes altered the surface properties of the original cellulose. The voltage and current outputs of the pure BC were 54. 4 V and 4. 96 μA. After treatments, the TENG output performances are changed. For the phosphorylated samples, the output voltage and output current were 76.7 V and 6.35 μA. Similarly, the output voltage and output current of the SBC was found to be 64 V and 5.94 μA. Thus, the surface modification of BC by either phosphorylation or sulfonation can enhance the TENG performance in comparison to pure BC (29).

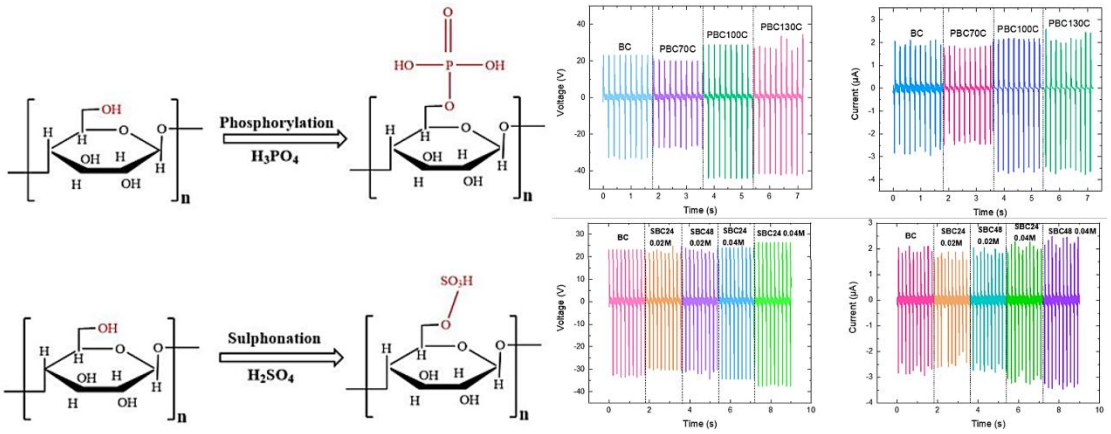

Figure 28 The schematic illustration of the phosphorylation and sulfonation of BC. The TENG voltage and current output of the BC phosphorylated BC and sulfonated BC.

Source: Boonchai (2022). Biointerface Research in Applied Chemistry p. 1587-600.

From all previous research, the process of improving the chemical functional groups of cellulose is an interesting process that can be applied to textiles for enhancing charge accumulation. However, the methods mentioned above are complex methods, with too many variables for the efficiency of functional groups. This makes it difficult to control quality. Therefore, this research uses a simple method to improve functional groups and increase the electrical efficiency of fabric based TENG. In this research, we are interested in charge accumulation by modified functional group by a simple method that is fabric dyeing.

2.8 Dyes

The dye is a water-soluble colorant and attaches to fiber molecules in different ways. Figure 29 shows the major constituents of the dye. It consists of the two main parts of chromophores to produce color and auxochromes to react with fibers. In the dyeing mechanism of dyes, the hydrogen atoms in the dye react with the hydroxyl groups of the fibers to absorb color into the fabric (31, 58).

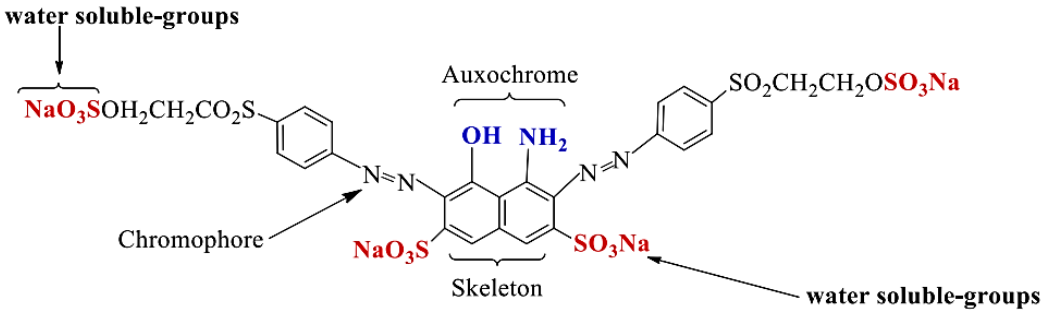

Figure 29 General structural molecule of dyes

2.8.1 Theory of dyeing

In the dyeing process, color is transferred to a textile material to make it permanently colored. In the dyeing theory, the interaction between dyes and the textile material along with different mordant includes of 3 stages (59).

1. Diffusion is dye migration from the solution to the surface of the fiber.
2. Absorption is dye diffusion to the interior of the fiber from the surface.
3. Migration is dye fixation by different types of bonds or entrapping inside the fiber pores.

2.8.2 The mechanism of dyeing on cellulose fabric

The mechanism of dyeing on cellulose fabric is shown in Figure 30. The reacting group of the dye is auxochromes. Cellulose fibers can be dyed under the action of alkaline substances. The functional groups of cellulose fibers can form covalent bonds with the hydroxyl groups in cellulose molecules to fix the auxochromes group of the dyes. In the functional group structure of the dye, substitution and addition reactions occur during the dyeing process due to dyeing and fixation via covalent bonds. This process causes color on cellulose fibers (60).

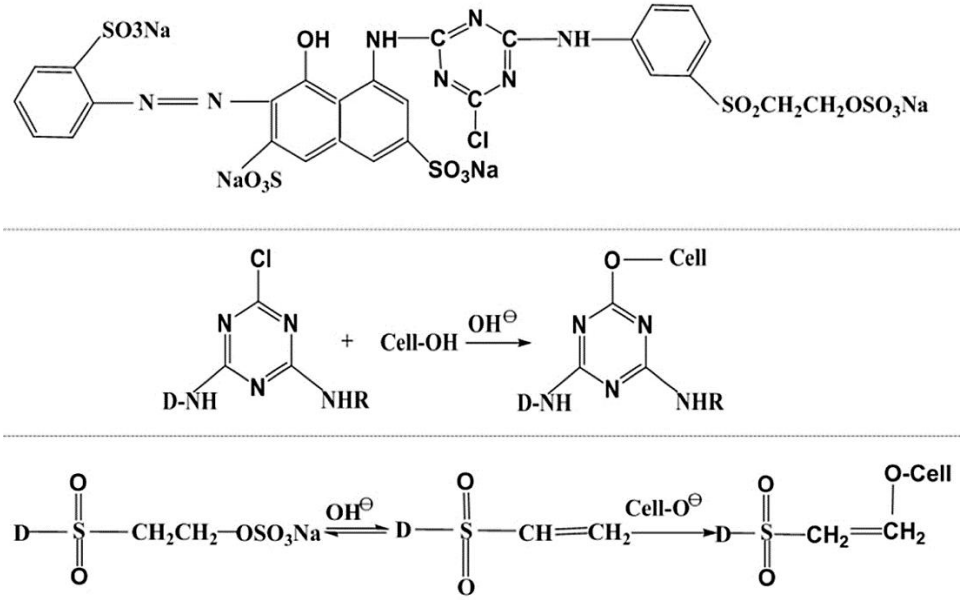

Figure 30 Substitution and addition reaction between the dye and cellulose fabric.

At present, there are many types of dyes, and each type of dye has a different functional group. This research therefore focused on synthetic dyes are readily available and have an uncomplicated dyeing method.

2.8.3 Synthetic dyes

Dyes derived from organic or inorganic compounds are known as synthetic dyes including Direct, Acid, Basic, and Reactive dye, among others (Figure 31). Synthetic dyes replaced traditional natural dyes. Dye has a chemical structure formula the properties of dyes and their methods are different (61).

Figure 31 Synthetic dyes

Source: https://www.etsy.com/listing/270714265/rit-dye-more-synthetic-fiber-dye-all

2.8.4 Functional group of dyes

2.8.4.1 Acid dyes

Acid dyes are water-soluble anionic dyes, containing sulfonic acid substituents or other acidic groups, as shown in Figure 32. Synthetic food colors are cataloged in these dyes. Acid dyes are dyed to fibers such as silk, wool, nylon, and acrylic fibers. Acid dyes are not important to cellulose fibers. The dyeing process is reversible and may be described as follows (62):

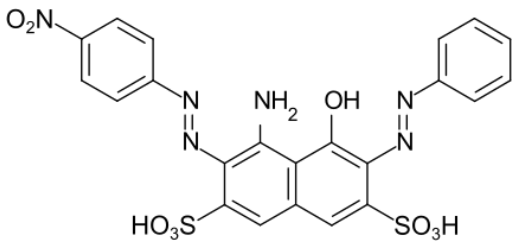

$$Dye^- + H^+ + Fiber \rightleftharpoons Dye^-H^+ - Fiber$$

Figure 32 Functional group of acid dyes

2.8.4.2 Basic dyes

Basic dyes are salts of organic bases, negatively charged, and water-soluble, as shown in Figure 33. These dyes are the first synthetic dyes to be extracted from coal derivatives used in discharge printing. Basic dyes were used to dye nylon, acrylic, etc. Basic dyes should not be used to dye natural fibers because they are not fastness to washing and light (63).

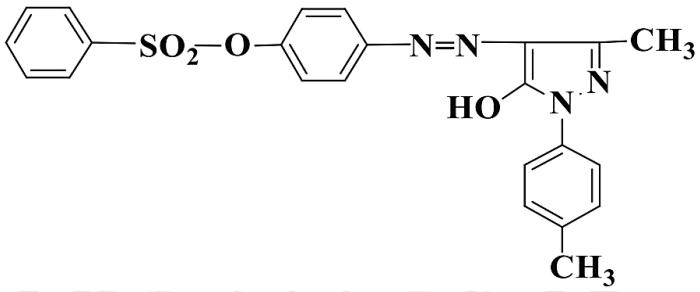

Figure 33 Functional group of basic dyes

2.8.4.3 Direct dyes

A direct dye or cotton dye is a cationic dye that is an azo compound, as shown in Figure 34. The direct dye contains a group of sulfonic acids that make the color soluble in water. The color is not as bright as the basic dye, but it has better light fastness and washing fastness. Direct dyes can be dyed to cellulose fibers such as cotton, linen, and rayon. The dye attaches to the fibers by dye molecules inserted between the fiber molecules and linked with hydrogen bonds (64).

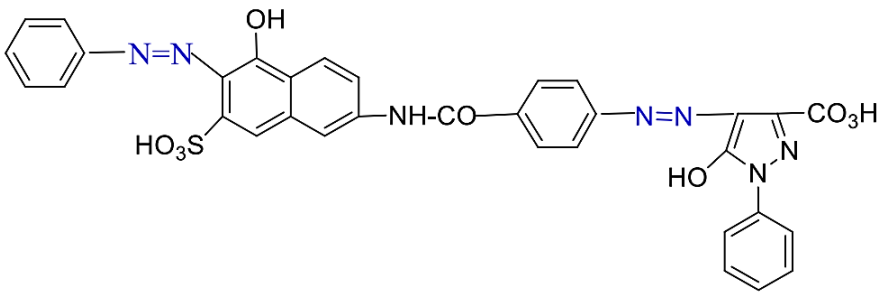

Figure 34 Functional group of direct dyes

2.8.4.4 Reactive dyes

Reactive dyes are water soluble and provide a positive charge, as shown in Figure 35. Amino groups of dye are linked to hydroxyl groups of cellulose by covalent bonds in alkaline conditions, forming a new compound with cellulose. Resulting in dyed fabric with high washing fastness properties. Cotton, wool, or silk can be dyed with this type of dyeing (65).

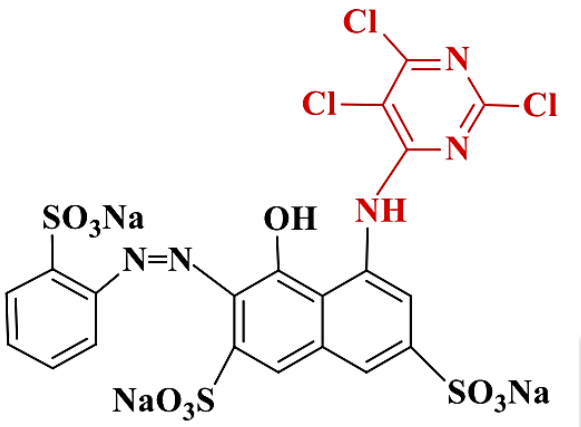

Figure 35 Functional group of reactive dyes

Therefore, controlling the functional group present in the dye molecule by dyeing it into cotton fabric has a high possibility of improving the charge accumulation and output efficiency of TENG. In this work, the textile TENG was fabricated by using cotton fabric as the primary friction material and modifying its functional group with six different colors of the inorganic dyes. All functional groups of cotton and dyes are identified. Studied the fabric morphology before and after dyeing. And studied the effect of the dye's functional group on the electrical output, including the output voltage (*V*), output current (*I*), and maximum output power (*P*).

CHAPTER 3
RESEARCH METHODOLOGY

This research fabricated the textile triboelectric nanogenerator (TENG) using cellulose-based fabric as the primary friction material and modified functional groups of cellulose-based fabric by using with the inorganic dyes to improve charge accumulation and electrical output performance. The preparation process is divided into three main steps, including pre-treatment of cellulose-based fabric, cellulose-based fabric dyeing with inorganic dyes, and fabrication of TENG device. After the preparation, the characteristic functional groups and morphology of the fabric were characterized. The electrical output performance of cellulose-based fabric TENG was measured, as shown in Figure 36. The details of chemicals, materials, preparation methods, and characterizations are the following.

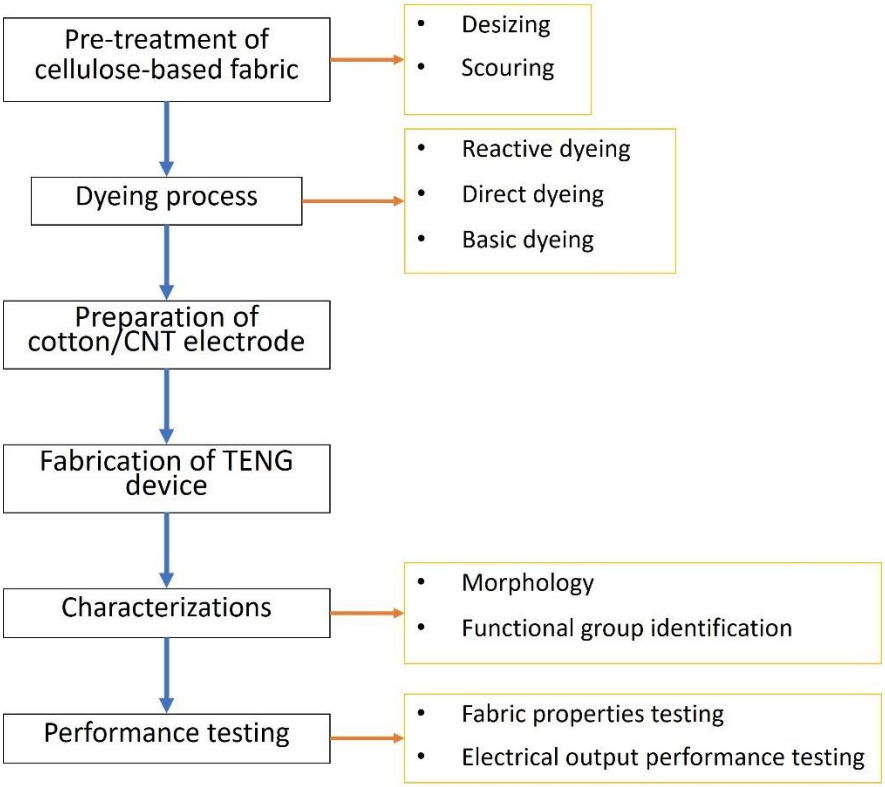

Figure 36 Diagram of research methodology

3.1 Materials, equipment, and chemicals

3.1.1 Materials and equipment

- 100 % cotton fabric (Bulliontex Co., Ltd.)
- 100 % linen fabric (Bulliontex Co., Ltd.)
- 100 % rayon fabric (Bulliontex Co., Ltd.)
- 100 % tencel fabric (Giansingh Co., Ltd.)
- Reactive dyes (KCB TEXTILE Co., Ltd.)
- Direct dyes (A.C. BURAPA Co., Ltd and SIAM DYECHEM Co., Ltd.)
- Basic dyes (A.C.S. Xenon Co., Ltd, dye content 85%.)
- Polytetrafluoroethylene (PTFE) film (commercial grade, Polytechindustry).
- Conductive aluminum tape (RS Components Co., Ltd.)
- Acrylic sheets (RS Components Co., Ltd.)
- Spring (RS Components Co., Ltd.)
- Electrical wire (RS Components Co., Ltd.)
- Laboratory Glassware (Pyrex LAB)

3.1.2 Chemicals

- Enzyme amylase (3,000 IU/ml, Reachbiotechnology Co., Ltd.)
- Sodium chloride (ACS reagent 99%, Sigma Aldrich)
- Sodium hydroxide (ACS reagent 97%, Carlo Erba Reactifs SA)
- Calcium chloride (ACS reagent 99%, Sigma Aldrich)
- Potassium iodide (analytical reagent 99%, Sigma Aldrich)
- Iodine solution (0.05 M, Chem Lab Co., Ltd.)
- Sodium carbonate (BioXtra 99%, Sigma Aldrich)
- Sodium sulphate (ACS reagent 99%, Sigma Aldrich)
- Acetic acid (glacial 100%, Sigma Aldrich)
- Nonionic surfactant (R&D grade, Sigma Aldrich)
- Carbon nanotubes (CNT)
- Deionized (DI) water

3.2 Pre-treatment of cotton fabrics

The commercial cellulose-based fabrics were prepared before use by desizing and scouring processes. The details are as follow:

3.2.1 Desizing of cotton fabrics

5 g of fabric was weighted and checked for water absorption by dropping 1 drop of water for 60 seconds. Prepare the solution for desizing by mixing 0.5 g of the enzyme amylase, 1 g of sodium chloride, 0.05 g of calcium chloride, and 0.1 g of nonionic surfactant in 100 ml of water with constant pH of about 6.5 and heat at 100 °C for 45 minutes. Then, the cotton fabric was boiled in boiling water for 10 minutes to remove the decomposed starch, rinsed with cold water and dried in air. The experimental procedures are shown in Figure 37. After the desizing process, the obtained fabric was tested by the recipe explained in the 3.2.1.1 subheading.

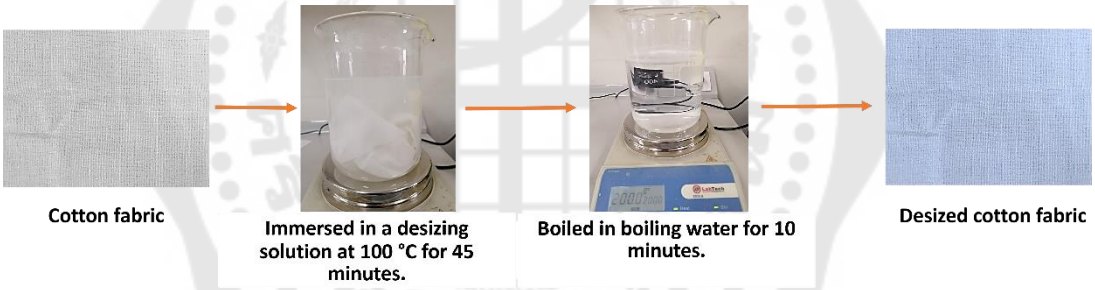

Figure 37 Experimental steps for the desizing process of cellulose-based fabric

3.2.1.1 Desizing efficiency testing

The iodine drop test is employed to check the desizing efficiency. The iodine solution was prepared by mixing 0.24 g of potassium iodide and 0.13 g of iodine in 100 ml of distilled water. 1-2 drops of the iodine solution were dropped on the surface of the fabric and compared with the Violet scale having a 1–9 rating, as shown in Figure 38. A rating of 9 indicates complete removal of starch from the fabric.

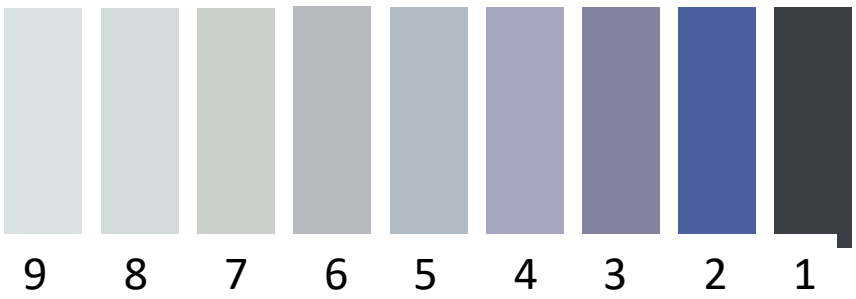

Figure 38 Scale of starch determination after testing with iodine

3.2.2 Scouring of cellulose-based fabrics

The chemical solution for scouring was prepared by mixing 0.2 g of sodium hydroxide and 0.01 g of nonionic surfactant in 100 ml of water. 5 g of the desized fabric was soaked in pre-mixed scouring solution at 95 °C for 60 minutes. Then, the fabric was rinsed with water at normal temperature and dried in air, according to the experimental diagram in Figure 39. After the process, the scoured fabric was tested to confirm its efficiency by the procedure in the 3.2.2.1.

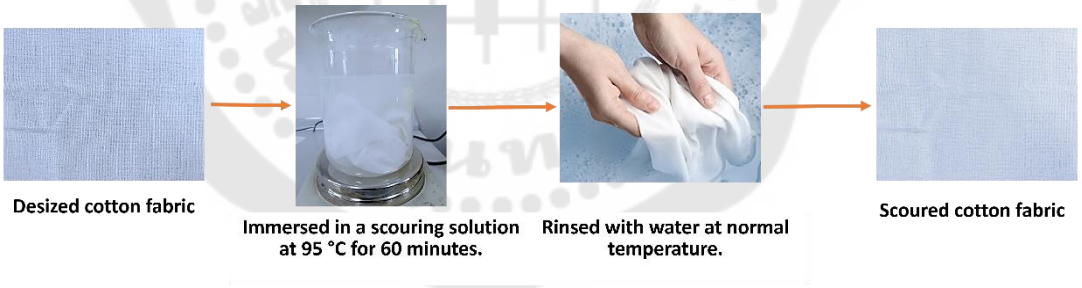

Figure 39 The scouring process of cellulose-based fabric

3.2.2.1 Scouring efficiency testing

The scoring efficiency of fabrics was tested by water absorption with the AATCC test method 79-2000, where a drop of water is allowed to fall onto the surface of a fabric test specimen. The time for the absorption of the water drop is measured and recorded. Generally, 5 seconds or less is considered to represent adequate absorption.

3.3 Inorganic dyeing process

After the fabric preparation, the dyeing process with three types of the dyes (reactive, direct, and basic) was performed according to the experimental steps in 3.3.1, 3.3.2 and 3.3.3 subheading, respectively.

3.3.1 Dyeing process of cellulose-based fabric with reactive dyes

The solution for reactive dyeing was prepared by mixing reactive dye of 2 % on weight of the fabric (%owf), 1 g of sodium carbonate, 2 g of sodium sulphate, and 0.5 g of anionic surfactants in 100 ml of water. Then, the cellulose-based fabric was immersed in a dyeing solution at room temperature and the temperature was raised to 80°C with a heating rate of 1.5°C/min for 30 min of soaking. After that, the dyed fabric was washed with cold water. Then, the dyed fabric was boiled in soaping water to remove the excess dye at 100 °C for 15 min, washed again in cold water to remove the soap, and dried by air blowing. All experimental steps of reactive dyeing are shown in Figure 40.

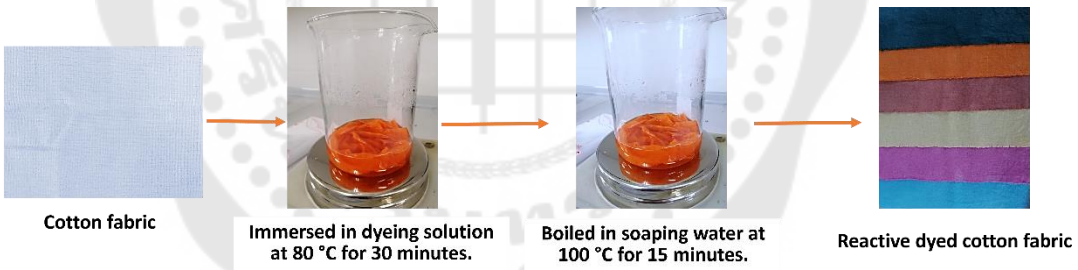

Figure 40 The dyeing process of cellulose-based fabric with reactive dyes

3.3.2 Dyeing process of cellulose-based fabric with direct dyes

The solution for reactive dyeing was prepared by mixing 2 %owf of direct dye, and 1.5 g of sodium chloride in 100 ml of water. Then, the cellulose-based fabric was immersed in a dyeing solution at room temperature and the temperature was raised to 90°C with a heating rate of 1.5°C/min for 30 min. After that, the dyed fabric was washed with cold water and dried by air blowing. All experimental steps of direct dyeing are shown in Figure 41.

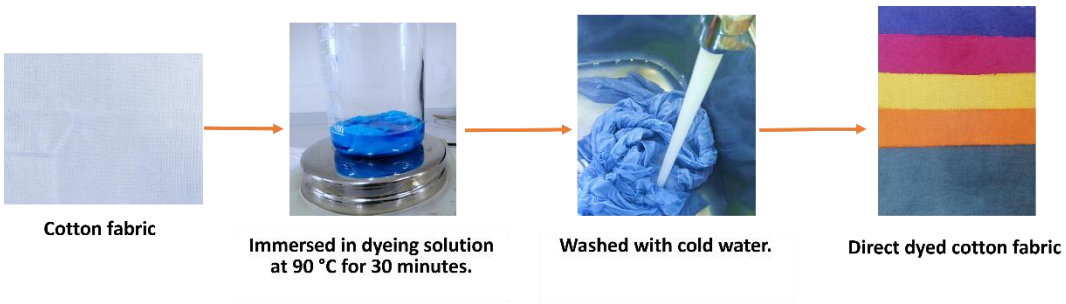

Figure 41 The dyeing process of cellulose-based fabric with direct dyes.

3.3.3 Dyeing process of cellulose-based fabric with basic dyes

The solution for reactive dyeing was prepared by mixing 2 %owf of basic dye, 0.5 g of sodium acetate, and 0.5 g of wetting agent in 100 ml of water. Then, the cellulose-based fabric was immersed in a dyeing solution at room temperature and the temperature was raised to 95°C with a heating rate of 1.5°C/min for 30 min of soaking. After that, the dyed fabric was washed with cold water. Then, the dyed fabric was washed with 0.2 g of non-ionic detergents in 100 ml of water to remove the excess dye at 60 °C for 15 min, washed again in cold water to remove the detergents, and dried by air blowing. All experimental steps of basic dyeing are shown in Figure 42.

Figure 42 The dyeing process of cotton fabric with basic dyes.

3.4 Preparation of cotton/CNT electrode

Two types of TENG electrodes, Al tape and cotton/CNT composite, were used for comparison. In the case of Al tape, the commercial product was used. Only cotton/CNT composite is necessary to be prepared according to the experimental steps in Figure 43. 0.15 g of CNT powder was mixed with 50 ml of DI water and continuously

stirred for 30 minutes. The cotton fabric glue was soaked in the CNT solution for 15 minutes and hung for drying in air. Two cycles of the soaking process were performed. After drying, the fabric glue impregnated with CNT was ironed onto the prepared cotton fabric. Then, acrylic was sprayed onto the fabric glue impregnated with CNT for protection.

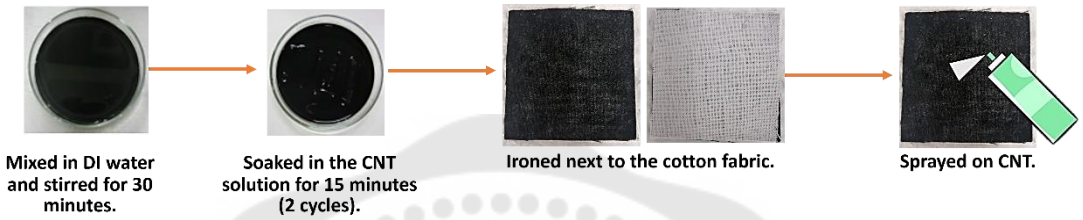

Figure 43 Cotton/CNT electrode preparation process.

3.5 Fabrication of triboelectric nanogenerator (TENG) device

In fabricating the device for triboelectric nanogenerator, 3x3 cm^2 dyed cellulose-based fabrics and 3x3 cm^2 polytetrafluoroethylene (PTFE) were assembled to a two-layer workpiece. The cotton/CNT electrode was placed on an acrylic substrate. The dyed cellulose-based fabric was placed on the cotton/CNT electrode. Meanwhile, the aluminum electrode tape was placed on an acrylic substrate and PTFE was placed on an aluminum electrode. The dyed cellulose-based fabric and a PTFE plate were used as friction materials in the upper and lower parts. Electrodes of each part were connected to the ground. The TENG measurement was tested under a vertical contact-separation mode. The schematic diagram of TENG components is shown in Figure 44.

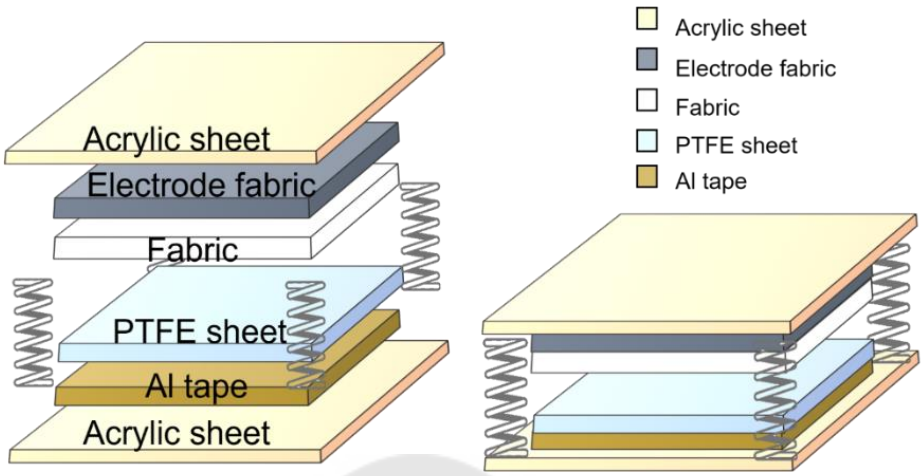

Figure 44 The schematic diagram of the TENG device.

3.6 Characterizations

3.6.1 Morphological observation by the scanning electron microscope (SEM)

A scanning electron microscope (SEM) (FEI, Quanta 250, USA) was used to observe the surface morphology of the samples (Figure 45). The sample stub was rubbed with sandpaper to remove rust. The samples of cotton/CNT and fabric glue impregnated with CNT were cut into 1x1cm^2 and attached to the stub. The samples were gold-coated for 90 seconds before imaging with the SEM to improve their conductivity.

Figure 45 Schematic diagram of SEM (Quanta 250 model, USA).

3.6.2 Structural and functional group inspection with Attenuated Total Reflectance Fourier transform Infrared (ATR-FT-IR) technique

The functional groups of the cellulose-based fabric and dyes were investigated using Attenuated Total Reflectance Fourier transform Infrared (ATR-FT-IR) spectroscopy (Thermo Scientific, Nicolet 6700, US). Samples were cut into the size of 1x1 cm^2 before analyzing the functional groups within a wavenumber range of 4000 to 400 cm^{-1} (Figure 46).

Figure 46 Schematic diagram of FTIR model Nicolet 6700 from the US.

3.6.3 Standard testing methods for textiles

3.6.3.1 Colorfastness to washing

The color fastness to washing is used to determine the color firmness of textiles in different detergents and different washing environments. The dyed fabric is sewn onto the multifiber fabric and washed with a soap solution in a laundering device at 40 °C for 30 minutes. After that, the sample fabric was rinsed and dried. Evaluation of the color change of the dyed fabric and the color staining of the multifiber fabric was achieved using a grey scale as shown in Figure 47. The color change assessment of the dyed fabric was compared with that of the pure fabric using a grey scale for evaluating change in color. The dyed fabric and the pure fabric were placed on a flat surface in the same direction. Then the grey scale was placed on the same flat surface. Before testing, the D65 standard light illuminated the surface at 45°. The direction of the view must be vertical to the surface. The color stain assessment is an assessment of the degree of

color staining on a multifiber fabric using a grey scale for color staining. The evaluation is the same as the color change assessment. The color difference between the various grey pairs indicates degrees of color change and color staining. According to the references, level 5 is the best fastness level and level 1 is the lowest fastness level (66).

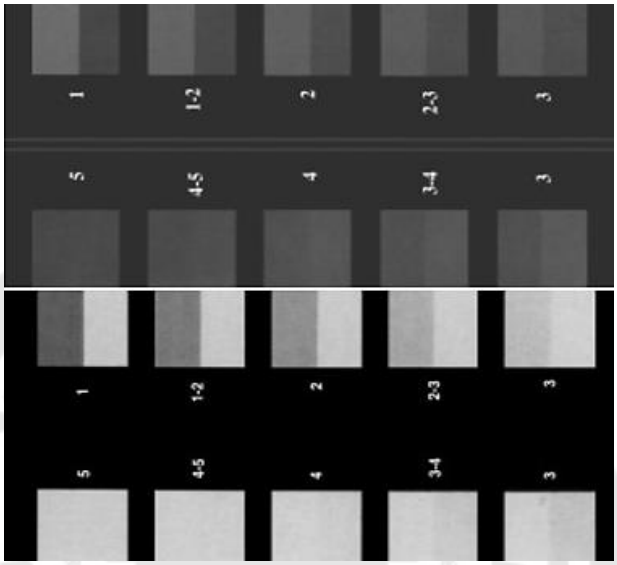

Figure 47 Grey scale for the assessment of color change and color straining.

3.6.3.2 Colorfastness to light

The colorfastness to light is tested under a xenon arc light as the light source. The cellulose-based fabric specimen and standard blue wool were cut to a size of 45x10 mm^2. The cellulose-based fabric specimen and standard blue wool were covered with paper without pressing (Figure 48). The cellulose-based fabric specimen and the standard blue wool were measured under the light at 64 °C, and 35% relative humidity. Colorfastness to the light of the cellulose-based fabric specimen was assessed. The color change of the cellulose-based fabric specimen was compared with that of standard blue wool (67).

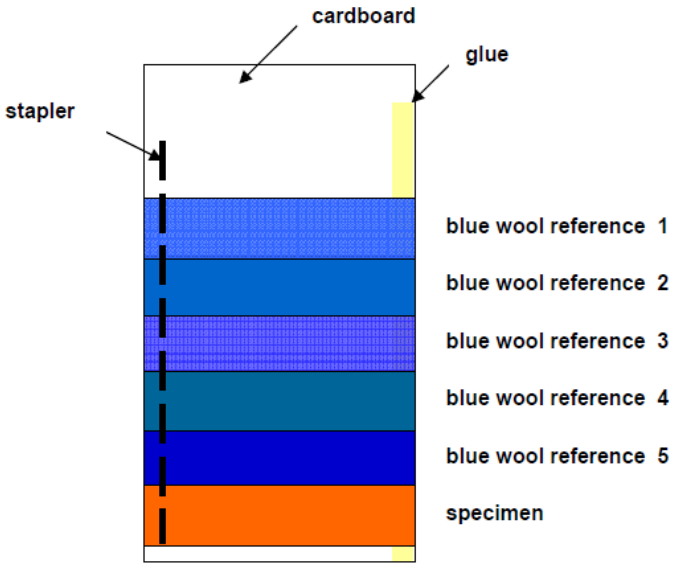

Figure 48 Placement of sample and standard blue wool for color fastness to light testing.

Source: http://garmentstech.com/colourfastness-to-light/

3.6.3.3 Colorfastness to rubbing test

Colorfastness to rubbing is a type of textile color fastness inspection (Figure 49). It refers to the ability of the color of textiles to resist friction. The degree of staining of white cloth is used as the evaluation basis, and it is graded against a set of standard colorfastness to staining gray scales. The gray sample card used to determine the fastness rating is divided into five grades (68).

Figure 49 rubbing test with electronic crock meter.

3.6.4 Monitoring electrical output performances of TENG device

Electrical output performance is performed by measuring the output voltage, output current, and maximum output power with using an automatic compressing machine (ACM), oscilloscope (DSO-x 2012A, Keysight), and a digital multimeter (DMM, DM3058E, Rigol) as shown in Figure 50. An ACM was utilized as an external force. Acrylic substrates of the CF-TENG device were stuck onto the upper and lower part of the ACM. The distance of the gap between the top and bottom of the acrylic substrate was 1.7 cm. The harvesting energy process was operated by a pneumatic system with the air pump at room temperature. The force applied by the ACM on the device was in the vertical direction. The output voltage, output current, and maximum output power in vertical contact separation mode were measured by an oscilloscope and DMM connected to a computer.

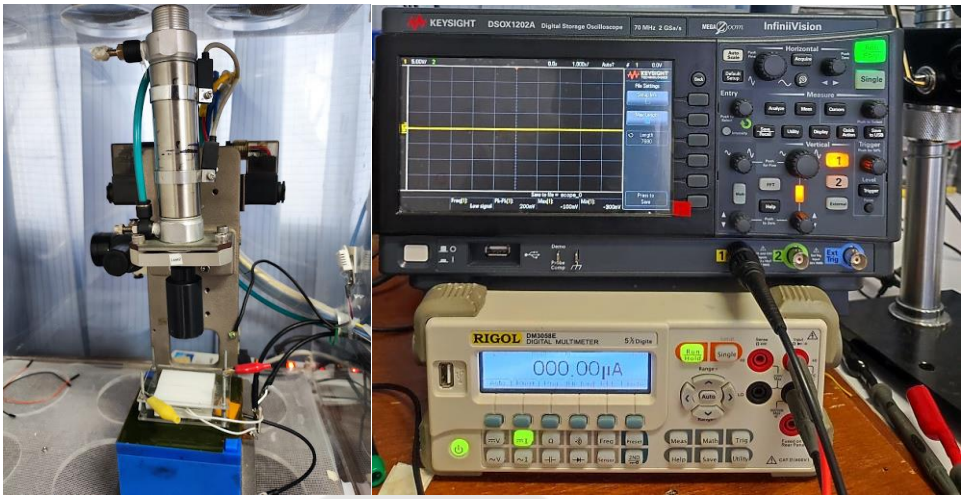

Figure 50 Diagram of an automatic compression machine, oscilloscope, and Multimeter for electrical output performances monitoring process.

CHAPTER 4
RESULTS AND DISCUSSIONS

This chapter provided the results and their discussion of controlling the triboelectric charges of cellulose-based fabrics with the inorganic dyes, including the physical properties, morphology and chemical characterization of cellulose-based fabrics and the inorganic dyes. The textile properties of fabrics before and after dyeing and the electrical output signal with application are also discussed.

4.1 The physical properties of cellulose-based fabrics before and after dyeing

The physical properties of cellulose-based fabrics to analyze the weaving structure characteristics and surface structure of cellulose-based fabrics. The result also includes the measurement and comparison of color values in four types of cellulose-based fabrics before and after the dyeing process.

4.1.1 Cellulose-based fabrics before dyeing

The image from a digital camera shows the weaving structures of cellulose-based fabrics according to Figure 51. Not all fabrics have the same weaving structures. The cotton, linen and rayon fabrics contain a plain weave structure (Figure 51a-c), which is a weaving where the weft contrasts with the warp at perpendicular angles. Meanwhile, the Tencel fabric shows a twill weave structure with a diagonal pattern that is parallel to each other (Figure 51d). The weft inserts under two or more warps with steps between the rows to create a diagonal pattern. The color of the cellulose-based fabric was measured by a spectrophotometer. The results of L*, a*, and b* values of fabrics are given in Table 1. The L* is the lightness or luminance value, which ranges from 0 to 100. Higher lightness values represent lower color yields. Meanwhile, a* and b* star denotes red to green and bule to yellow region. a* values run from negative (green) to positive (red) and b* values run from negative (blue) to positive (yellow) (69). It was found that all the fabrics show a similar value of L*, Tencel contained the most L* value at 94.5 followed by rayon, linen, and cotton at 92.6, 91.6, and 90.7, respectively. The results showed that all fabrics have a high L* value because it is a pristine fabric with no dye.

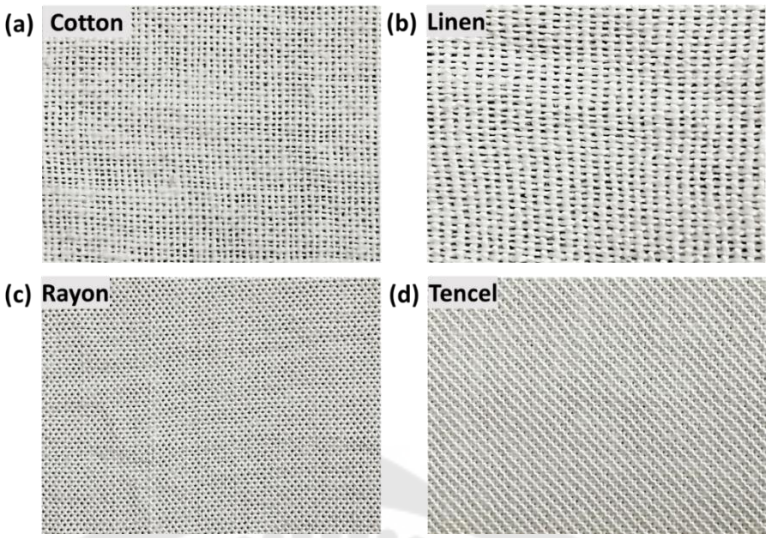

Figure 51 Cellulose-based fabrics before dyeing by digital camera, (a) cotton, (b) linen, (c) rayon, and (d) Tencel fabric.

Table 1 Color measurement values of fabrics.

Fabrics	D65		
	L*	a*	b*
Cotton	90.7	0.9	-0.8
Linen	91.6	0.7	-1.2
Rayon	92.6	-0.3	-0.5
Tencel	94.5	-0.6	-0.7

4.1.2 Color measurements of cellulose-based fabrics after dyeing

Color shades of dyed cellulose-based fabrics with three types of inorganic dyes were reported. This part shows the color of dyed cellulose-based fabrics and color measurement values of dyed cellulose-based fabrics with reactive, direct, and basic dyes.

4.1.2.1 Color measurements of cellulose-based fabric with basic dyes

Figure 52 shows the color measurement results obtained from the cellulose-based fabrics dyeing with basic red dyes indicating that all fabrics can be dyed and

produce consistent coloration. The L*, a*, and b* values for all fabrics are provided in Table 2. The dyed fabrics demonstrate varying degrees of color intensity. The a* value of red is positive for all the dyed fabrics. Rayon displayed the highest value at 42.8, followed by tencel, linen, and cotton at 28.9, 23.4, and 16.5, respectively. The b* value is negative for linen, rayon, and Tencel. In lightness value, rayon shows the lowest L* value at 48.5, followed by linen, tencel, and cotton with values of 50.2, 59.3, and 65.7, respectively. The color measurement values showed that rayon fabric had the lowest L* value and the highest a* value. Therefore, rayon fabric is the best dyed fabric in basic dye.

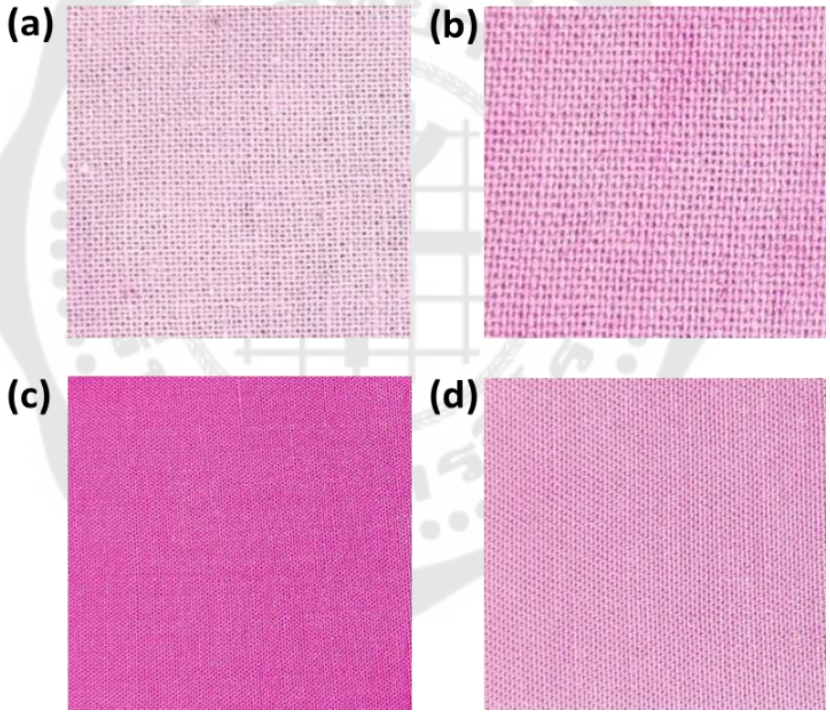

Figure 52 Cellulose-based fabric with basic dyes, (a) cotton, (b) linen, (c) rayon, and (d) Tencel fabric

Table 2 Color measurement values of dyed cellulose-based fabric with basic dyes.

Fabrics	Dyes	D65		
		L*	a*	b*
Cotton	Basic Red	65.7	16.5	2.1
Linen	Basic Red	50.2	23.4	-12.6
Rayon	Basic Red	48.5	42.8	-14.7
Tencel	Basic Red	59.3	28.9	-20.7

4.1.2.2 Color measurements of cellulose-based fabrics with reactive dyes

The cellulose-based fabrics were dyed with six differently commercial color of reactive dyes, including red (Reactive Red 195), blue (Reactive Blue 21), yellow (Reactive Yellow 167), orange (Reactive Orange 122), green (Reactive Green 19), and brown (Reactive Brown 18). The results show that all types of cellulose-based fabrics, including cotton, linen, rayon and Tencel, are dyeable with a uniform color throughout the fabric. However, each type of fabric illustrated a different shade as shown in Figure 53. The shade of color could be measured with the color measurement testing. Table 3 illustrates that reactive red, orange, and brown exhibit positive values of a*, whereas reactive blue and green demonstrate negative values of b*. In the same concentration of dyes, the value of L* for reactive green is lower than all colors which represents higher color yields than other colors. Additionally, fabric dyeing involves the L* value. A higher L* value close to 100 indicates that the fabric is less white due to the dye being absorbed into the fabric. Based on the result, reactive red, yellow, and green dyes are the most absorbed for rayon fabric with lower L* values than other fabrics. Similarly, reactive blue and orange dyes are appropriate for cotton with lower L* values than other fabrics. Moreover, reactive brown dye is best dyed for Tencel fabric, as it has the lowest L* value compared to all colors. In contrast, have not the best dyes for dyed linen fabric.

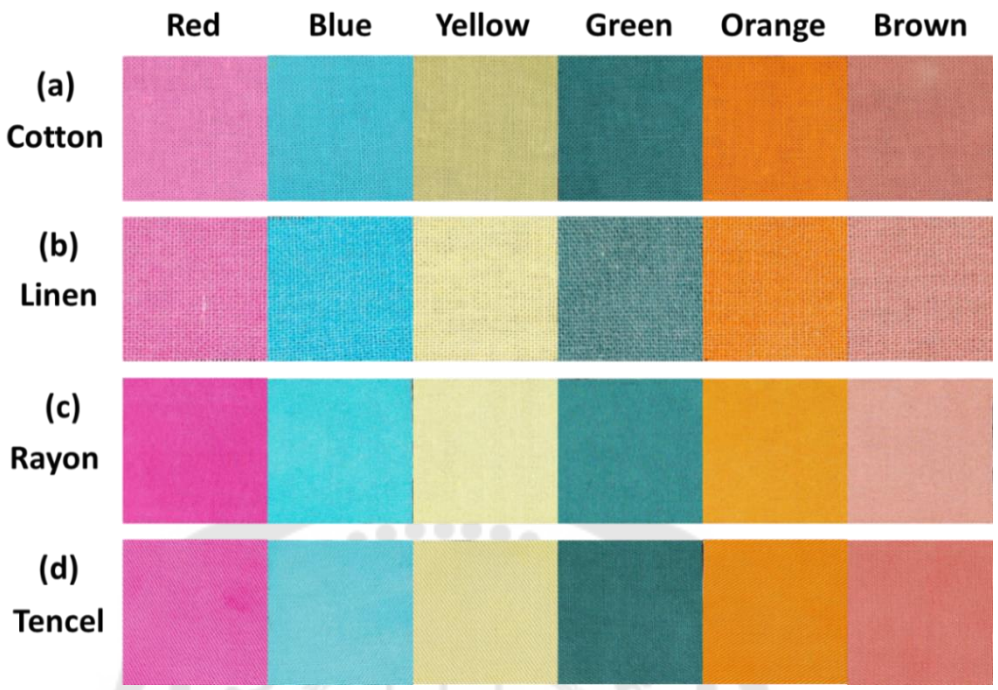

Figure 53 Cellulose-based fabric with reactive dyes, (a) cotton, (b) linen, (c) rayon, and (d) Tencel fabric

Table 3 Color measurement values of dyed cellulose-based fabric with reactive dyes.

Fabrics	Dyes	D65		
		L*	a*	b*
Cotton	Reactive Red	62	25.5	16.5
	Reactive Blue	73.4	-27.1	-19.4
	Reactive Yellow	88.3	-4.3	44.1
	Reactive Green	44.5	-16.2	-4.1
	Reactive Orange	44	-46.7	-3.6
	Reactive Brown	68.3	40.3	54.2

Table 3 Color measurement values of dyed cellulose-based fabric with reactive dyes (Continued).

Fabrics	Dyes	D65		
		L*	a*	b*
Linen	Reactive Red	60.7	34	-10.4
	Reactive Blue	73.8	-30.5	-21.4
	Reactive Yellow	87.4	-5.6	44
	Reactive Green	44.2	-14.3	-4.1
	Reactive Orange	68.8	41.1	56.5
	Reactive Brown	59.5	32.7	18.8
Rayon	Reactive Red	49.6	48.7	-9.5
	Reactive Blue	89	-5.3	-39.9
	Reactive Yellow	87.3	-4.7	47.5
	Reactive Green	42.9	-16.2	-3.5
	Reactive Orange	66.3	41.2	48
	Reactive Brown	60.5	41.1	12.5
Tencel	Reactive Red	53.1	42.7	-9.5
	Reactive Blue	75.4	-29.4	-21.3
	Reactive Yellow	88.7	35	47.5
	Reactive Green	46	-16	-3.8
	Reactive Orange	68.7	39.5	50.3
	Reactive Brown	57.7	42.1	15.1

4.1.2.3 Color measurements of cellulose-based fabric with direct dyes

The cellulose-based fabrics were dyed with five different commercial colors of direct dyes, including red (Direct Red 243), blue (Direct Blue 201), yellow (Direct Yellow 86), orange (Direct Orange 39), and green (Direct Green 6). Similar to the reported results of cellulose-based dyeing with reactive dyes. The direct dyes were also able to be attached with all cellulose-based fabrics. However, each type of fabric shows a different shade, as can be observed in Figure 54. Table 4 summarizes the L*, a*, and b* values of the dyed fabrics, which show varying degrees of color intensity. For both direct green and blue dyes, the a* value is negative, while the value of b* is negative for direct blue dye. Additionally, upon comparing the same dye concentrations, the L* value for

direct dyes is consistently lower than of all reactive dyes. Furthermore, when analyzing the L* value of each dyed fabric, it can be inferred that cotton has the lowest L* value compared to other fabrics in every dye. This result emphasizes that direct dye is an ideal dye for cotton fabric.

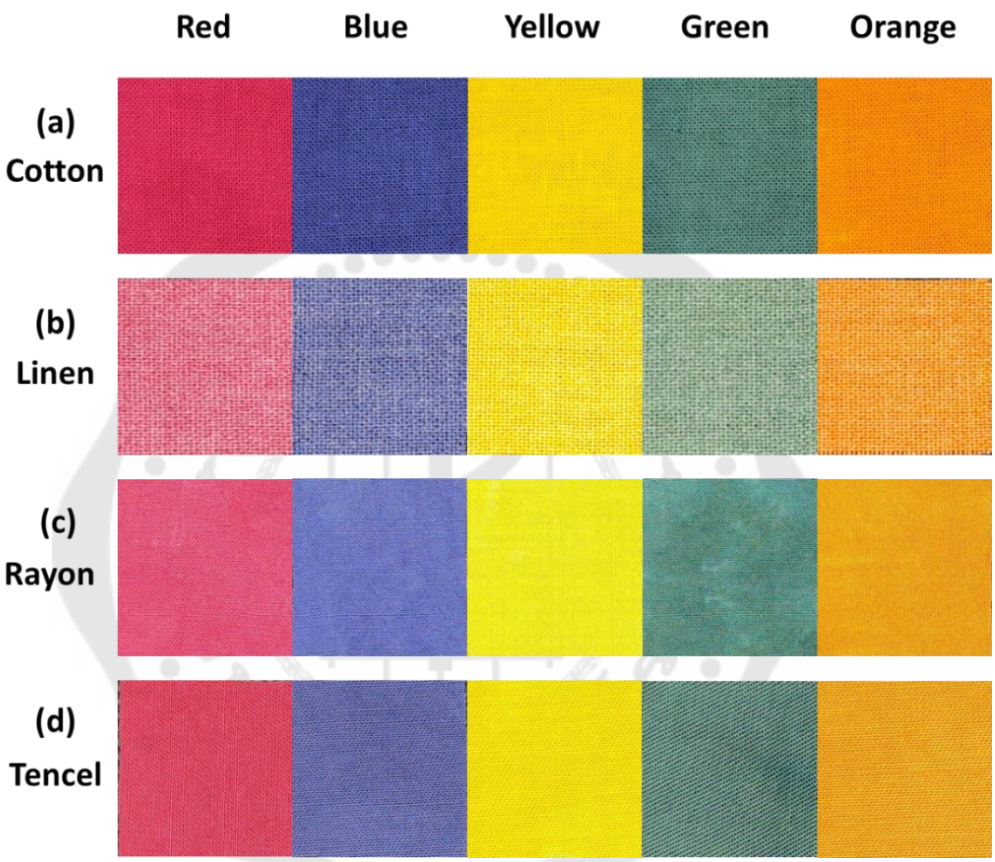

Figure 54 Cellulose-based fabric with direct dyes, (a) cotton, (b) linen, (c) rayon, and (d) Tencel fabric

Table 4 Color measurement values of dyed cellulose-based fabric with direct dyes.

Fabrics	Dyes	D65		
		L*	a*	b*
Cotton	Direct Red	33.9	43.8	6.8
	Direct Blue	71.2	-31.3	24.4
	Direct Yellow	31.6	7.8	-28
	Direct Green	34.6	-27.4	9.7
	Direct Orange	31	44.4	4.1
Linen	Direct Red	57.3	32.4	8.1
	Direct Blue	27.8	6.3	19.8
	Direct Yellow	76	2.8	-25.8
	Direct Green	72.7	-9.9	3.8
	Direct Orange	58.5	42.2	6
Rayon	Direct Red	39.1	34.5	9.2
	Direct Blue	30.3	7	23.6
	Direct Yellow	70.2	3.7	-25.4
	Direct Green	29.8	-13.9	2.4
	Direct Orange	56.5	43.3	5.1
Tencel	Direct Red	34.6	36	5.7
	Direct Blue	36.5	5.6	24
	Direct Yellow	73.6	5.3	-28.1
	Direct Green	48	-11.7	9
	Direct Orange	61	38	6.6

4.2 Standard testing methods for textiles

4.2.1 Colorfastness to washing of cellulose-based fabrics

4.2.1.1 Colorfastness to washing of cellulose-based fabrics with basic dye

The colorfastness of washing is used to determine the color firmness of textiles in different detergents and different washing environments. Evaluation of the color change of the dyed fabric and the color staining of the multifiber fabric was achieved using a grey scale ranging from 1-5 values. According to the references (66), the level 5 of scale is the best fastness level, meanwhile level 1 denotes the lowest fastness level. The results of color fastness in washing the dyed cellulose-based fabrics with basic dye is shown in Table 5. The color change ratings showed a score of 5 for all

fabrics, indicating good colorfastness of the dyed fabrics. The color staining ratings also revealed a similar trend with all the dyed fabrics receiving a rating of 4 to 5. The observation of the multifiber fabric revealed a significant degree of color staining. This suggests that dyed fabrics with basic dye exhibit less staining. The table of colorfastness to washing indicates that basic dyed fabrics have a staining level rating of 4 to 5. The basic dye performs at an excellent level and the colorfastness is quite good. Furthermore, this indicates that the basic dye adheres well to the fabric, causing less excess dye and less staining. The uniform diffusion rate of the dye molecules is responsible for the dyed fabric's color fastness to washing. (70).

Table 5 Colorfastness to washing of dyed cellulose-based fabric with basic dyes.

Fabrics	Dyes	Gray scale	
		Color staining	Color change
Cotton	Basic Red	4-5	5
Linen	Basic Red	5	5
Rayon	Basic Red	4-5	4-5
Tencel	Basic Red	5	5

4.2.1.2 Colorfastness to washing of cellulose-based fabrics with reactive dyes

Using reactive dyes (Figure 55-58), the color change ratings were found in the ranging from 4 to 5. Whereas Tencel fabric with reactive red and blue (Figure 58) were found the color change ratings of 2 to 3 and 3 to 4, respectively. The wash fastness of the dyed fabrics in color change is a good rating to an excellent rating. The wash fastness of dyed fabric is influenced by the diffusion rate of dye molecules inside the fabric. When dyes already diffuses within the fabric, the resulting fabric has good colorfastness. The color staining ratings for all the dyed fabrics were found from 3 to 5. Only Tencel fabric with reactive blue dye has a 2 rating for the color staining. There was very slight staining observed on the multi-fiber fabric in the case of Tencel with reactive

blue and almost no staining on the multi-fibers of the other dyed fabric. Thus, cotton, linen, and rayon have a stronger bond between the fibers and the dyestuffs than Tencel. Thus, cotton, linen, and rayon fabrics have less color staining than Tencel fabric. Reactive dyes have a higher number of dye molecules than direct and basic dyes, respectively (71). Consequently, reactive dyes can bond more effectively between the fibers, resulting in better colorfastness than the other dyes. In conclusion, reactive dyes are more effective for achieving colorfastness in dyed fabrics than basic and direct dyes.

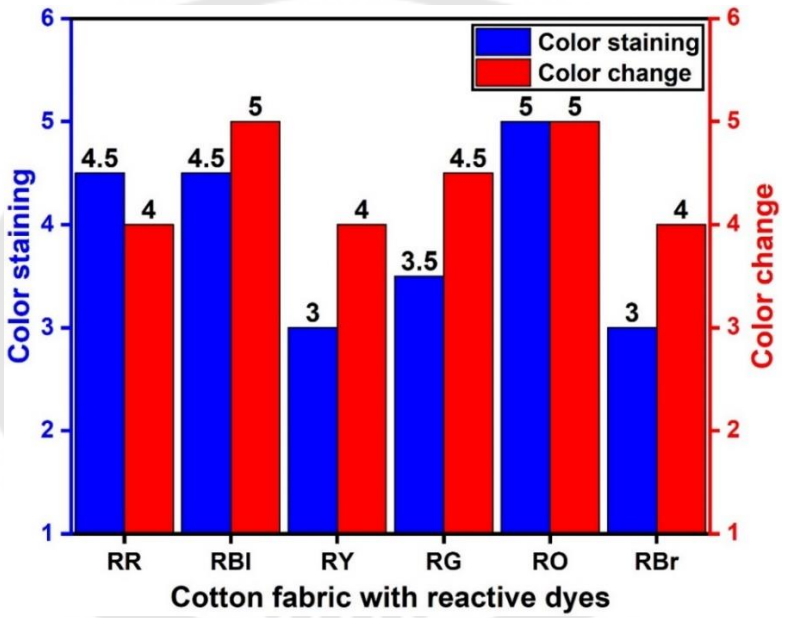

Figure 55 Colorfastness to washing of dyed cotton fabric with reactive dyes

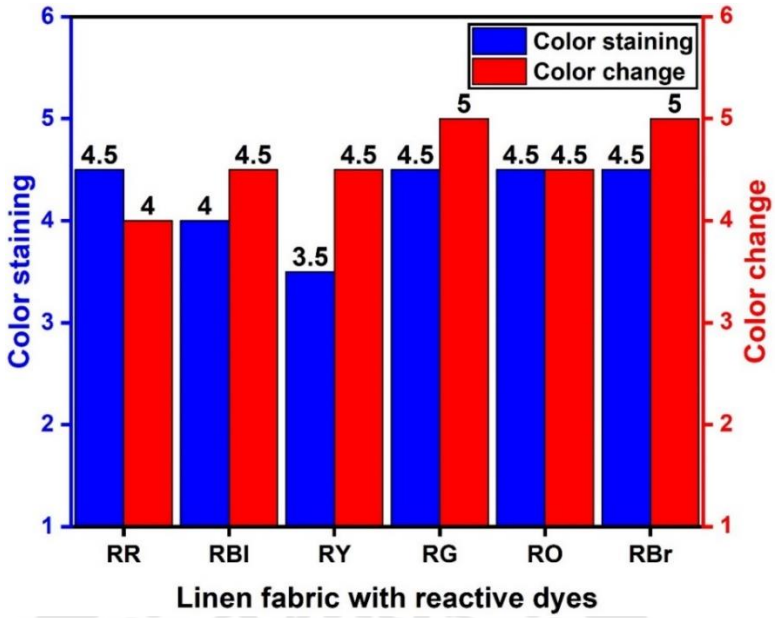

Figure 56 Colorfastness to washing of dyed linen fabric with reactive dyes

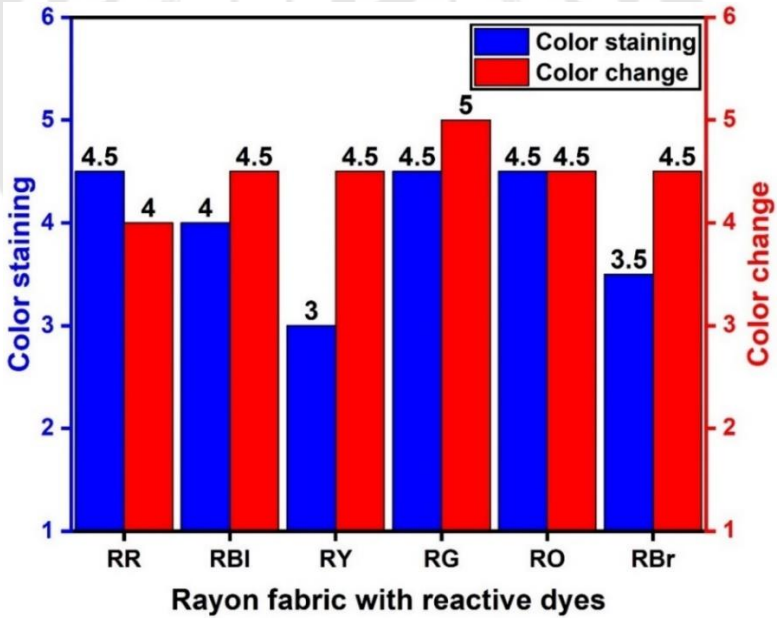

Figure 57 Colorfastness to washing of dyed rayon fabric with reactive dyes

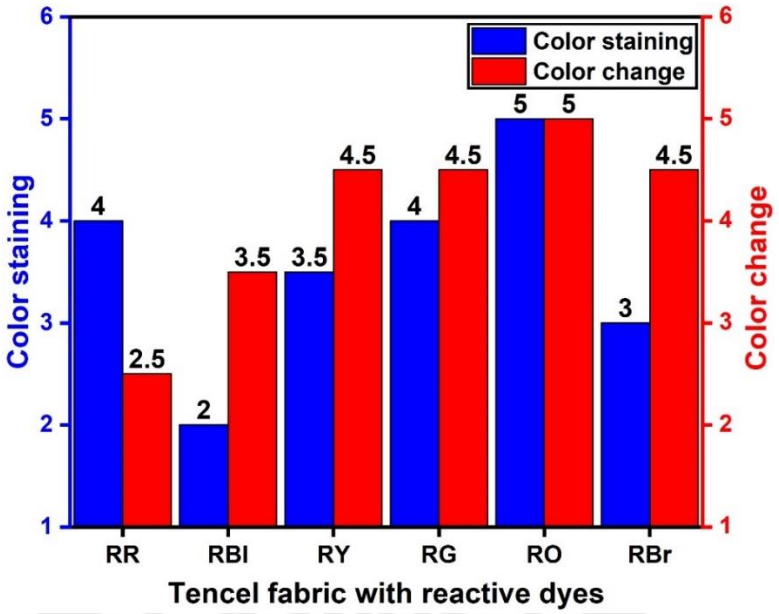

Figure 58 Colorfastness to washing of dyed tencel fabric with reactive dyes

4.2.1.3 Colorfastness to washing of cellulose-based fabrics with direct dyes

The results in Figure 59-62 reveal the colorfastness of dyed fabrics using direct dyes after washing. The color change ratings for these fabrics range from 2 to 5. Overall, the colorfastness for these dyed fabrics in terms of color change is rated as fair to excellent. For the color staining, the ratings ranged from 1 to 3 for all the dyed fabrics, except for Tencel with direct red, which received a higher rating of 4 to 5. Interestingly, the multifiber fabric showed significant staining when dyed with direct dyes. Meanwhile, the Tencel fabric with direct red showed almost no staining on its multifiber. This finding suggests that all fabrics dyed with direct dyes have less bonding between the fibers and the dyestuffs, resulting in more color staining as compared to those with reactive dyes.

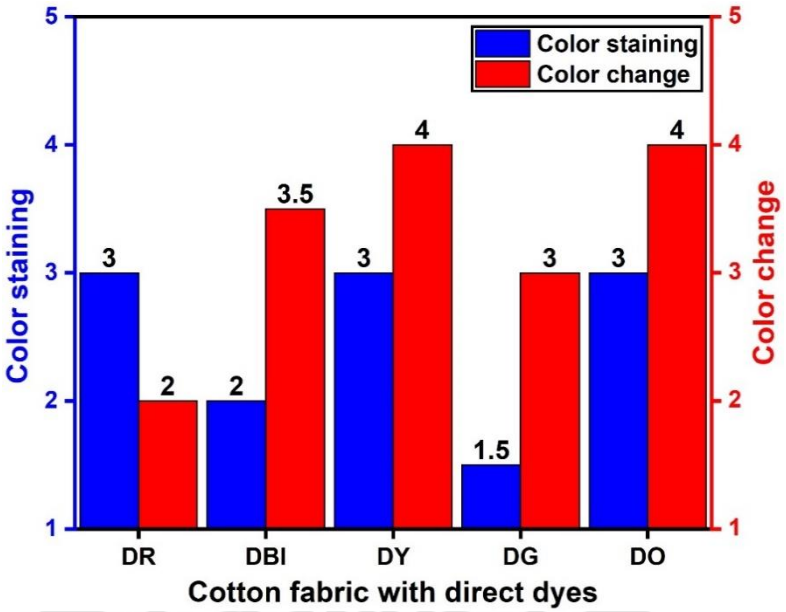

Figure 59 Colorfastness to washing of dyed cotton fabric with direct dyes

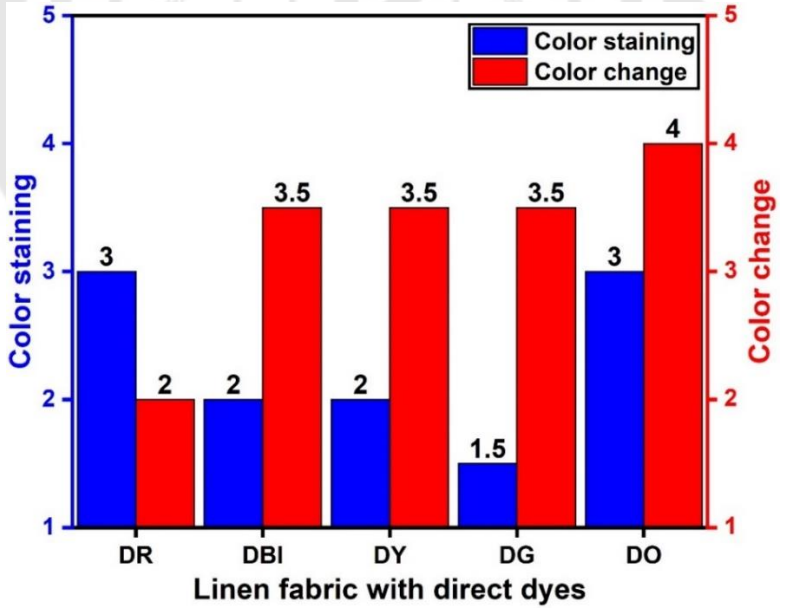

Figure 60 Colorfastness to washing of dyed linen fabric with direct dyes

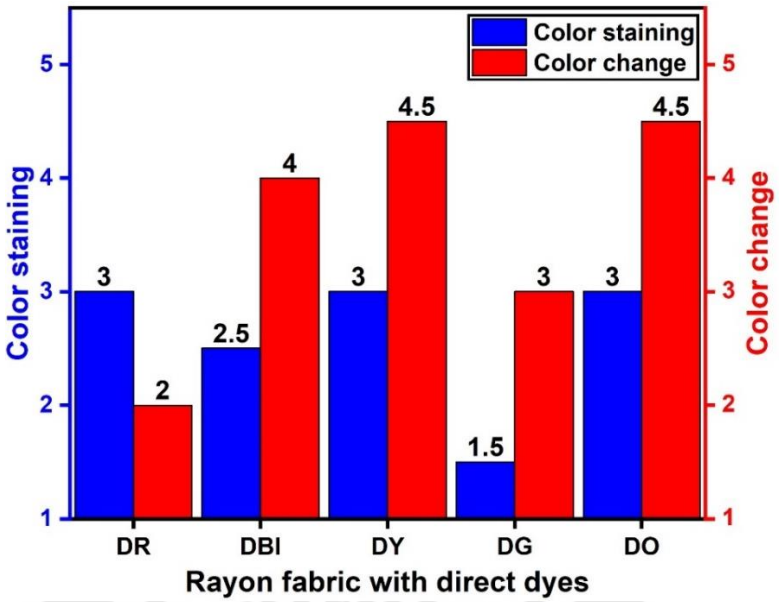

Figure 61 Colorfastness to washing of dyed rayon fabric with direct dyes

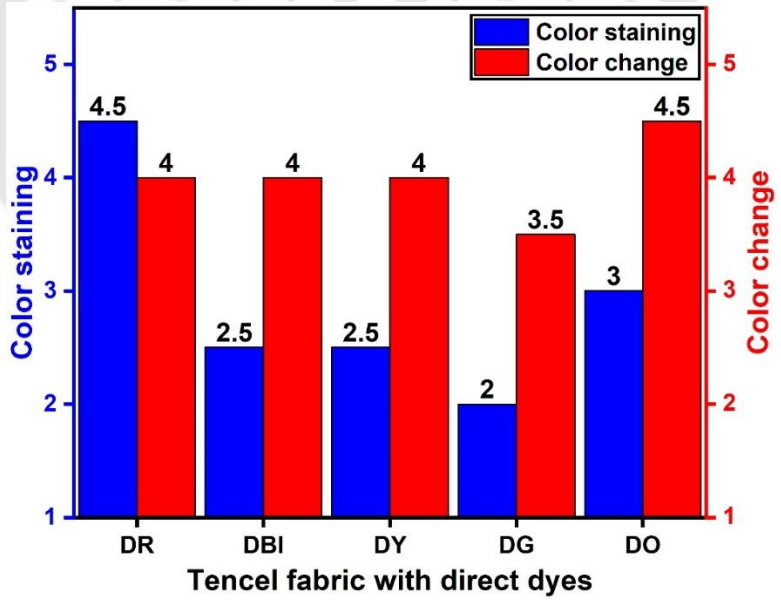

Figure 62 Colorfastness to washing of dyed Tencel fabric with direct dyes

4.2.2 Colorfastness to rubbing of cellulose-based fabrics

4.2.2.1 Colorfastness to rubbing of cellulose-based fabrics with basic dye

Colorfastness to rubbing was tested. The degree of staining of white cloth is used as the evaluation basis, and it is graded against a set of standard colorfastness to

staining gray scales. Table 6 reveals that the color change and color staining of dyed fabrics with basic dyes change from 4 to 5. The rubbing tests show that all evaluated dyed fabrics were rated good to excellent due to their colorfastness properties to rubbing. This result is attributed to the nature of the color and the construction of the fabric.

Table 6 Colorfastness to rubbing of dyed cellulose-based fabric with basic dyes.

Fabrics	Dyes	Gray scale	
		Color staining	Color change
Cotton	Basic Red	4-5	5
Linen	Basic Red	5	5
Rayon	Basic Red	4-5	4-5
Tencel	Basic Red	5	5

4.2.2.2 Colorfastness to rubbing of cellulose-based fabrics with reactive dyes

The scale used to measure rubbing is composed of levels ranging from 1 to 5, with level 1 representing the least durable and level 5 the most durable. This measure of fastness can be determined by comparing tested dyed fabric against a grayscale to assess the degree of color change. To gauge the extent of color change on the dyed fabric, a white cloth used for polishing and the dyed cloth are compared, and the degree of staining is measured using a grayscale. This method is also useful in determining the level of staining of dyed fabric on white fabric. Dyed fabrics with reactive dye in Table 7 show grades 4 to 5 of color change. Dyed fabrics have well to excellent ratings for rubbing tests. The color staining test results on white fabric for dyed fabrics with reactive dye indicate a color staining grade of 4 to 5. However, Tencel with reactive green, orange, and brown exhibits a color staining grade of 2 to 3. The rubbing test evaluation reveals that Tencel with reactive green, orange, and brown dyes have poor to fair rating for colorfastness to rubbing tests. The poor rating of rubbing fastness indicates that the dye molecules do not adhere well to the fabric, causing excess color

to form on the surface of the dyed fabric. When rubbing the test, the color will come off and stain the white cloth during the test.

Table 7 Colorfastness to rubbing of dyed cellulose-based fabric with reactive dyes.

Fabrics	Dyes	Gray scale	
		Color staining	Color change
Cotton	Reactive Red	4-5	5
	Reactive Blue	5	5
	Reactive Yellow	5	5
	Reactive Green	4-5	4-5
	Reactive Orange	4	4-5
	Reactive Brown	4-5	5
Linen	Reactive Red	5	5
	Reactive Blue	5	5
	Reactive Yellow	5	5
	Reactive Green	5	5
	Reactive Orange	5	5
	Reactive Brown	5	5
Rayon	Reactive Red	4-5	5
	Reactive Blue	4	4
	Reactive Yellow	5	5
	Reactive Green	4-5	4
	Reactive Orange	5	5
	Reactive Brown	4-5	4-5
Tencel	Reactive Red	5	5
	Reactive Blue	4	4-5
	Reactive Yellow	4	4-5
	Reactive Green	2-3	4
	Reactive Orange	2	4-5
	Reactive Brown	2-3	4-5

4.2.2.1 Colorfastness to rubbing of cellulose-based fabrics with direct dyes

Table 8 presents color fastness to rubbing test on the color change of dyed fabrics with direct dyes. The ranges for color change were obtained in a period of 4 to 5. A thorough evaluation of the dyed fabrics showed that their colorfastness to rubbing

tests was good to excellent rating. The color staining on the white fabric of the dyed fabrics with direct dye showed grades ranging from 4 to 5. Except Tencel with direct blue, green, and orange, which demonstrated grades of 2 to 3. The Tencel fabric is poor to fair ratings, which is consistent with the trend observed in reactive dyes. Poor rating of Tencel fabric as a result of the dye not being sufficiently fixed to the fabrics. A slight external force can easily separate the dye from the fabric. Therefore, residual color stains white fabric. The results of Tencel fabric, with a different fabric structure, have a different impact on the color fastness of rubbing. Continuous friction and washing can affect lint on the dyed fabric surface. When rubbing, the adhesion of the fabric is low and some short lint from the dyed fabric may stain the white fabric.

Table 8 Colorfastness to rubbing of dyed cellulose-based fabric with direct dyes.

Fabrics	Dyes	Gray scale	
		Color staining	Color change
Cotton	Direct Red	4	4-5
	Direct Blue	4-5	4-5
	Direct Yellow	4	4-5
	Direct Green	4-5	4
	Direct Orange	4	4-5
Linen	Direct Red	5	5
	Direct Blue	4-5	5
	Direct Yellow	4-5	5
	Direct Green	4-5	5
	Direct Orange	4-5	5
Rayon	Direct Red	4-5	4-5
	Direct Blue	4-5	4-5
	Direct Yellow	4	4-5
	Direct Green	4-5	4-5
	Direct Orange	4	4-5
Tencel	Direct Red	4-5	4-5
	Direct Blue	2	4
	Direct Yellow	4-5	4-5
	Direct Green	2-3	4
	Direct Orange	2-3	4-5

4.3 Characterizations

4.3.1 Morphological characterization of cellulose-based fabrics

The SEM images are shown in Figure 63a-d. The surface morphology of cellulose-based fabrics was found with different weaving structures depending on the fabric type. The SEM pictures revealed a plain weave for cotton, linen, rayon, while Tencel showed a twill weave structure. The difference in weaving structure contributes to the unique characteristics and properties of each cellulose-based fabric.

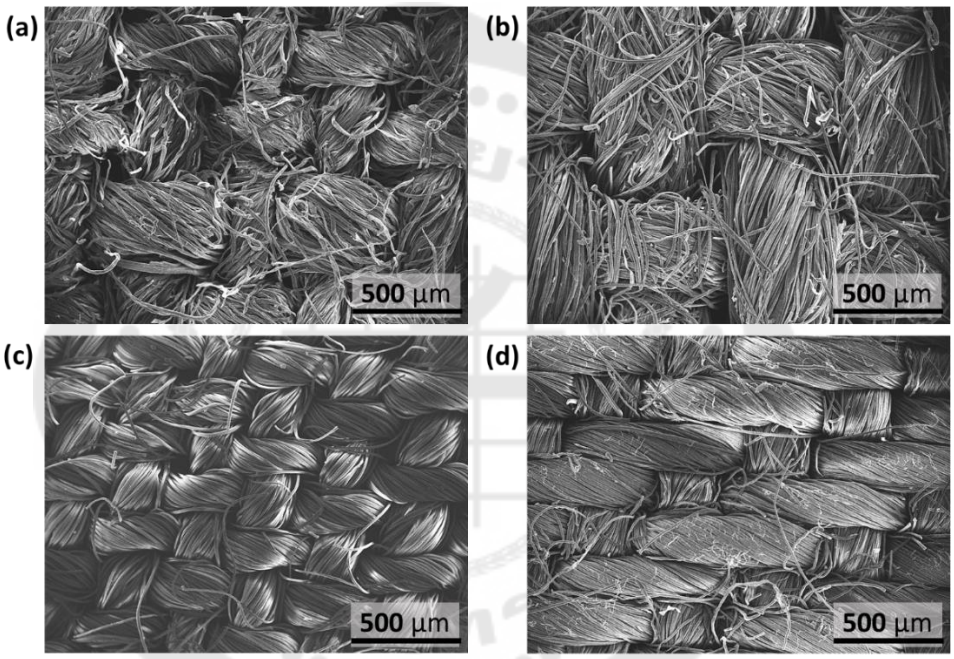

Figure 63 SEM images of surface morphology at 60x for (a) cotton, (b) linen, (c) rayon, and (d) Tencel fabrics

The fiber diameter for different types of fabrics could be estimated from SEM images according to Figure 64 using the ImageJ software. Figure 64a shows that the cotton fiber has 21.8 ± 8 µm of average diameter with many ribbons shape along its length. The ribbon shape of fiber gives an uneven fiber surface of cotton. The linen fiber (Figure 64b) shows the presence of fiber nodes or joints that are small, soft, and irregular lumps. The fiber nodes occur randomly along the length of the fiber with 25.6 ± 11 µm of the average diameter. A characteristic of rayon fiber contains a lengthwise

striated surface with an average diameter of about 18.8 ± 6 μm, as illustrated in Figure 64c. Figure 64d shows the longitudinal surface of Tencel fiber that is smooth without striation. The average diameter of the Tencel was found to be 19.3 ± 7 μm.

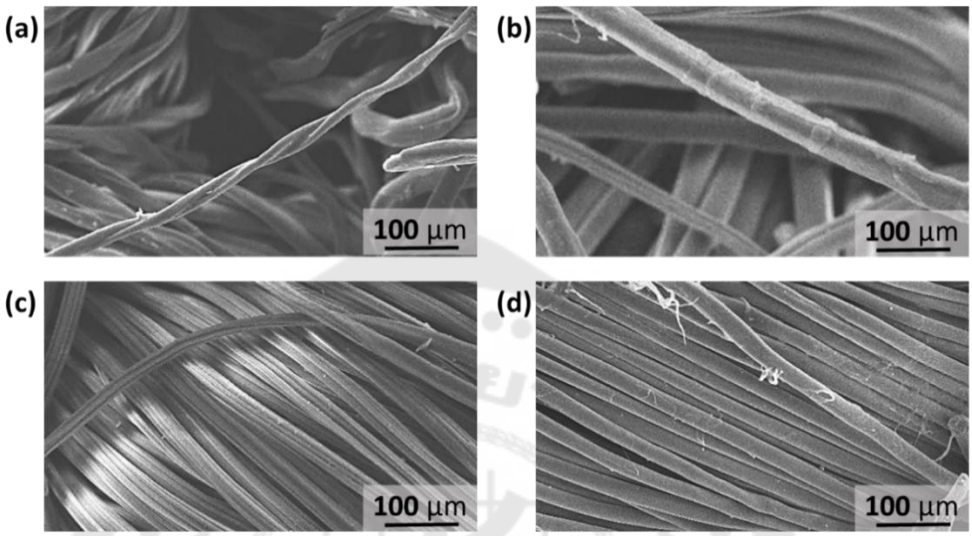

Figure 64 SEM images of cellulose-based fabrics at 200x including (a) cotton, (b) linen, (c) rayon, and (d) Tencel fabrics

The total surface area can be calculated using the area of fabric (M^2) divided by the mass of the fabric (G) according to equation (1) (72). The total surface area of all fabric was found to be 0.0054, 0.0044, 0.0085, and 0.0079 m^2/g for cotton, linen, rayon, and Tencel fabrics, respectively. The rayon fabric shows the highest total surface area with the consistency of having smallest diameters of fibers.

$$\text{Surface area of fabric} = M^2/G \qquad (1)$$

The data of fiber diameters for cellulose-based fabrics was further collected to calculate the total surface area of fabrics with another method as shown by the equations (2)-(4) (73). The calculation is done by using the same dimensions of all fabrics at 3x3 cm^2.

$$C_1 = p_1 \times d_1 \quad (2)$$

$$C_2 = p_2 \times d_2 \quad (3)$$

$$C_f = (C_1 + C_2 - C_1C_2) \times 100 \quad (4)$$

According to equation (2)-(4), the C_f is the total contact surface area, C_1 is the contact surface area of the warp thread, and C_2 is the contact surface area of the weft thread. p_1 is warp spacing = 1/number of warp yarns per unit width of fabric and p_2 is weft spacing = 1/number of weft yarns per unit length of fabric. d_1 and d_2 represent the diameter of warp and weft yarns. The results were found in the same trend with using the equation (1) that the contact surface area is in order as rayon (73.4%) > Tencel (72.7%) > cotton (45.9%) > linen (18%). Therefore, it can confirm that rayon has significantly higher surface area and total contact area than that of others in the group of cellulose-based fabric. Having a high surface area directly affects the electrical output efficiency for TENG owing to its high opportunity to produce more charge after triboelectrification process as compared to lower surface area. The output signal in terms of open circuit voltage (V_{OC}) and short circuit current (I_{SC}) are provided by session number 4.5.3.

4.3.2 Chemical functional group examination

4.3.2.1 Chemical functional group of cellulose-based fabrics

Figure 65 shows the ATR-IR spectra of cellulose-based fabrics including cotton, linen, rayon, and Tencel. The absorption peak of all fabrics at 3330 cm^{-1} is attributed to the hydroxyl (-OH) stretching vibration, which is the primary functional group of cellulose. The absorption peak at 2896 cm^{-1} is characteristic of the stretching vibration of C-H, presenting in cellulose and hemicellulose. Meanwhile, the peak at 1630 cm^{-1} is associated with H-O-H bending vibrations of water in cellulose. The peaks at 1360 cm^{-1} is relative to the C-H bending vibration of cellulose polysaccharides. At the absorption peak of 1051 cm^{-1}, the C-O stretching is observed. The absorption peak at 894 cm^{-1} indicates the presence of β-glycosidic linkages between monosaccharides. The absorption peak list of all cellulose-based fabrics is shown in Table 9. Previous

research by Yetria Rilda et al. have reported the IR spectrum analysis of cellulose-based fabric and revealed the absorption peak, which is consistent with the results reported above (74). The IR results in this work are also consistent with the work reported by Emanoel Henrique Portella and co-workers (75) that, therefore, confirms the similar cellulose chemical structure in all of the fabrics. However, the absorption peak at 1732 cm^{-1}, which corresponds to the C=O stretching of a carboxyl group (-COOH) in hemicellulose, is only found for linen fabric. This peak is not presented in other fabrics due to their low or nonexistent composition of hemicellulose, as reported by Comnea-Stancu et al (76) and Titok et al (77). Hemicellulose is usually found from incompletely washing out during the scouring process. In linen and cotton, the complex mixing components is usually found from nature source, including waxes, pectin, lignin, hemicellulose, and cellulose (78). However, the amount of hemicellulose in linen structure is higher than that of cotton. The peak of hemicellulose then was not detected by IR technique. In contrast, the component of rayon and Tencel is simpler and cleaner because the production process is produced by regenerated cellulose. Therefore, they are only containing the cellulose component without any other impurity before spinning into yarn (79). That is the reason why the hemicellulose was not found for rayon and Tencel.

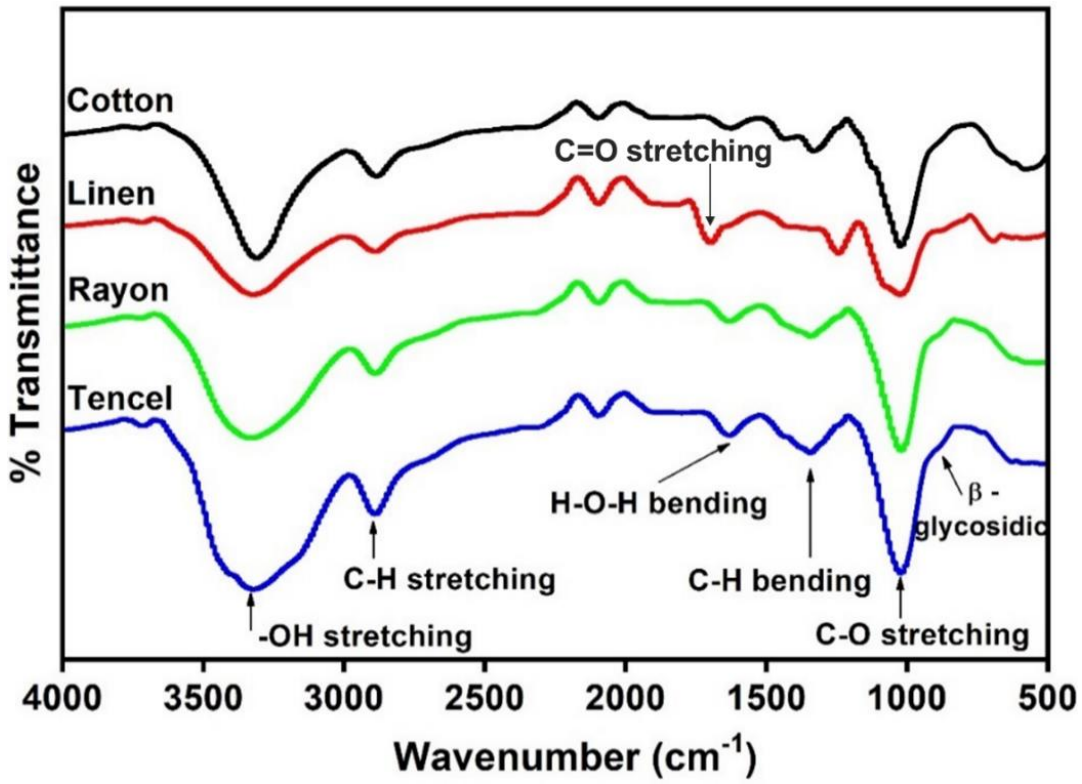

Figure 65 ATR-IR results of four types of cellulose-based fabrics including cotton, linen, rayon, Tencel fabrics

Table 9 ATR-IR peak identification list for cellulose-based fabrics

Wavenumber (cm^{-1})	Characteristic bond
3330	-OH stretching
2896	C-H stretching
1732	C=O stretching
1630	H-O-H bending
1360	C-H bending
1051	C-O stretching
894	β-glycosidic

4.3.2.2 Chemical functional group of basic dyes

The characteristic functional groups of basic dye, namely red was analyzed by IR as shown in Figure 66 Table 10 show the list of absorption peak of basic dye. The absorption peak of basic dye at 3432 and 3291 cm^{-1} represents the stretching vibration of N-H, corresponding to the amine group. In the infrared spectrum of basic dye, various absorption peaks are observed, indicating different vibrational modes of the molecule. One of the prominent peaks can be seen at 3137 cm^{-1}, which represents the C-H stretching of the aromatic ring. Another peak is observed at 1625 cm^{-1}, corresponding to the bending vibration of N–H. The stretching vibration of C–C in the aromatic ring is represented by two peaks at 1567 and 1450 cm^{-1}. Additionally, the absorption peak at 1321 cm^{-1} is related to the stretching vibration of C–N. The in-plane C–H bending vibration is observed at 1159 cm^{-1}, while the out-of-plane C–H bending vibration is represented by the absorption peak at 898 cm^{-1}. These results are in agreement with the findings reported by Osman Duman et al. (80) that identified similar peaks in the IR spectrum of basic red 9.

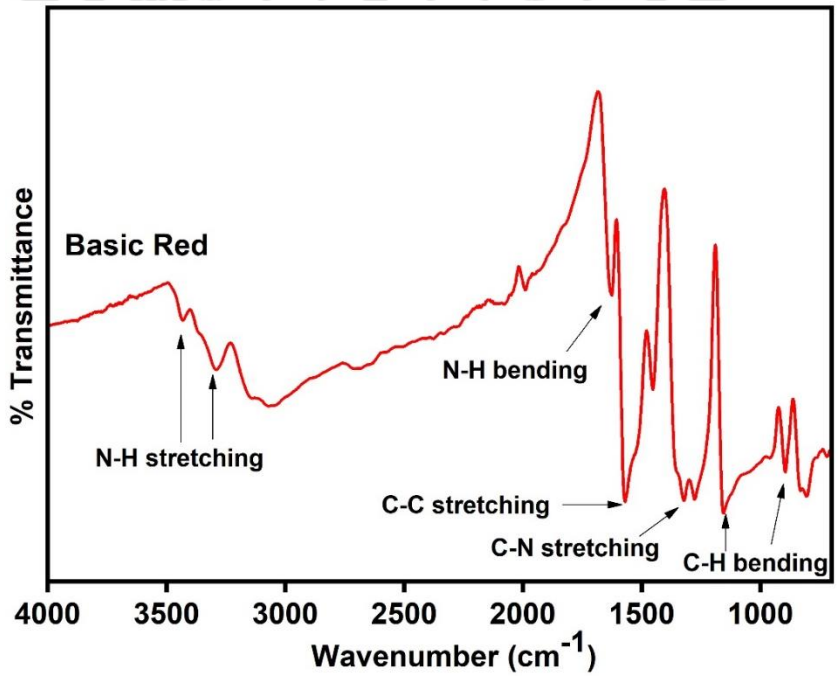

Figure 66 ATR-IR spectra of basic red dyes

Table 10 ATR-IR peak identification list for the basic red dyes

Wavenumber (cm^{-1})	Characteristic bond
3432	N-H stretching
3291	N-H stretching
3137	C-H bending
1625	N-H bending
1567	C-C stretching
1450	C-C stretching
1321	C-N stretching
1159	C-H bending
898	C-H bending

4.3.2.3 Chemical functional group of reactive dyes

The characteristic functional groups of 6 reactive dyes, namely red, blue, yellow, green, orange, and brown, were analyzed by ATR-IR within the wavenumber ranging from 4000-700 cm^{-1}. The results are shown in Figure 67. The absorption peak of all dyes at 3740 cm^{-1} corresponds to the N-H stretching vibration of the amine group indicating the main functional group of the reactive dye. The absorption peak at 2970 cm^{-1} is assigned to the C-H stretching vibration of $-CH_2$. The prominent peak at 1700 and 1650 cm^{-1} correspond to the -NH- bending and the -C=N- stretching of secondary aromatic amines. The absorption peak at 1430 and 1110 cm^{-1} are attributed to the C-S asymmetric stretching vibrations and the $-SO_2$ symmetric stretching vibrations of meta-sulfonyl. The absorption peak at 864 cm^{-1} is the wagging vibration of the β-naphthalene indicating mononuclear and polynuclear aromatic rings of the reactive dyes. All absorption peaks of reactive dye are listed in Table 11. The -NH stretching vibration of aromatic amines, the -C=N- stretching and the -NH- bending of secondary aromatic amines are observed owing to an auxochrome group of reactive dye that reacts with fabric. The beta-naphthalene rings with two contiguous hydrogen atoms of reactive dye

correspond to the chromophore of the reactive dye (81). All chemical characteristic results of the dye confirm the dye is a reactive dye.

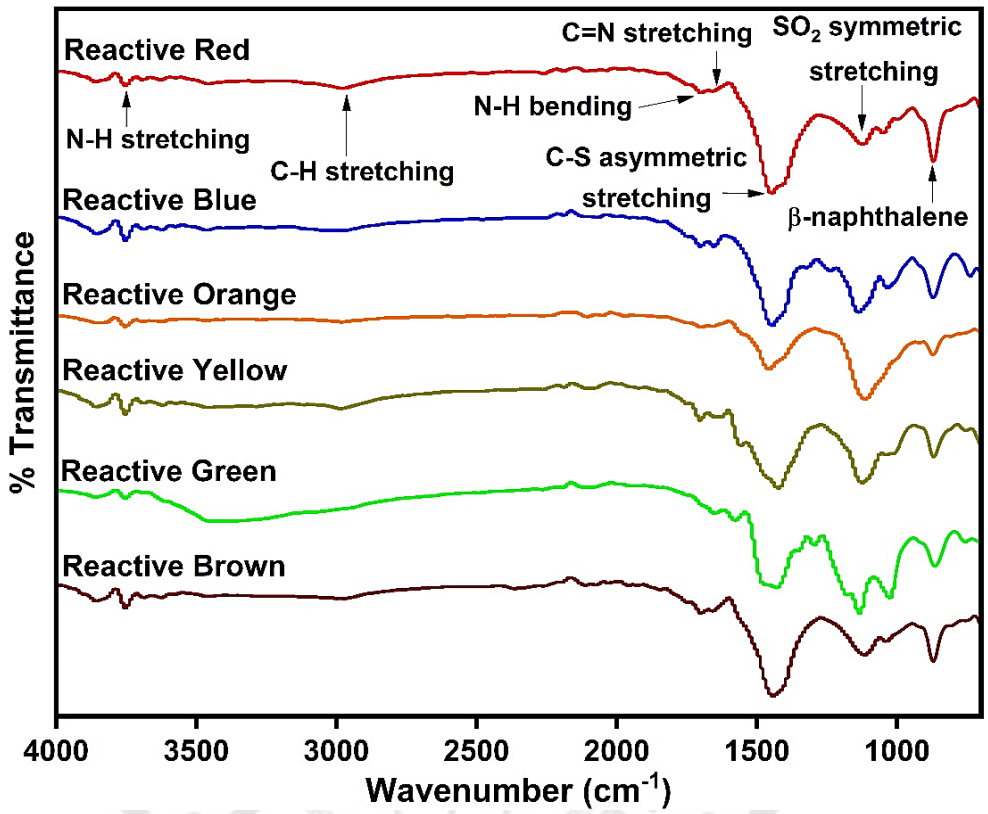

Figure 67 ATR-IR spectra of 6 different color of reactive dyes

Table 11 ATR-IR peak identification list for reactive dyes

Wavenumber (cm^{-1})	Characteristic bond
3740	N-H stretching
2970	C-H stretching
1700	-NH- bending
1650	-C=N- stretching
1430	C-S asymmetric stretching
1110	$-SO_2$ symmetric stretching
864	Aromatic ring

4.3.2.4 Chemical functional group of direct dyes

Figure 68 display the analysis of the characteristic functional groups in five direct dyes, including red, blue, yellow, green, and orange. All characteristic vibrations relative to peak position of the direct dyes are tabulated in Table 12. The characteristics of the direct dyes are observed at 3355 cm^{-1}, indicating to the O-H stretching vibration of the hydroxyl group. The presence of N=N stretching vibration at 1547 cm^{-1} indicates the presence of azo groups, while the N-H bending vibration at 1475 cm^{-1} confirms the presence of an amine as the primary functional group. The NO_2 stretching vibration at 1343 cm^{-1} corresponds to a nitro group, and the S-O bond stretching vibration at 1124 cm^{-1} indicates the presence of a sulfoxide group. The results are also consistent with the IR results from Qunshan Wei et al. (82) and Juan Lozano-Alvarez et al. (64)'s reports, confirming the symmetrical and asymmetrical vibrations of a primary amine of direct dye.

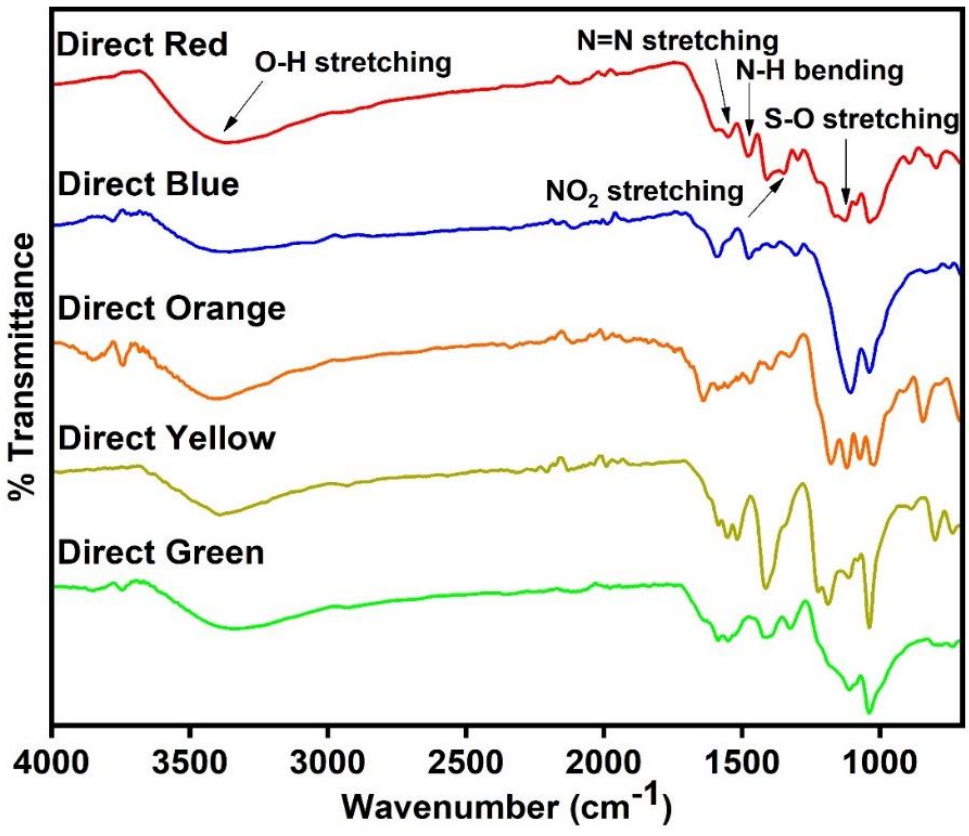

Figure 68 ATR-IR spectra of five different color for direct dyes

Table 12 ATR-IR peak identification list for direct dyes

Wavenumber (cm^{-1})	Characteristic bond
3355	O-H stretching
1547	N=N stretching
1475	N-H bending
1343	NO_2 stretching
1124	S-O stretching

4.3.2.5 Chemical functional group of cellulose-based fabrics with inorganic dyes

The functional group of the cellulose-based fabrics with the inorganic dyes was characterized as shown by the results in Figure 69-71. It was found that the IR peaks of cellulose-based fabrics after dyeing are similar to the IR result of cellulose-based fabrics before dying. This indicates that the dye molecules were probably stuck with a small amount on the fabric. Therefore, the absorption peak of the dye is not noticeable. However, based on the results from literature, Reazuddin Repon et al. reported ether linkage between reactive dye and cellulose together with the N-H deformation of dye (83). The results found that the absorption peak of literature is consistent with dyed cellulose-based fabric in this research.

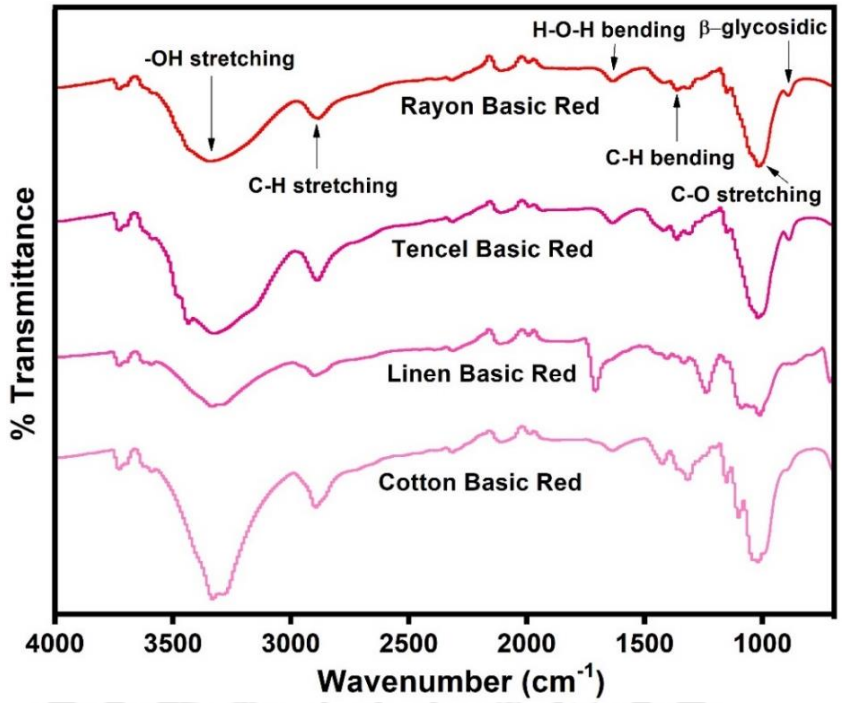

Figure 69 ATR-IR spectra of cellulose-based fabrics dyeing with basic dye

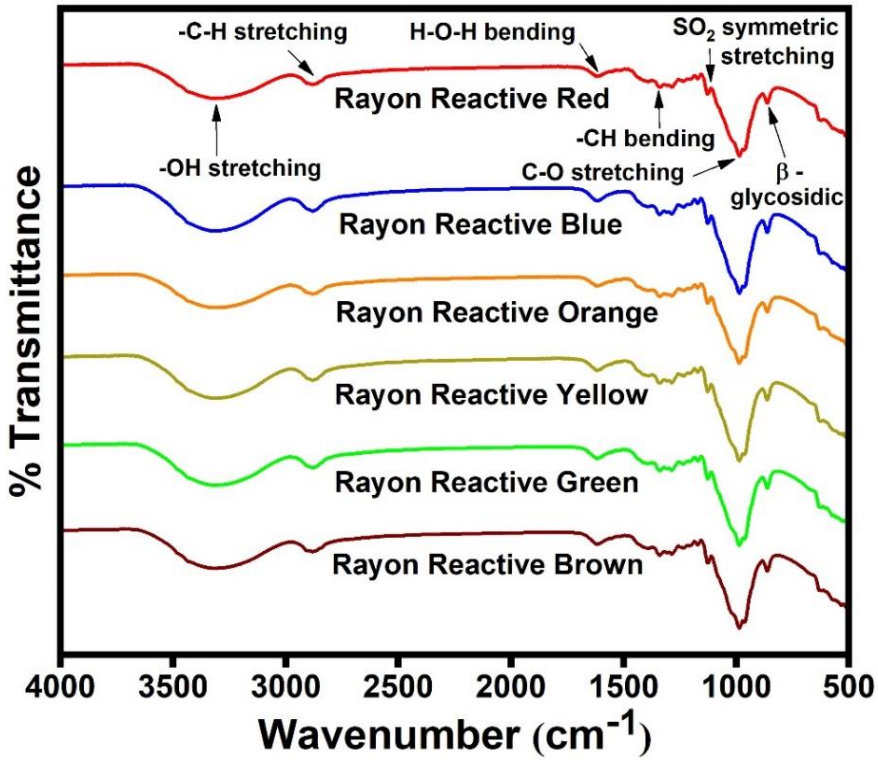

Figure 70 ATR-IR spectra of rayon fabric dyeing with reactive dyes

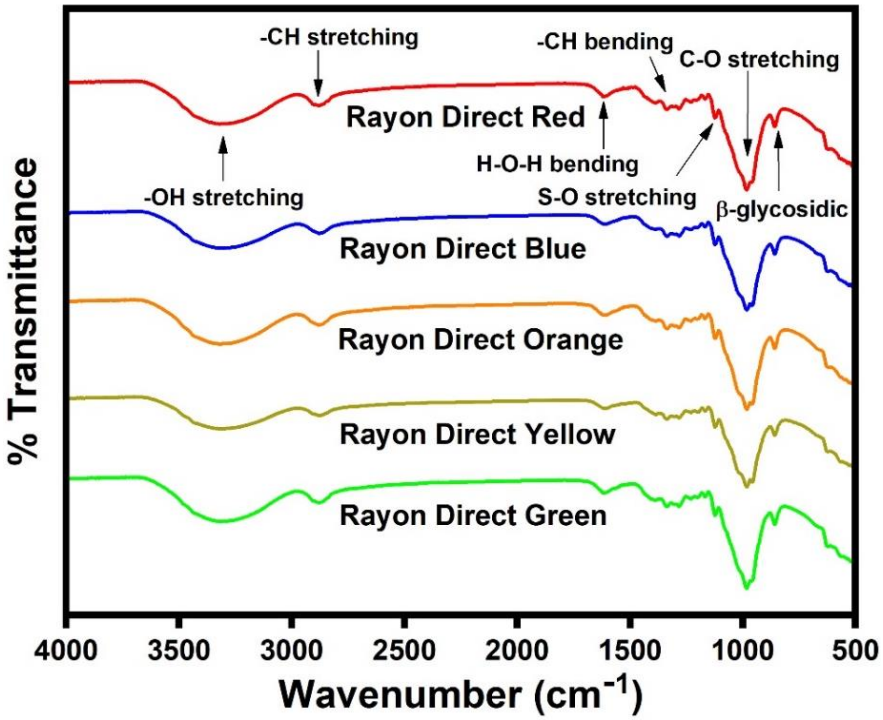

Figure 71 ATR-IR of rayon fabric dyeing with 5 different colors of direct dyes

4.4 Characterization and electrical properties of cotton/CNT electrode

To fabricate the TENG for flexible devices, its electrodes are one of critical components that need to be developed for being flexibility with firmly sticking to the device during operation. Generally, the electrodes used in the TENG device are solid film materials which are not appropriate for attaching by fabric. It is necessary to fabricate fabric electrodes. Therefore, a conductive fabric has been developed in this work by coating adhesive cotton fabric with specifically 0.15 g CNT, similar to the best condition from literature (84). Its electrical conductivity was tested every time before actual use. This session shows the characteristics of adhesive cotton/CNT fabric with its electrical properties including conductivity and resistivity.

4.4.1 Morphological characterization of cotton/CNT electrode by scanning electron microscope (SEM)

Figure 72a shows the image of cotton/CNT fabric from a digital camera. The CNT solution has a black particle cover on adhesive cotton fabrics. Figure 72b displays the SEM image of cotton/CNT fabric at 200x magnification. The CNT particles were

dispersed and formed on the surface of adhesive cotton fibers after coating as can be seen by the solid particle on surface of fabric. The SEM image at 30,000x magnification (Figure 72c) and 60,000x (Figure 72d) magnification represent the significant particles of CNT on the adhesive cotton fabric. The carbon particles are arranged in a long sheet. It is shaped like a network of carbon and rolled together to form a cylinder or tube. This indicates that CNTs have been successfully absorbed into the adhesive cotton fabrics.

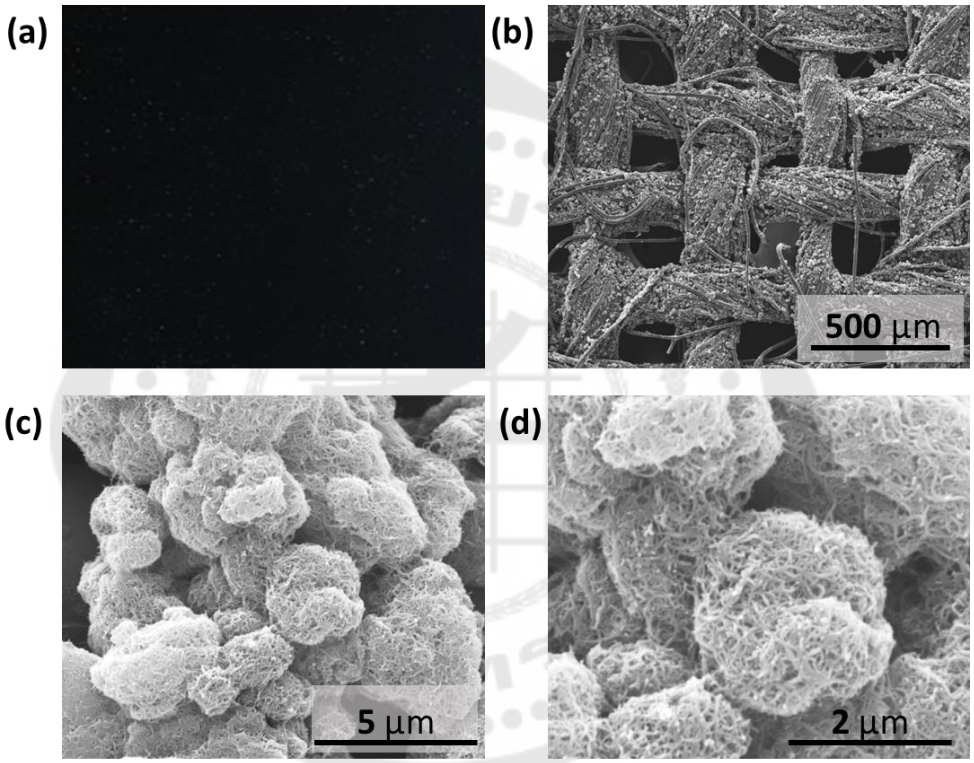

Figure 72 (a) Photograph of cotton/CNT fabric by digital camera, (b) SEM image of cotton/CNT fabric at 200x magnification, (c) 30,000x magnification, and (d) 60,000x magnification

4.4.2 The Energy Dispersive Spectroscopy (EDS) analysis of cotton/CNT electrode

The EDS analysis was conducted to identify elements on the surface of the cotton/CNT electrode. The results are displayed in Figure 73. The number of elements on the surface of the pristine cotton fabric and cotton/CNT electrode were analyzed in Figures 73a and 73b, respectively. Figure 73c displays the elements of C (yellow), O

(blue), and Au (purple) on the surface of the cotton/CNT electrode. Cotton/CNT fabric analysis revealed larger amounts of C elements compared to pristine cotton. This indicated that a considerable amount of CNT was coated into cotton fabric. This result can be confirmed by the weight ratio of 48.54%, illustrating the C atoms of pristine cotton fabric. The weight ratio of C atoms increased to 71.24% after the cotton fabric was coated with CNTs. In addition, pristine cotton fabric contains O elements derived from -OH groups with a weight ratio of 44.01%, and the weight ratio decreased to 21.75% for cotton/CNT electrodes. The amount of carbon is 3.3 times higher than that of oxygen because CNT is an element that consists of only one carbon atom. Therefore, it can be concluded that the cotton fabric can be completely coated with CNT.

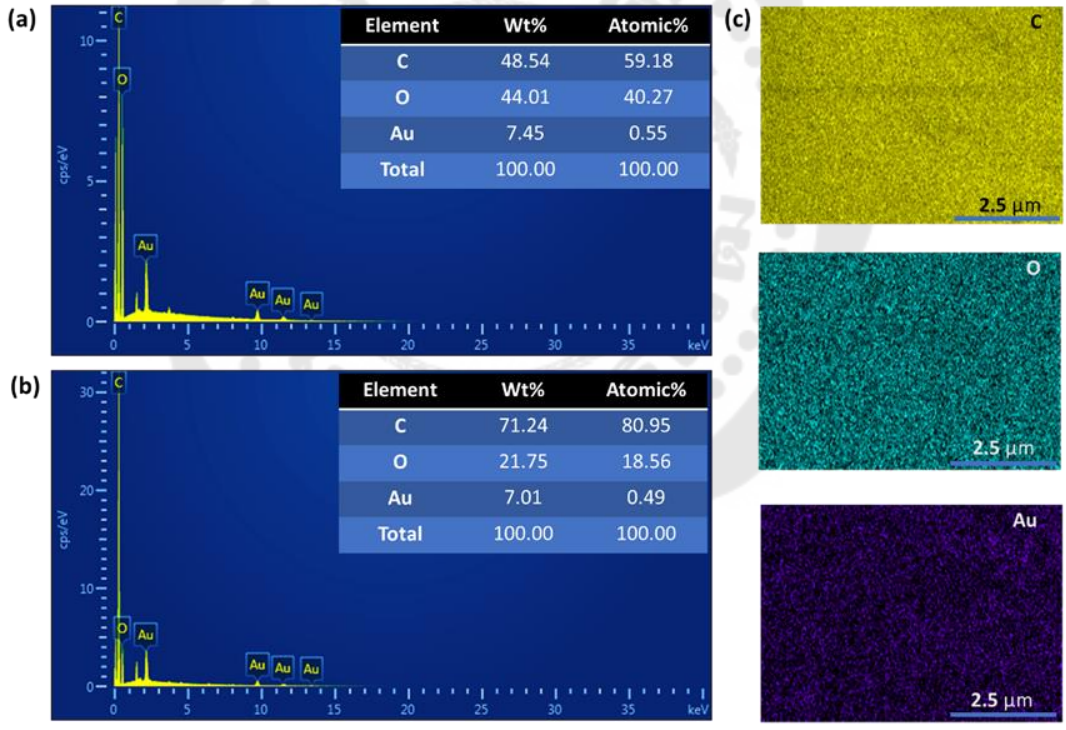

Figure 73 The EDS analysis of cotton/CNT electrode, including (a) the number of elements on the surface of the pristine cotton fabric and (b) cotton/CNT electrode, (c) mapping results of each element on the cotton/CNT electrode.

4.4.3 The dispersion of CNT in cotton/CNT electrode by Synchrotron Radiation X-ray Tomographic Microscopy (SR-XTM)

The SR-XTM technique was used to analyze the dispersion of CNT within the cotton/CNT electrodes, revealing some interesting findings in terms of 3D virtualization images. Figure 74a shows the non-adhesive side of the cotton fabric with a porous weaving structure. It was found that similar spheres of adhesive beads stuck on cotton fabric as illustrated in Figure 74b. This adhesive side will be ironed to the dyed cellulose-based fabric. When the cotton fabric turns 90 degrees, it shows the adhesive and non-adhesive sides of the cotton fabric as illustrated in Figure 74c. Figure 74d-f shows only the CNT phase distribution at different point of view to indicate the distribution of CNT inside the cotton fabric. This result shows that the CNT can disperse both on the surface of non-adhesive side and adhesive side together with incorporating inside of the cotton fabric at elevated amount.

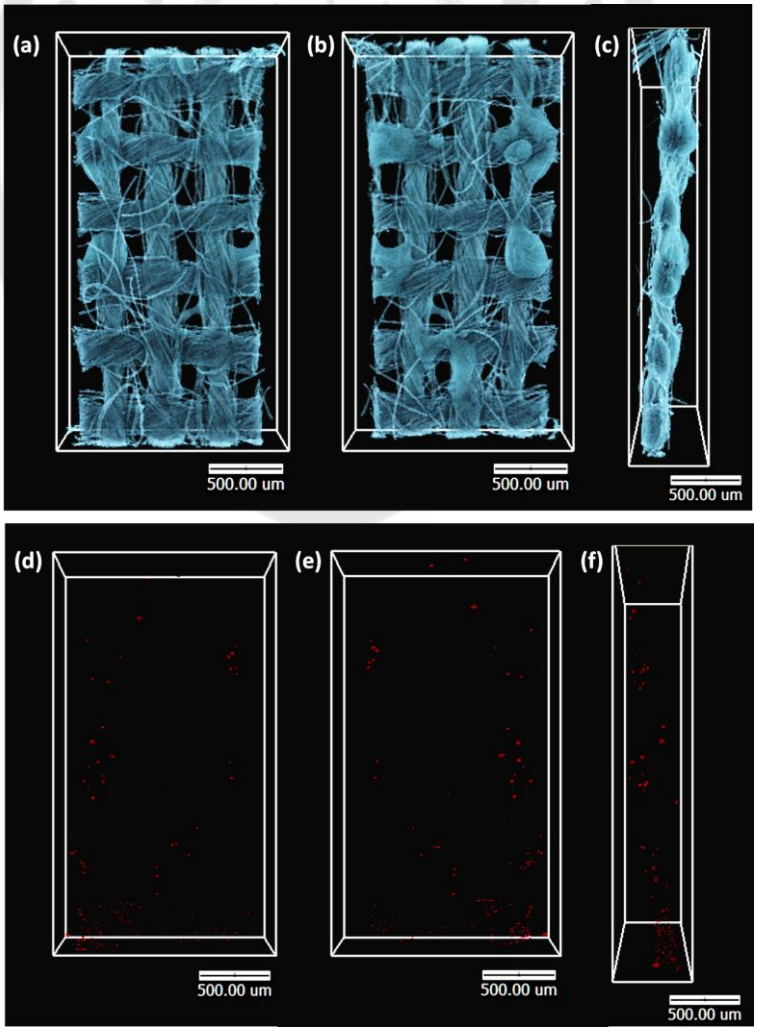

Figure 74 SR-XTM 3D visualization images of cotton/CNT electrode, including (a-c) cotton fabric and (d-f) CNT phase dispersion in cotton fabric

4.4.4 Chemical structure characterization of cotton/CNT electrode by Raman spectroscopy

Raman spectroscopy is employed to analyze the characteristics of cotton/CNT electrodes (Figure 75). The Raman spectrum of the pristine cotton fabric was examined, the Raman spectrum shows the peak at 1295 cm^{-1} corresponding to C-C stretching of backbone structure. The band at 1620 cm^{-1} is the bending of CH_2. The Raman spectra also represent C=C stretching vibrations at 1734 cm^{-1}, related to the crystalline form of polypropylene (PP). PP is the adhesive component that is used to coat cotton fabric. The Raman spectrum of the cotton/CNT shows two specific signals at 1342 cm^{-1} and 1574 cm^{-1}, corresponding to the D band and G band of CNT. The D band is associated with the structural disorder arising from amorphous carbon. The G band corresponds to the tangential stretching vibrations of the carbon atoms. The spectrum of CNT/cotton exhibits a similar profile to Rui Costa et al. presented the Raman spectra of the CNT (85).Therefore, the Raman analysis of cotton/CNT confirms that the cotton fabric was coated successfully with the CNT.

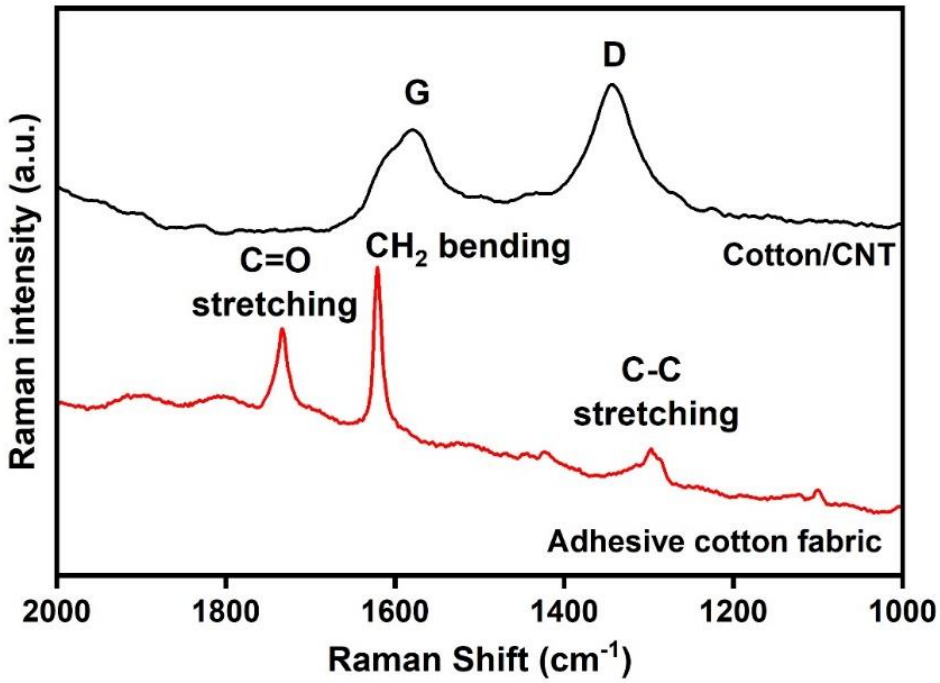

Figure 75 Raman spectra of the adhesive cotton fabric coated with CNT and adhesive cotton fabric

4.4.5 Resistivity and conductivity of cotton/CNT fabric

In this work, the flexible electrode of cotton/CNT fabric is utilized. The electrical resistivity and conductivity were analyzed. Figure 76 shows the resistivity of pristine cotton and cotton/CNT that changes with increasing frequency. It is seen that with the increased frequency, the resistance of cotton/CNT is lower than pristine cotton. The increased CNT content reduces the electrical resistance and allows electric current to flow through the cotton/CNT better than pristine cotton. From the frequency of 10^4 Hz onwards, the resistance value of cotton/CNT improves to approximately 10^5 Ω. On the other hand, the electrical conductivity increases with increasing frequency. The electrical conductivity of cotton/CNT is higher than the conductivity of pristine cotton. As the frequency increases from 100 Hz to 10^5 Hz, the electrical conductivity of cotton/CNT increases from 0 to 7.8 μSm^{-1} (Figure 77), which indicates the electrical conductivity of cotton/CNT. Therefore, cotton/CNT can be effectively used as a conductive electrode fabric for TENG devices.

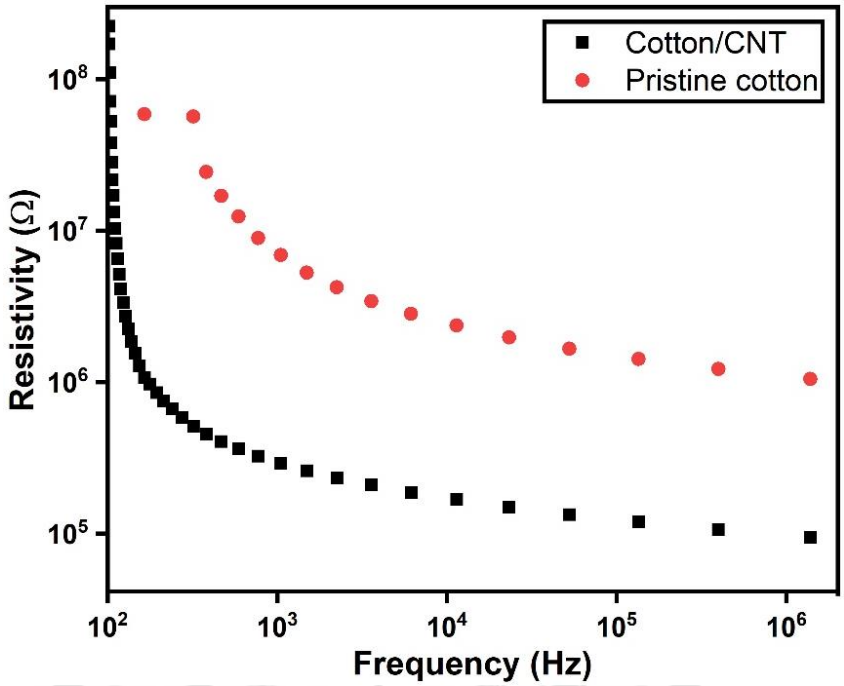

Figure 76 Resistivity of pristine cotton and cotton/CNT fabric

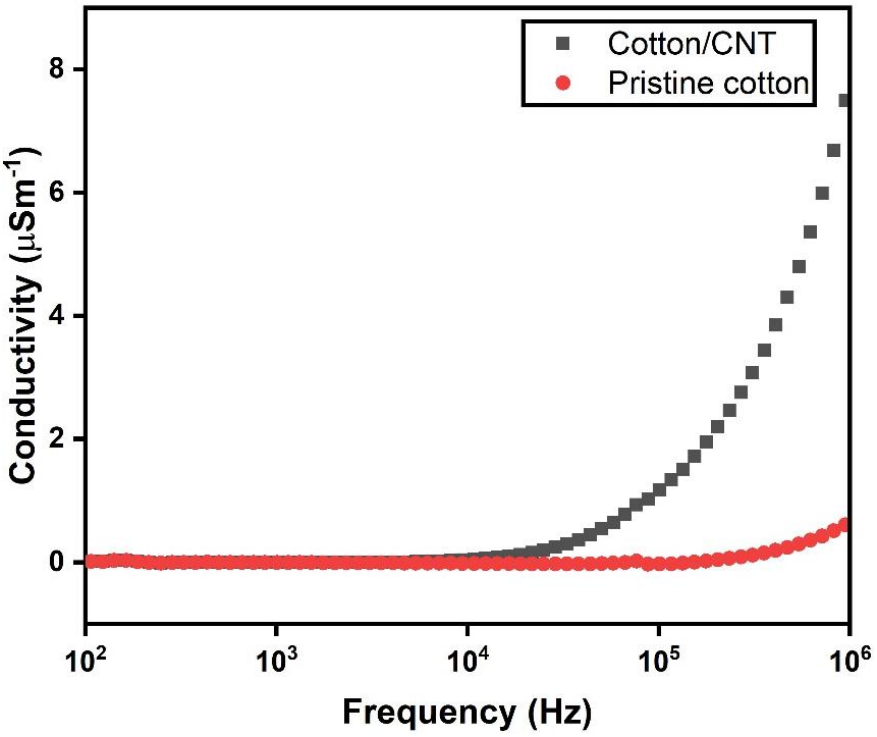

Figure 77 Conductivity of pristine cotton and cotton/CNT fabric

4.5 Electrical output performance testing

4.5.1 Electrical output performance of cellulose-based fabric triboelectric nanogenerator (CF-TENG) by comparing negative triboelectric pair.

The electrical output of the CF-TENG device was tested using an oscilloscope and a digital multimeter to demonstrate the open circuit voltage (V_{OC}) and short circuit current (I_{SC}) under vertical-contact separation mode. The positively charged contact layer of CF-TENG is cotton, a cellulose-based fabric. Two types of contact layer materials, Al tape and PTFE film were compared to select for using as standard negatively charged materials for CF-TENG along with cellulose-based fabric. Figure 78a and 78b shows the electrical output of cotton fabric with Al tape (Cotton/Al tape) and cotton fabric with PTFE (Cotton/PTFE) film with V_{OC} and I_{SC} of 0.9 V, 2.93 μA, and 28.1 V, 50.3 μA, respectively. The results showed that Cotton/PTFE has a higher electrical output than that of using Cotton/Al tape. From the results, it can be explained that cotton fabric can donate electrons, while the PTFE has a high ability to accept electrons. When cotton fabric comes into contact with PTFE, the electrical output is higher than when cotton fabric comes into contact with Al tape (86). By considering and comparing the working mechanism between cotton/Al tape and cotton/PTFE, the electron donor and acceptor behavior of materials play a crucial role. The mechanism of cotton/Al tape is an exchange of the charge between the metal and the dielectric materials, meanwhile, cotton/PTFE contacting mechanism occurs between dielectric-to-dielectric materials. The working mechanism of cotton/Al tape is shown in Figure 78c. When the Al tape contacts the cotton fabric (i), the cotton will accept electrons from the Al tape and the Al tape to have a positive charge on the surface. During the separation process (ii), the electrons in the electrode move to the Al tape, the separated electrical charges generate the electrical current flows. After perfect separating of the Al tape from the cotton fabric (iii), the Al tape becomes electrically neutral, while the electrode is positively charged due to lack of electrons. Once the Al tape and the cotton fabric becomes close again (iv), the electrons in the Al tape move back to the electrode and this state generates electricity. Herein, since the Al tape and cotton contain high potential of electron donating tendency with small different electronegativity in

triboelectric series position, their triboelectrification therefore causes poor exchange of electron and gives a slight electrical output value. Meanwhile, the cotton/PTFE mechanism of action involves the exchange of charges is different, as shown in Figure 78d. In this case, the PTFE film and cotton fabric exhibit a significant difference in electronegativity in the triboelectric series position making the high potential for electron exchanging between them. The PTFE can gain electrons easier while cotton can simply donate electrons. Thus, the triboelectrification of the cotton/PTFE results in a good electron exchanging and generates a higher electrical output value as compared to the cotton/Al tape pair. According to Figure 78d, when two materials have different electronegativity in contact (i), the cotton will give electrons and create a positive charge on the surface. PTFE will receive electrons from the cotton, creating a negative charge on the surface. When they are separated (ii), the charges induce an electron flow from the negative electrode to the positive electrode through an external circuit and create electricity. After the complete separation of the cotton fabric from PTFE film (iii), the contact materials become electrically neutral. As the cotton and PTFE film come into contact again (iv), the electrons in the positive electrode move back to the negative electrode and generate electricity. The result has proven that the PTFE film is ideal for a negative contact layer of cellulose-based fabric TENG devices.

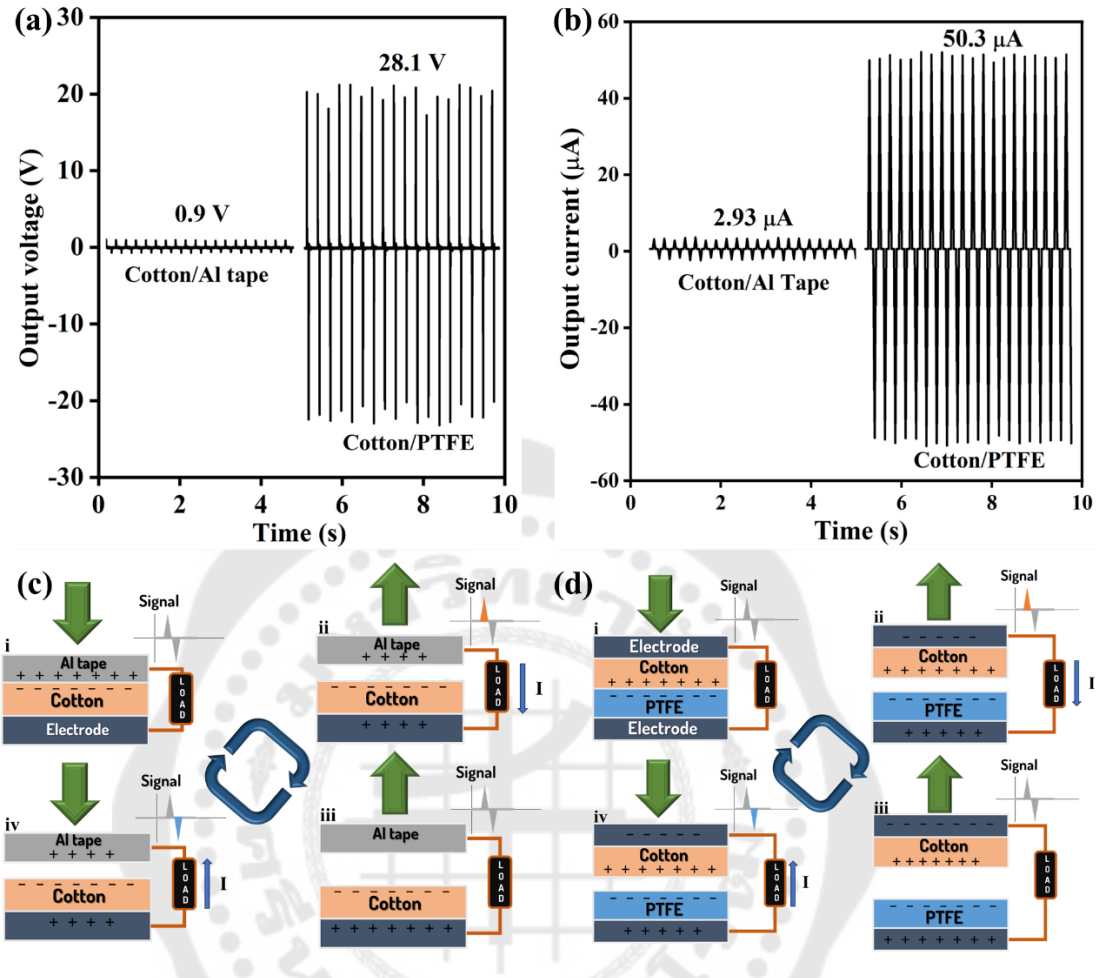

Figure 78 The electrical output performance including (a) output voltage and (b) output current of CF-TENG by comparison of using Al and PTFE as contacted material, and the working mechanism between (c) cotton/Al tape and (d) cotton/PTFE.

4.5.2 Electrical output of cellulose-based fabric triboelectric nanogenerator (CF-TENG) by comparing electrodes.

After selecting the PTFE film as negatively charged material, the electrical results of TENG devices were studied by comparing three types of electrodes: Al tape, CNT, and graphene. The results of V_{OC} and I_{SC} are illustrated in Figure 79a and 79b. Utilizing Al tape (Cotton/Al tape) provided the highest V_{OC} and I_{SC} of 28.1 V and 50.3 μA, respectively. However, Al tape is not good at adhering to fabrics in case of using in application. The electrode materials for textile TENG should be the fabric that will be

subjected to varying strain rates and deformation according to the unpredictable movements of the body (87). Consequently, the electrodes for CF-TENG should be designed in such a way as to accommodate these conditions with a stable yield of desired output and skin comfort. Therefore, CNT and graphene were used to render high performance for CF-TENG electrodes. Both of them were dispersed in solvent and coated on the glue fabric by dipping for attaching to cellulose-based fabric before fabricating the TENG device. The result shows that using CNT electrode (Cotton/CNT) provided a higher performance than that of using the graphene electrode (Cotton/graphene) with the V_{OC} and I_{SC} of 28.9 V and 39.6 μA. The result shows that CNT has better electrical conductivity than graphene because CNT has a 1D structure while graphene has a 2D structure (88). Therefore, it can be concluded that higher electrical conductivity and 1D structure result in the electrical output of Cotton/CNT higher than Cotton/graphene. Therefore, a CNT is an electrode layer for a CF-TENG device.

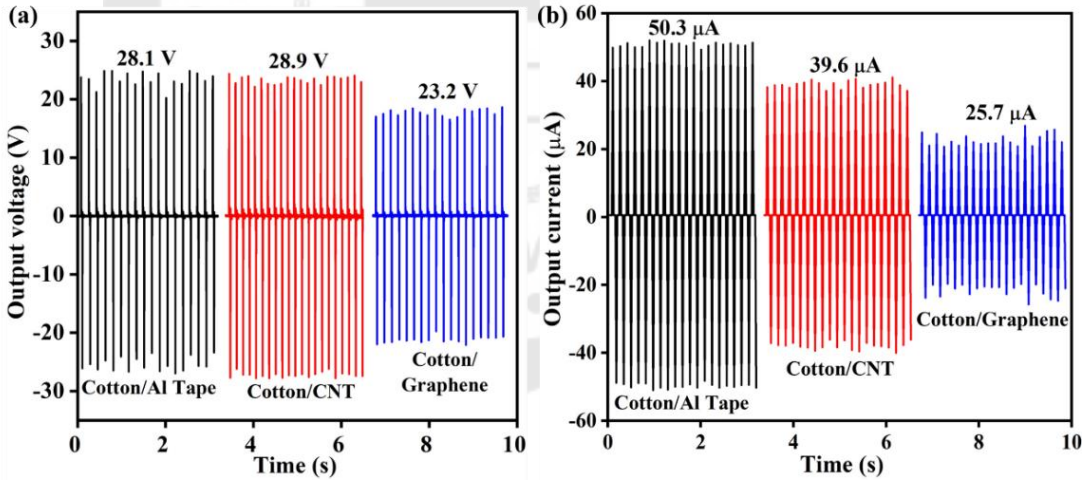

Figure 79 The electrical output performance including (a) V_{OC} and (b) I_{SC} of CF-TENG by comparison of using different electrodes

4.5.3 The electrical output performance of cellulose-based fabric triboelectric nanogenerator (CF-TENG)

4.5.3.1 The electrical output performance of CF-TENG with various types of cellulose fabrics.

The electrical output performance of CF-TENG was measured by comparing 4 types of cellulose fabric including cotton, linen, rayon, and Tencel. PTFE film is used as a negative charged contact layer and cotton/CNT fabric is used as electrode. Figure 80a and 80b show the electrical output of CF-TENG with different types including cotton, linen, rayon, and Tencel fabric. The V_{OC} of 12.69 V, 17.46 V, 23.17 V, and 18.71 V for cotton, linen, rayon, and tencel fabric, respectively. While the I_{SC} of all cellulose-based fabric was 9.48 μA, 9.07 μA, 13.08 μA, 8.44 μA, respectively. It was found that the rayon fabric showed higher electrical output than that of other fabrics because of its surface area. According to the fiber morphology and total surface area, rayon has the smallest diameter with the highest total surface area as per the total surface area calculations above (72). The surface area has an effect significant on the efficiency of TENG. As a result of the total surface area of fabrics, rayon fabric can produce a larger triboelectric charge on the triboelectric layer due to large surfaces can generate more triboelectric charge on the surface of fabric. Meanwhile, other types of fabrics with larger fiber sizes result in less total surface area than rayon fabric. Containing lower contact area results in a lower electrical output signal. The result can confirm the significance of the material surface area on the electrical output performance of the TENG device. Hence, only rayon fabric with the greatest total surface area has been researched.

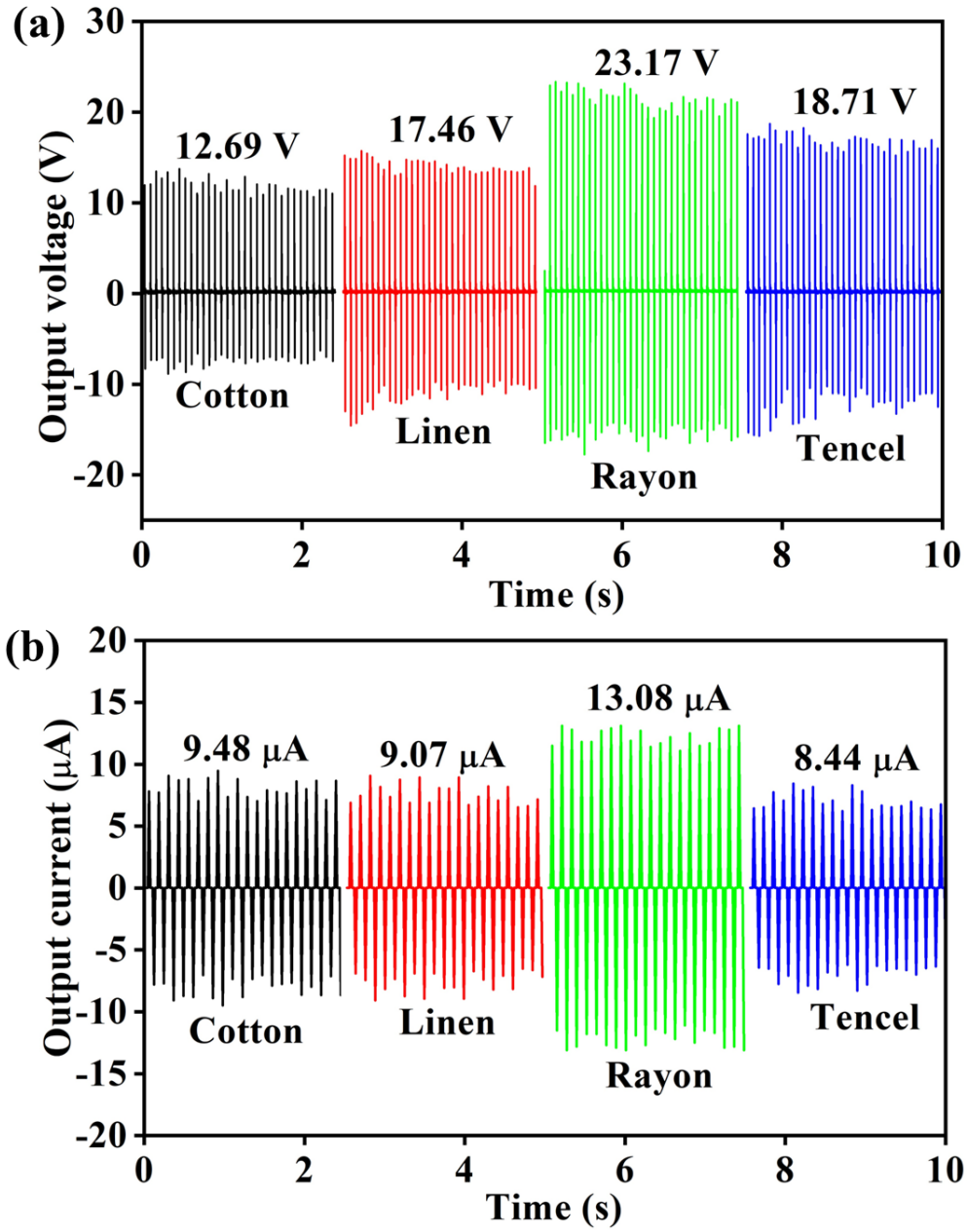

Figure 80 The electrical output performance of CF-TENG including (a) V_{OC}, (b) I_{SC} of cotton, linen, rayon, and Tencel fabric

4.5.4 The electrical output performance of dyed rayon fabric based TENG with three types of the dyes for red colors.

In this work, after measuring output signal of CF-TENG with various types, the rayon was used to study further about the effect of dyes. Three types of red color,

including reactive dye, direct dye, and basic dye, were used first for dyeing with rayon to compare the effect of functional groups. The red dyed rayon with reactive dye, direct dye, and basic dye are shortly called R-RR, R-DR, and R-BR. The electrical output of V_{OC} and I_{SC} for the red dyed rayon fabrics are shown in Figures 81a and 81b. The V_{OC} and I_{SC} of pristine rayon fabric were 23.2 V and 13.08 μA. After the rayon fabric was dyed with red dyes, the electrical output increased. The V_{OC} of rayon fabric after dyeing reactive red (R-RR), direct red (R-DR), and basic red (R-BR) was found to be 36.7 V, 42.7 V, and 46.6 V, respectively. Meanwhile, the I_{SC} of R-RR, R-DR, and R-BR increased at 17.85 μA, 18.85 μA, and 22.95 μA, respectively. The electrical output results showed that the electrical efficiency of rayon fabric increased from dyeing. Considering each color further, it was found that all three types of dyes have the same main functional group, namely the amine group, and have different numbers of amine groups. Rayon fabric with basic red dye shows the highest electrical outputs of 46.6 V and 22.95 μA. The result means that the rayon fabric dyed with all types of red dyes can provide higher electron than that of pristine rayon after contacting with a high negative PTFE film contact layer. According to chemical structure of the dyes in Figure 82-84), having amino functional groups (auxochrome) in the dye structure plays a significant role for controlling the rayon to be more positive. Containing (O=S=O) or other groups of chromophores does not affect the producing charge ability. However, as compared to dyeing with reactive and direct red dyes, the basic red dye can introduce a more positive charge on the fabric surface because of containing higher number of NH_2 auxochrome in molecules. As shown in Figure 82, the molecular structure of basic red dyes consists of three amine groups as an auxochrome in one molecule that can react with the hydroxyl groups from the fabric more than dyeing with the direct (Figure 83) and reactive dyes (Figure 84). Even though the reactive and direct red dyes have a higher amount of chromophore group, the existence of the auxochrome is more significant.

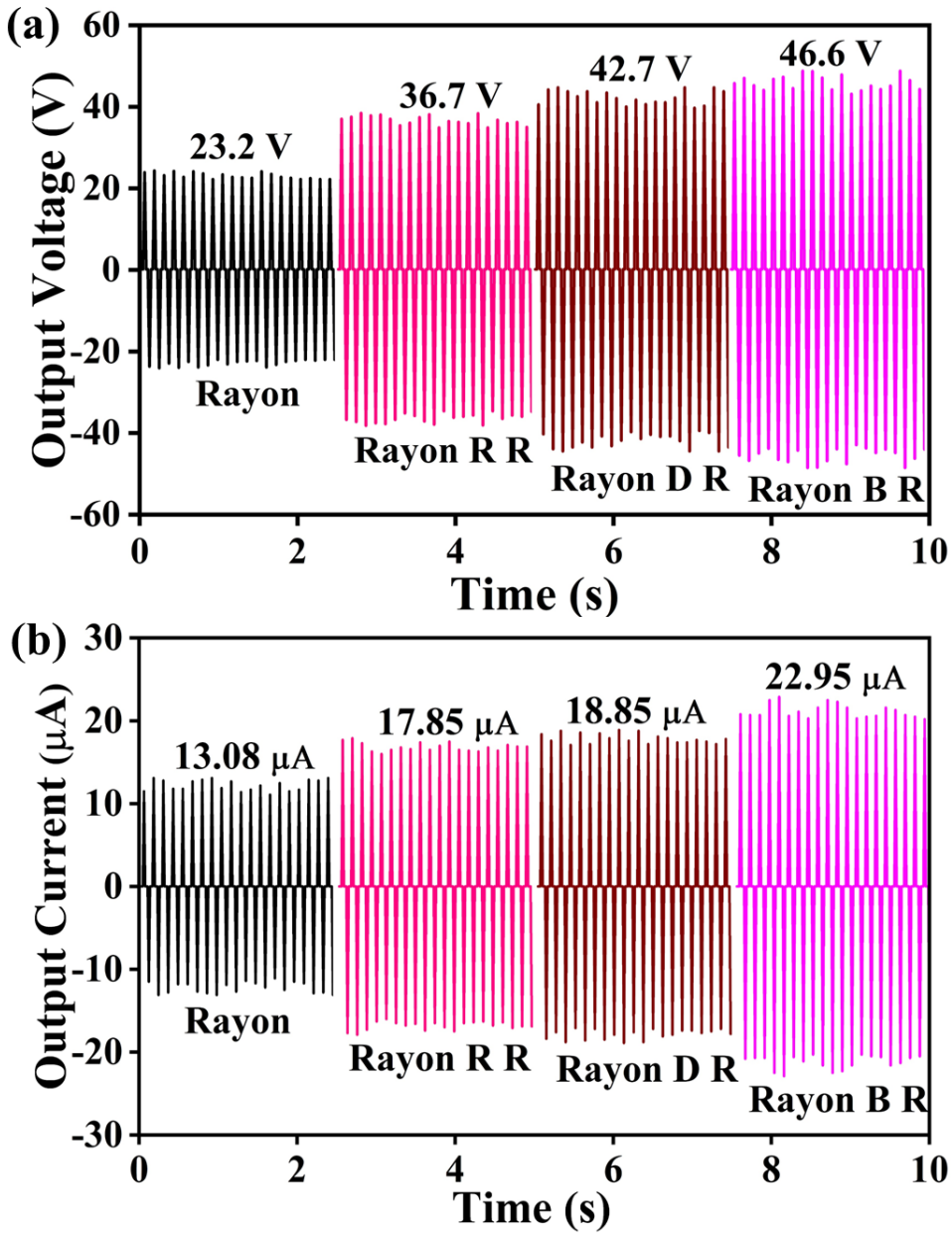

Figure 81 The electrical output performance including (a) V_{OC} and (b) I_{SC} of rayon fabric and rayon fabric with red dyes

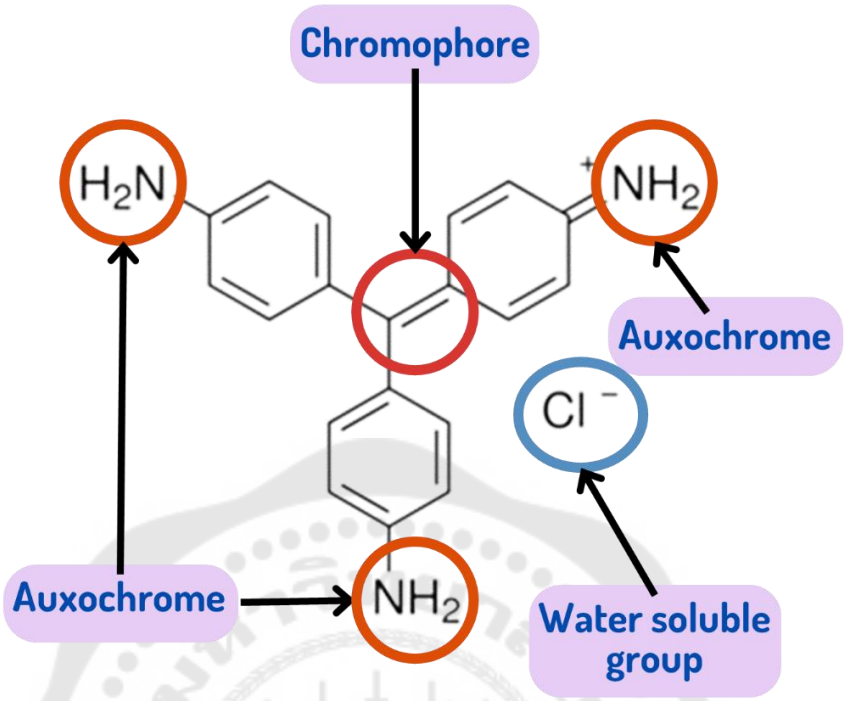

Figure 82 Molecule structure of Basic red dyes

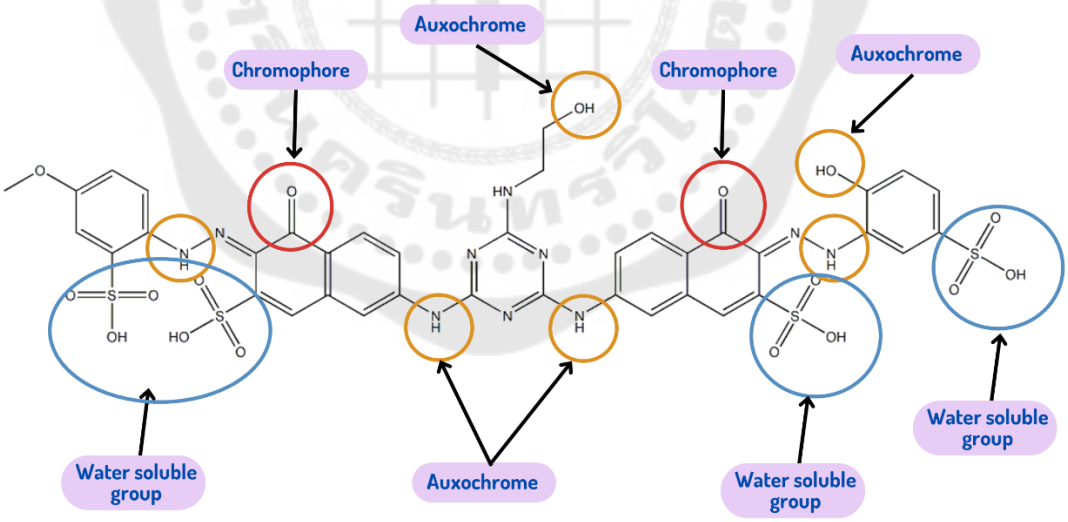

Figure 83 Molecule structure of Direct red dyes

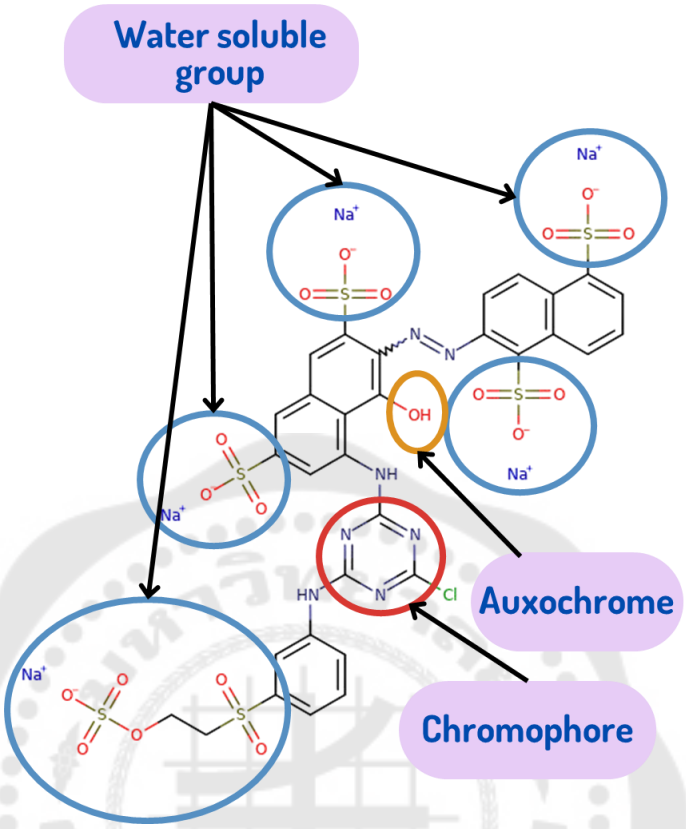

Figure 84 Molecule structure of Reactive red dyes

The maximum output power (P_{max}) of rayon fabrics and dyed rayon fabric with the red color from reactive dye, direct dye, and basic dye was checked under the resistivity 100 Ω - 15 MΩ. The output power depends on the amount of current flowing and the electrical output. The output power is a relationship that follows Ohm's Law, V=IR. The output voltage increases with the external load resistance from 100 Ω to 15 MΩ, and the output current decreases until the external load resistance reaches 15 MΩ, as in Figure 85. Therefore, the pristine rayon fabric exhibits P_{MAX} of 53 μW at a resistance of 1 MΩ, as depicted in Figure 85a. Figure 85b shows the dependence of the output power of rayon fabric with reactive red dye (R-RR) on the resistances. The I_{SC} decreases from 25 to 1 μA and the V_{OC} increases from 0.01 to 24.5 V as the load resistance increases from 100 Ω to 15 MΩ. The P_{MAX} of 83 μW could be achieved when the load resistance is 1 MΩ. In the same load resistance, the P_{MAX} of rayon fabric with

direct red dye (R-DR) increases to 102 μW, as in Figure 85c. Moreover, the rayon fabric with basic red dye (R-BR) has a maximum resistance of 1 MΩ with a P_{MAX} is 110 μW as shown in Figure 85d. The R-BR reveals a higher power than the other rayon fabric. The results show that the power output of all rayon fabrics tended according to the external load resistance. In addition, all output power result of dyed rayon fabric is consistent and in the same trends as the electrical output results. Table 14 shows other research on the output power of cellulose-based fabric. According to rayon fabric has the highest surface area and flexibility, it is compatible with the human body and its electrical output can be controlled by dyeing. Therefore, rayon fabric based TENG can be used in various electrical systems without requiring a lot of complicated circuits to function.

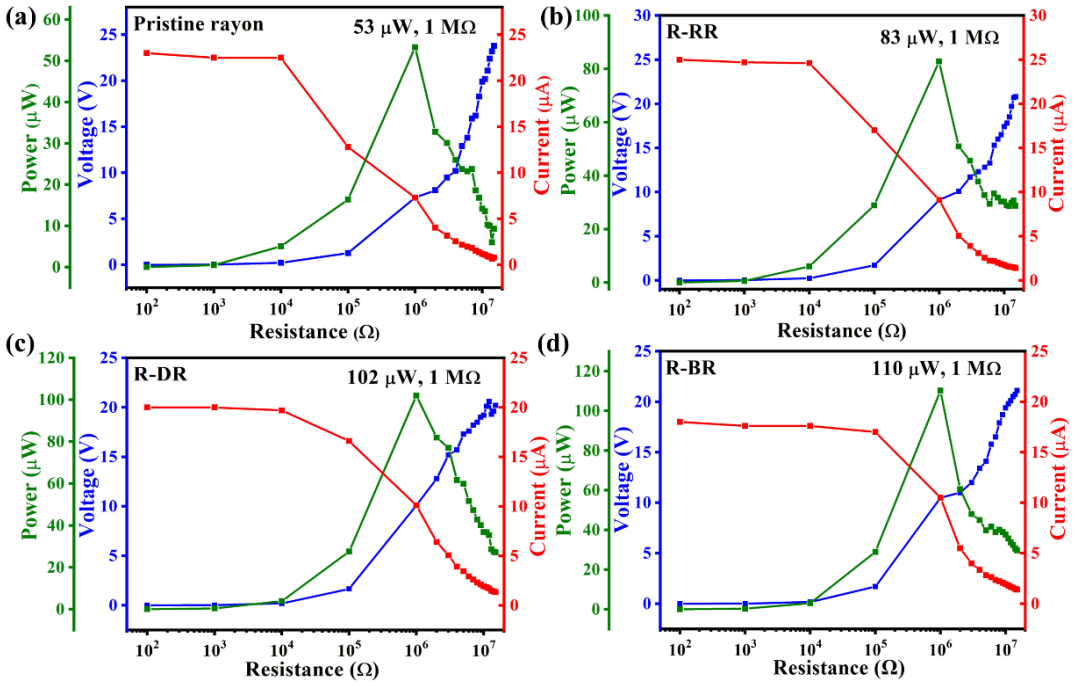

Figure 85 Output power of rayon fabric-based TENG, including (a) pristine rayon, (b) R-RR, (c) R-DR, and (d) R-BR fabric

Table 13 Comparison of the output power of cellulose-based fabric TENG in this work with literature

Positive materials	Negative materials	Working mode	Output power (W)	Reference
Cotton fabric	PTFE	CS	2.64 mW	(89)
Cotton fabric	PTFE	CS	2.26 W/m^2	(90)
Cotton fabric	PTFE	CS	0.66 mW/cm^2	(89)
Cotton fabric	FEP	CS	1.89 mW	(91)
Cotton fabric	Silicone rubber	CS	225 mW/m^2	(92)
Cotton/CO	PTFE	CS	13.5 W/m^2	(93)
Cotton fabric	PP tape	CS	0.90 μW/cm^2	(94)
Rayon BR fabric	PTFE	CS	110 μW	This work

4.5.5 The electrical output performance of dyed rayon fabric based TENG with reactive dyes.

Figure 86 shows the electrical output of pristine rayon fabric and dyed rayon fabric based TENG with seven colors of reactive dyes. The V_{OC} and I_{SC} of pristine rayon fabric is found to be 23.2 V and 13.08 μA. After dyeing rayon fabric with reactive dyes blue, green, yellow, orange, brown, and red, the electrical output signal was higher for all colors. The V_{OC} are 65.6 V, 61.4 V, 52.6 V, 51.3 V, 49.8 V, and 36.7 V, respectively (Figure 86a). The Voc was sorted by the positive charge on dyed fabric from most to least positive charge. Meanwhile, the I_{SC} at 29.9 μA, 29.4 μA, 28 μA, 25.3 μA, 25.2 μA, and 17.9 μA, respectively (Figure 86b). The results show that rayon fabric with reactive blue illustrated the highest electrical output of 65.6 V and 29.9 μA because the reactive blue molecular structure consists of a copper (Cu) atom with a low EN value (Figure 87). It also has an amine group that can react with the hydroxyl group of the fabric to provide high ability of electron donation. Therefore, rayon dyed with reactive blue has a good ability to donate electrons. Dyed rayon fabric with reactive blue is improved to have a

higher positive charge. When fabric is contacted with a high negative charge of PTFE, it results in more electron induction from the material surface to the electrode and higher electrical output. The results show that the functional groups have a significant effect on the electrical output of rayon fabric. This is because pristine rayon fabric has the main functional group of hydroxyls (-OH). Upon dyeing with reactive dyes containing amine (-NH_2) functional groups, the -NH_2 group can donate more electrons than the -OH group. Therefore, the electrical effect of the rayon fabric dyed with reactive dyes increased to a positive value. While sulfonate (-SO_3) and chlorine (Cl^-) groups are present in the dye structure, they still have less influence because they are less reactive groups. Moreover, each dye structure contains different molecules or functional groups that interact with fibers, causing a variety of electrical outputs.

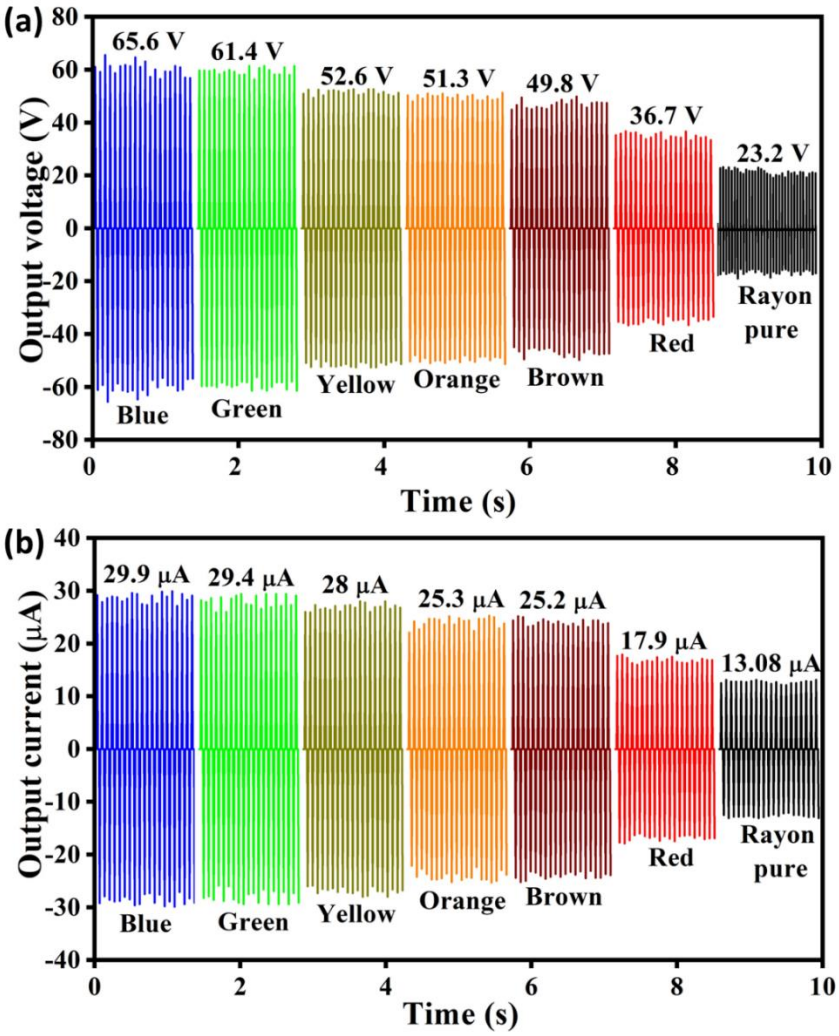

Figure 86 Electrical output performance of rayon fabric dyeing with reactive dyes, (a) V_{OC}, (b) I_{SC} of rayon fabric dyeing with reactive dyes

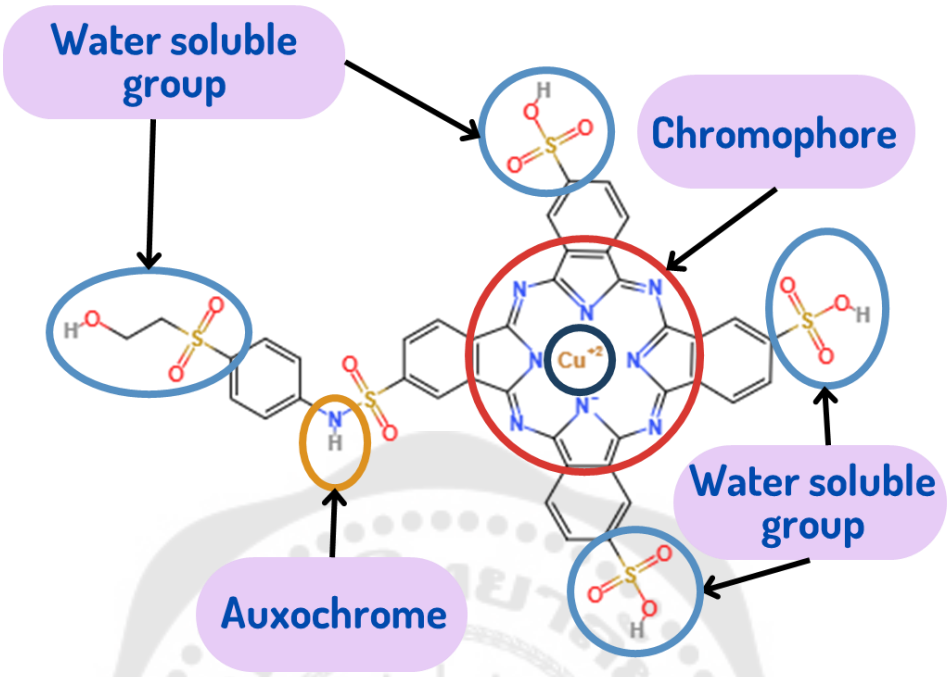

Figure 87 Molecule structure of Reactive blue dyes

4.5.6 The electrical output performance of dyed rayon fabric based TENG with direct dyes.

In this work, the authors also used six different colors of direct dyes for dyeing with rayon and study their electrical output. The electrical output of pristine rayon fabric and dyed rayon fabric based TENG with direct dyes is shown in Figure 88. It can be seen in Figure 88 that the trend of V_{OC} and I_{SC} after dyeing is similar to dyeing with reactive dyes. In the case with dyeing by direct dyed, the results of V_{OC} and I_{SC} were also found to be higher than that of pristine rayon. After dyeing rayon fabric with direct blue, green, yellow, orange, and red dyes, the V_{OC} was higher for all colors with 58.6 V, 55.4 V, 53.3 V, 42.7 V, and 41.7 V, respectively. Meanwhile, the I_{SC} of dyed rayon fabric are 23.8 μA, 22.7 μA, 20.9 μA, 20.5 μA, and 18.9 μA for blue, green, yellow, orange, and red dyes, respectively (Figure 88b). Dyed rayon fabric with direct yellow showed the highest electrical outputs at 58.6 V and 23.8 μA. The result for having the highest output signal from the yellow can be explained by chemical structure of the dyes as shown in Figure 89. As mentioned earlier in the last part, containing the hydroxyl and

amino group together in the fabric results in higher ability to give the electron to provide many positive charges on its surface. Then, it can generate more electrical output than that of using pristine as charge-generating layer. Moreover, by considering the molecular structure of the direct yellow dye, its molecule consists of the azo (-N=N-) as a chromophore functional group. Even though the direct dyes contain the same auxochrome group, having -N=N- as secondary functional group also affect to the output efficiency by improving electron donating ability. On the other hand, sulfonate groups present in the dye structure have less influence as they are not the reactive groups and dissolve in water during dyeing. However, the chemical structure of other color of direct dyes contains a carbonyl (-C=O) group as an element that shows lower ability of electron donating as compared to the -N=N-. Therefore, even dyeing with direct dyes of orange, red, blue, and green can enhance the electrical output of pristine rayon but still provide less electrical output than that of dyeing with yellow color.

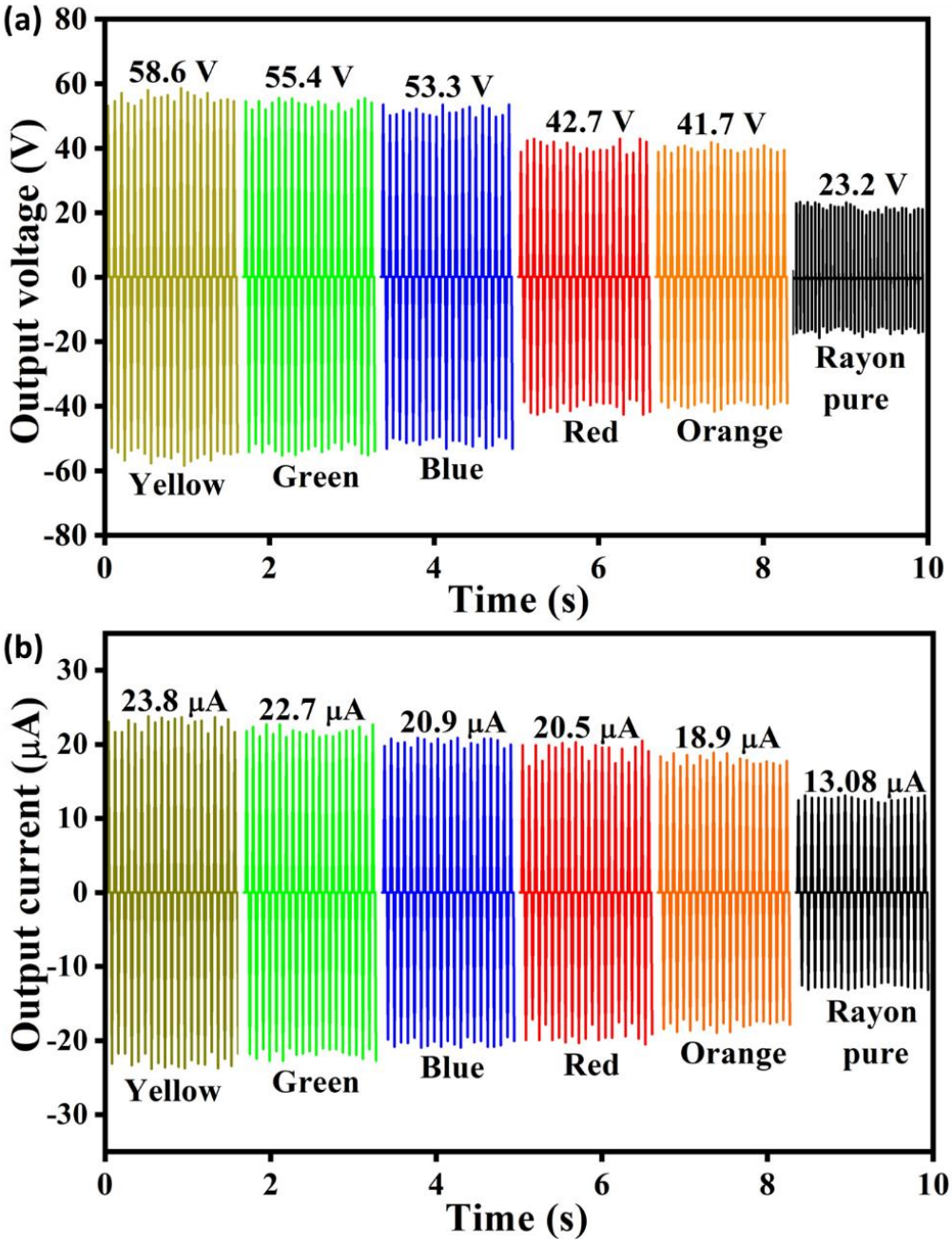

Figure 88 Electrical output performance of rayon fabric dyeing with direct dyes (a) V_{OC}, (b) *and* I_{SC} of rayon fabric dyeing with direct dyes

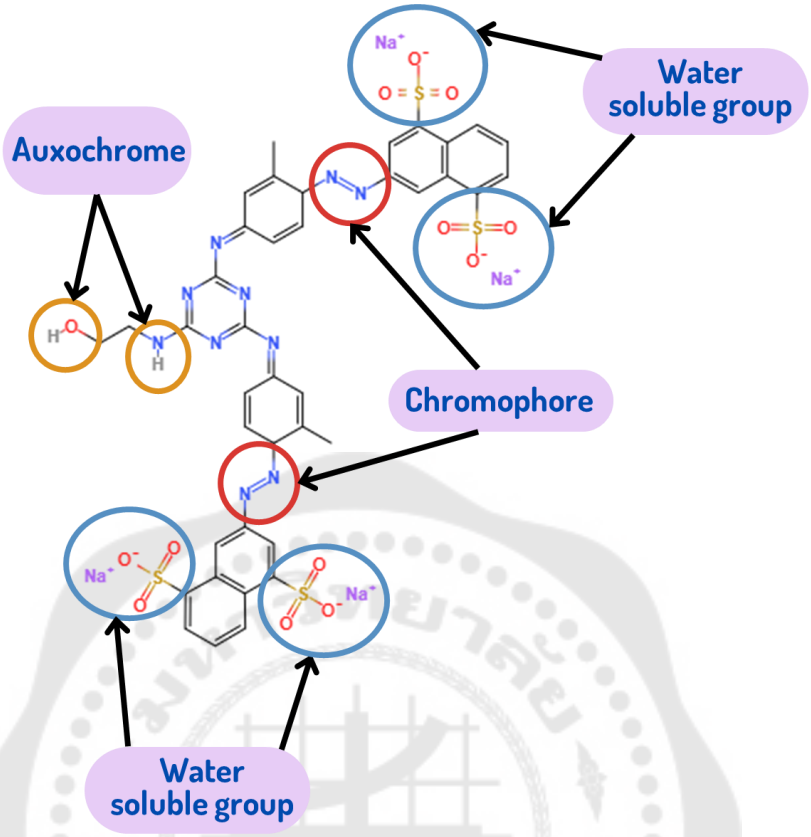

Figure 89 Molecule structure of direct yellow dyes

4.5.7 Triboelectric series of cellulose-based fabrics with the inorganic dyes

The results of dyeing four types of cellulose fabrics with three types of inorganic dyes. It shows that all fabrics can be dyed with all colors. The dyed cellulose-based fabric has different shades and different electrical outputs of TENG according to the type and color of the dye. Therefore, it can be concluded that the dye could control the triboelectric charge of cellulose-based fabric. All electrical output results can be generated into a triboelectric series of fabrics dyeing with 12 inorganic dyes, including 6 reactive dyes, 5 direct dyes, and 1 basic dye. The dyed fabric triboelectric series arranges the data from most to least positive dyes as shown in Figures 90-93. The triboelectric series of dyed cotton fabric in Figure 90 shows that all dyes created more positive charges on cotton fabric, especially reactive blue dye. The color that makes the cotton have the smallest positive charges is direct green at the below triboelectric series. Meanwhile, the triboelectric series of dyed linen fabric shows reactive blue with

the most positive charges and direct yellow with the least positive charges on linen fabric (Figure 91). The dyed rayon fabric triboelectric series in Figure 92 shows that the reactive blue shows the most positive charge while rayon fabric with a reactive red showed the least positive charge. Finally, the triboelectric series of Tencel fabric indicates the tendency of different dyes to become electrically charged when they dye on the fabric. According to Figure 93, dyed Tencel fabric exhibits a range of positive charges, with reactive yellow dye having the most positive charge and basic red dye showing the least positive charge. This triboelectric series information will help select the material in various dyes for the TENG device.

Figure 90 Triboelectric series of cotton fabric with the inorganic dyes

Figure 91 Triboelectric series of linen fabric with the inorganic dyes

Figure 92 Triboelectric series of rayon fabric with the inorganic dyes

Figure 93 Triboelectric series of rayon fabric with the inorganic dyes

The dyed cellulose-based fabrics were arranged in a triboelectric series, as illustrated in Figure 94. Basically, this study aims to highlight the significance of functional groups in dyes that can control the electrical properties of cellulose-based fabrics to be more positive and negative by dyeing. However, the experimental results demonstrated that the electrical output value of the fabrics increased after dyeing with inorganic dyes by meaning of the increasing ability to lose electrons. It can be seen from the results that the cellulose-based fabrics cannot be changed to have ability for accepting electron as expected. This phenomenon explanation arises due to the

presence of amine groups in the functional groups or auxochrome of all dyes exhibits high reactivity with fibers and can donate electrons to provide the high positive charges on pristine surface. The auxochrome is the most important role affecting to electrical properties and electrical output of fabrics. Meanwhile, having other functional groups does not affect much. The chromophore group is secondary effective parameter and sulfonate group does not affect by meaning of its dissolving in water during dyeing. However, the knowledge of this work can provide the triboelectric series arrangement of all dyed fabrics providing potential as a guideline for selecting materials for TENG device.

Figure 94 Triboelectric series of cellulose-based fabric with the inorganic dyes

4.6 The electrical output performance of rayon fabric based TENG with reactive red dyes under single-electrode mode.

In inventing applications for use in textiles, skin touching is important. Therefore, it is necessary to create a rayon fabric based TENG device to further tests in

a single-electrode mode. Rayon fabric and rayon fabric with reactive red dye (rayon RR) are ironed to the electrodes and the wires are connected to the electrodes. Testing in single-electrode mode by touching the workpiece with hand. Figure 95a, 95b shows the V_{OC} and I_{SC} of pristine rayon fabric at 0.73 V and 6.62 μA, respectively. Rayon RR fabric showed V_{OC} of 0.81 V and I_{SC} of 7.62 μA. These values correspond to the electrical output measured by the vertical-contact separation mode.

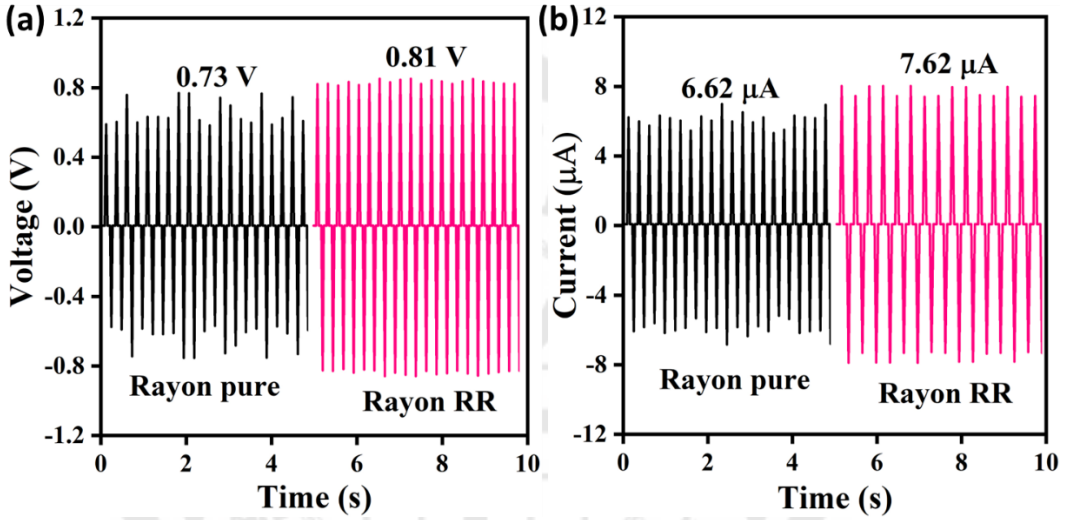

Figure 95 Electrical output of rayon fabric dyeing with reactive red dye under single-electrode mode, (a) V_{OC}, (b) I_{SC} of rayon fabric dyeing with reactive red dye

4.7 Pillow sensor TENG application for head position during sleeping

4.7.1 Fabrication of pillow sensor based TENG from rayon fabric with reactive red dye (rayon RR).

The analysis of electrical performance data of rayon fabric and rayon RR fabric by vertical contact-separation mode and single electrode mode, it can be concluded that the electrical output of rayon fabric with reactive red dye is suitable for use as a pillow sensor TENG to monitor the head position during sleep. To demonstrate the practical usage of the pillow sensor TENG as a triboelectric sensor, a flexible pillow-based triboelectric sensor was fabricated. Eight cotton/CNT electrodes (area: 5*10 cm^2) were designed as a working electrode. Then cotton/CNT electrodes were ironed

together with the eight positions on a pillowcase from rayon RR fabric. Electrical wires were connected to each sensor and Kapton tape was stuck to protect the electrical wire from drop off the triboelectric sensor. Eventually, a 40 * 20 cm^2 pillow sensor TENG was obtained. The completed flexible pillow sensor TENG is shown in Figure 96. The signals of all 8 sensors are connected through the electrical wire to the analog multiplexer, and the data are obtained by a multichannel data acquisition system (Figure 97). Then, the ADC was selected as the sensor channel that detects and changes the signal from analog to digital form. The digital data from ADC was sent through the MCU to be saved in a memory card. The data in the memory card was saved in the data logger and can be analyzed as a signal of the P-TES by the Arduino program.

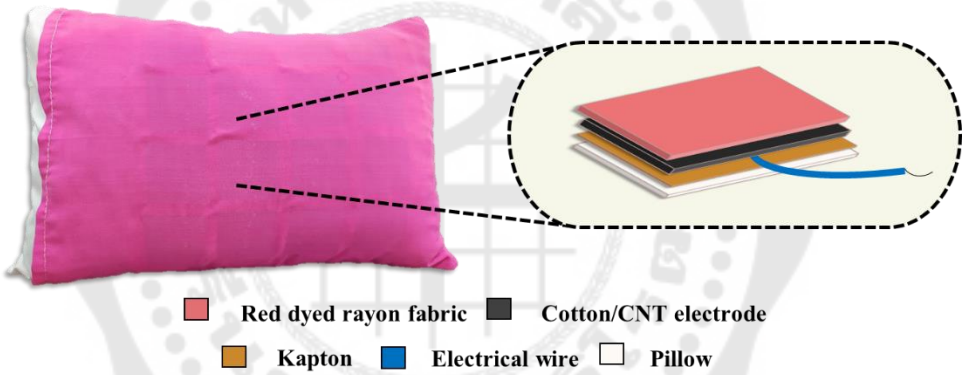

Figure 96 Photograph of pillow sensor based TENG form rayon fabric with reactive dye

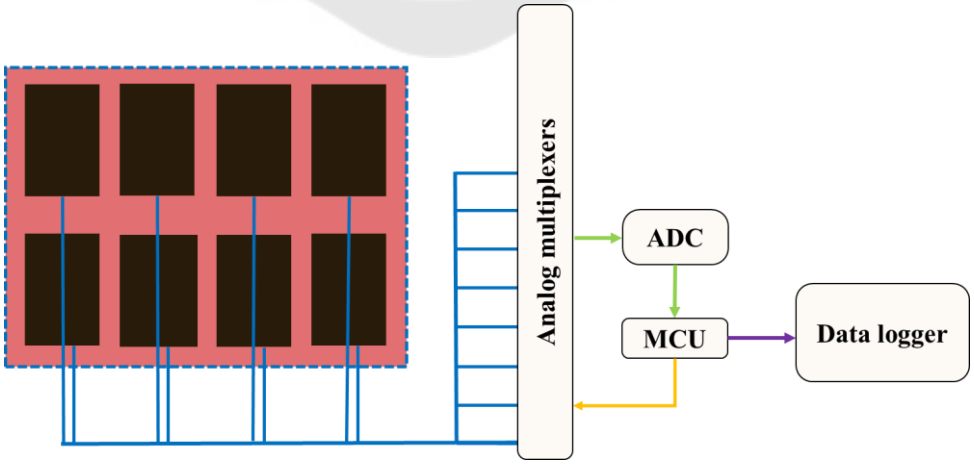

Figure 97 Diagram of pillow sensor based TENG on electronic circuit board

4.7.2 The electrical output performance of rayon fabric based TENG with reactive red dye under laundering stability.

The washability of rayon fabric with reactive red dye (rayon RR fabric) was evaluated by laundering the fabrics in repeated standard washing cycles by following the standard test method for textiles (TIS121-3) (66). The color after washing can be seen in digital photographs according to Figure 98. The result shows that the color of rayon RR fabric dropped dramatically after one wash and after 5, 10, and 20 cycles of washing, the color of rayon RR fabric reached a significantly similar color.

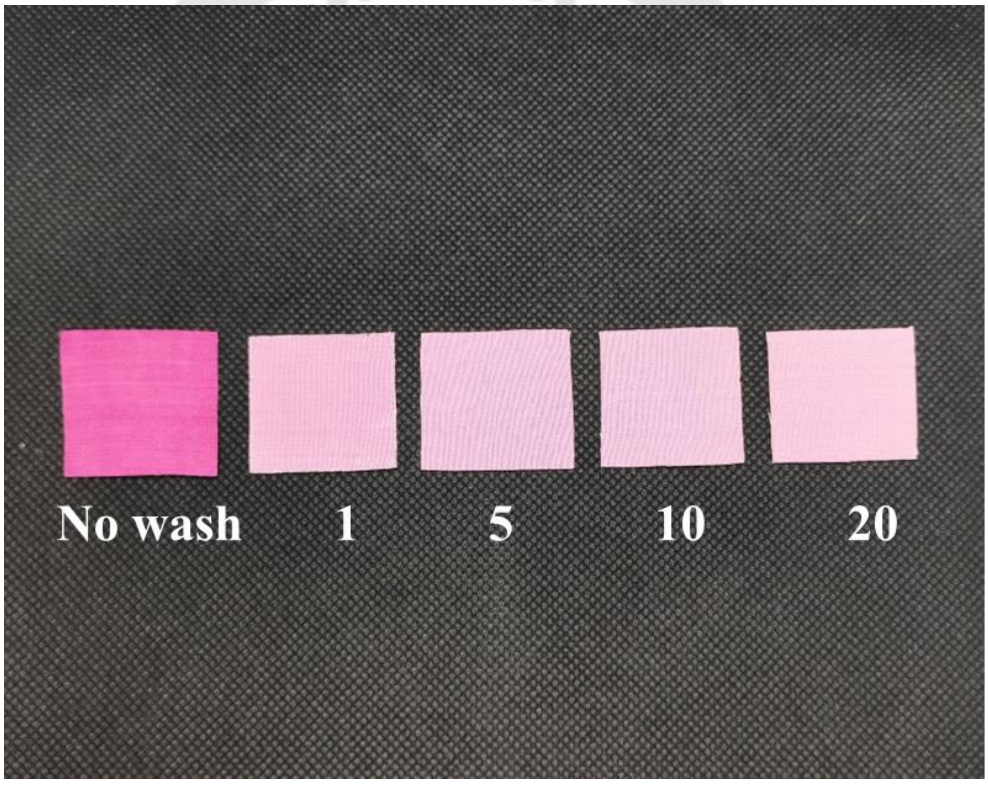

Figure 98 Photograph of rayon fabric with reactive red dye under wash fastness 20 cycles

Figure 99 shows the electrical output of the washability of rayon RR fabric after one wash and after 5, 10, and 20 cycles. The result shows that the electrical output of rayon RR fabric decreased obviously between no wash and 1 of the washing cycle.

While the electrical output was maintained at a similar level in 5, 10, and 20 of the washing cycles. No wash of rayon RR fabric and rayon RR fabric after 1, 5, 10, and 20 of the washing cycles show the decrease of electrical output from 46.6 V to 26.6 V and 22.95 μA to 14.97 μA, respectively, after 1 of the washing cycle. The electrical output decreased to 23.5 V and 12.71 μA in 20 of the washing cycle. In another research by Pei-Yong Feng and co-workers enhanced the triboelectric performance of commercial velvet fabric by enriching the fiber surface with a polyamidation reaction. Considering the washing of fabric based TENG in practical usage, the TENG was washed in warm water under a constant stirring rate of 100 rpm for up to 24 h. It was found that the output voltage and current were decreased from 119 to 109 V and 13 to 12 μA after washing for 5 h. When the washing time was increased from 12 to 24 h, the output voltage and current were maintained constant at 103 V, 10 μA and could be maintained when the washing time exceeded 12 h. Noticeably, the TENG based on modified velvet fabric could maintain a stable output after washing for some time (95). The electrical output of the washability of rayon RR fabric shows the same trend, in decreasing electrical output of the rayon RR fabric that has resulted from the peel-off of the dye in washing cycles.

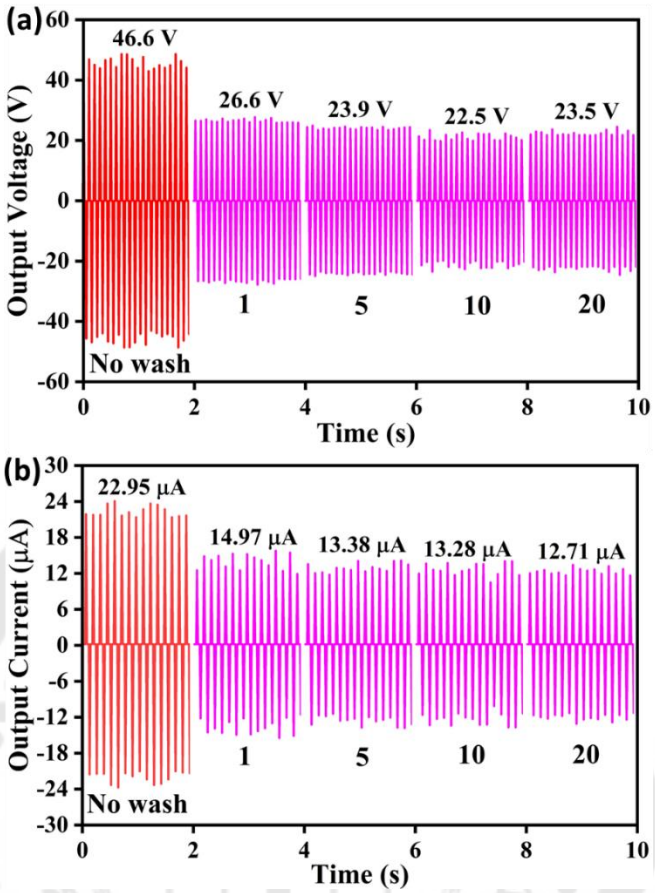

Figure 99 Electrical output of rayon fabric dyeing with reactive red dye, (a) output voltage, (b) output current of rayon fabric under wash fastness 20 cycles

4.7.3 Electrical output of pillow sensor TENG and analysis of head position during sleeping.

The pillow sensor TENG was used to test the head position during sleep in humans by using the dummy to test the head position. Figure 100 shows the head of the dummy in different positions on the sensor pillow: left-lateral position (Figure 100a), supine position (Figure 100b), and right-lateral position (Figure 100c). When placing the head of the dummy in the supine position in the middle of the pillow sensor TENG, which corresponds to positions c, d, and e (3, 4, 5, 6) in Figure 101a. Resulting in the signal from the dummy was detected at the positions of the pillow sensor TENG. The voltage signal is recorded at different sensor positions, with corresponding pressure mappings. The voltage of channel 1,2 was decreased, and the voltage of channels 3, 4, 5, and 6

(light blue, green, and yellow) increased. The signal shows higher electrical values than other sensor regions about 1.8-2.4 V, as shown in Figure 101b. When changing the head position to right lateral, which corresponds to the g, f position (5, 6, 7, 8), the voltage only channels orange, and red was reach increased. The signal from the pillow sensor TENG on the right lateral is higher than the other sensor positions, about 0.6 V. This test confirms that the pillow sensor TENG from rayon fabric with reactive red dye can emit electrical signals and can detect signals from the head position.

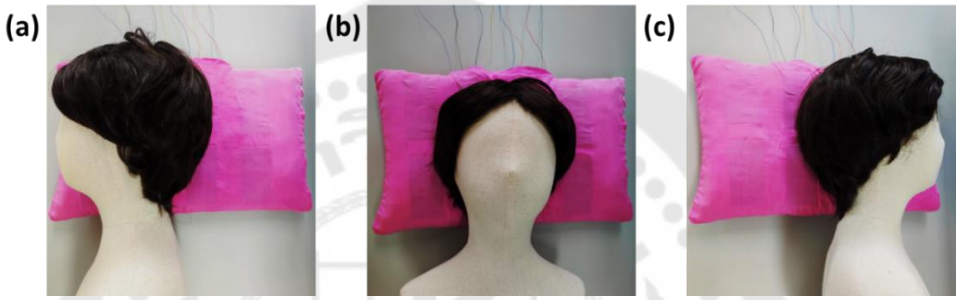

Figure 100 Head position of dummy on pillow sensor TENG, (a) left lateral position, (b) supine position, (c) right lateral position

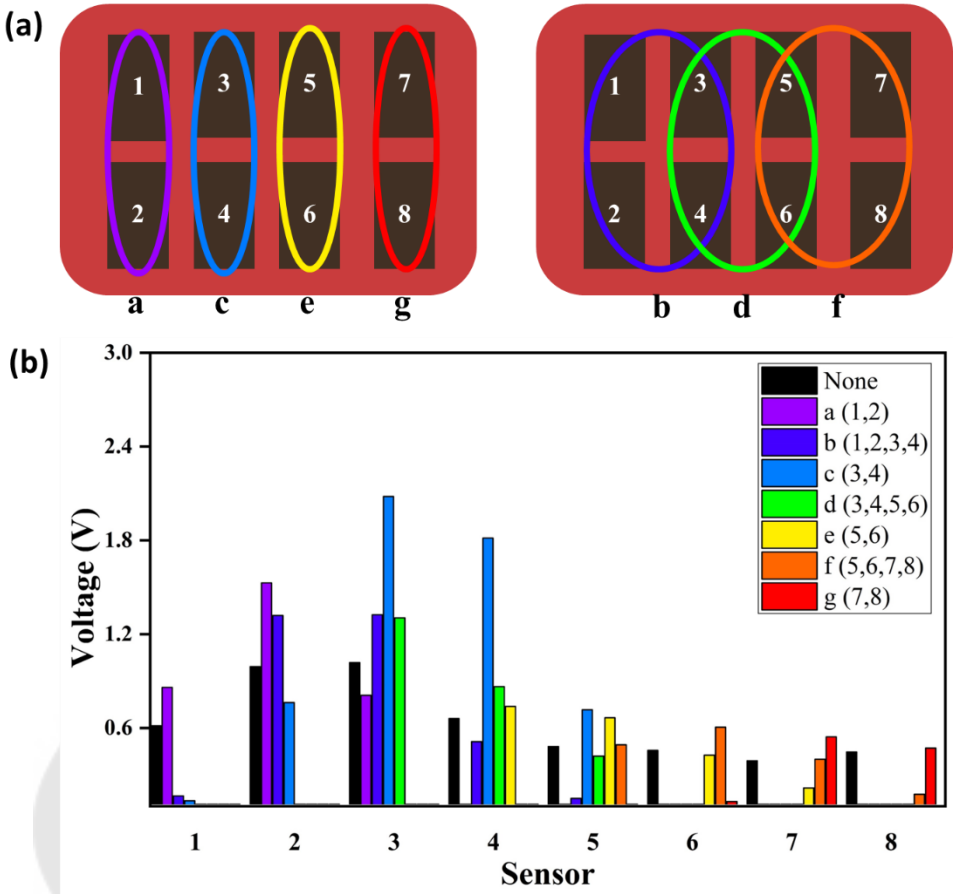

Figure 101 Electrical output of pillow sensor TENG, (a) position of dummy on pillow sensor TENG, (b) output voltage of pillow sensor TENG

The above results demonstrate that the pillow sensor TENG has the potential to be applied to real-time tactile sensing and motion monitoring of external objects, such as head monitoring. Figure 102a shows a supine position, a head facing either straight up or tilted slightly to left or right with <45° from vertically, or a head facing straight up and not tilted laterally. The pillow sensor showed the weight pressure gradient of the head at the correct supine position (i), most of the weight of the head is centered on the pillow. The incorrect supine position, head facing either straight up with more or less than 45° from vertically (ii, iii). The weight pressure gradient of the head indicates that the weight of the head is mostly at the bottom of the pillow. Figure 102b shows a left/right lateral, laying on either side and head facing the direction of their shoulders

and/or torso angled at 90º with the bed. The weight pressure gradient of the head is at the correct lateral position (i), most of the weight on the pillow is sided in the same direction as the head. The incorrect lateral position, head facing the direction of their shoulders and/or torso angled with more or less than 90º (ii, iii). The weight pressure gradient of the head indicates that the weight is sided in the same direction as the head but has a wider distribution of weight on the pillow. This demonstration shows that the pillow sensor TENG can provide a decent working range and high sensitivity for practical applications in real circumstances which can be used as key information for evaluating sleep quality.

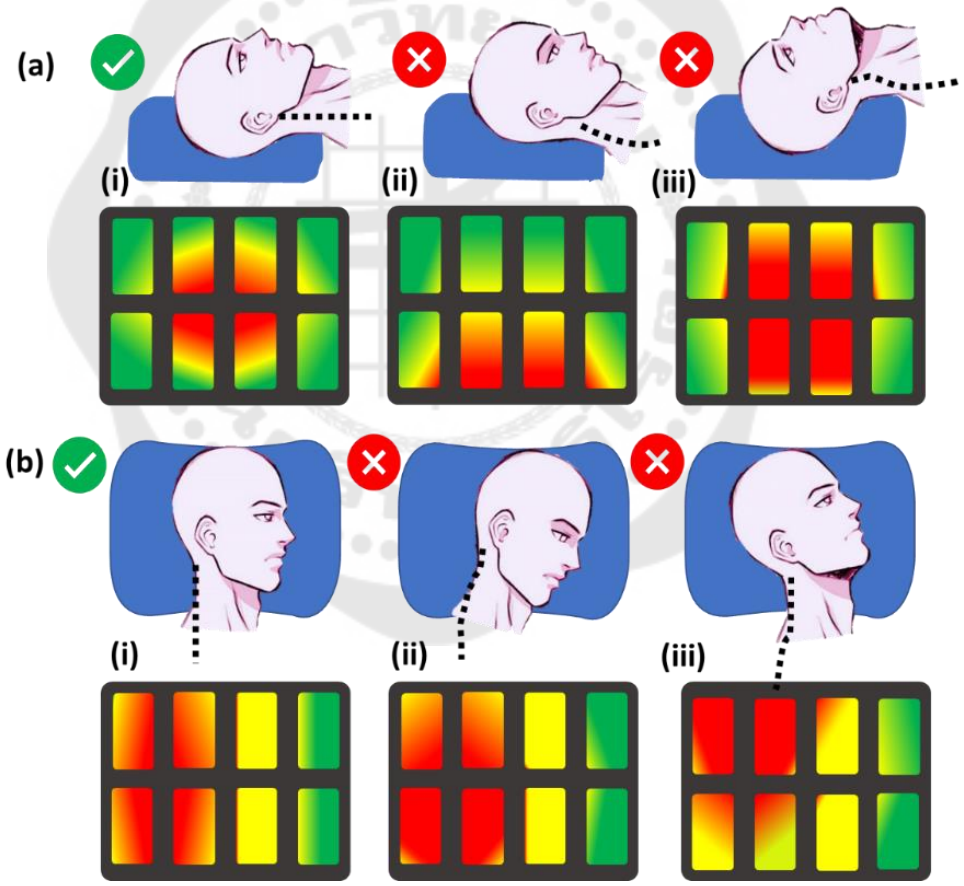

Figure 102 Position of dummy on pillow sensor TENG with (a) supine position and (b) lateral position

CHAPTER 5
CONCLUSIONS

Four types of cellulose-based fabrics were studied, including cotton, linen, rayon, and tencel fabrics. All the fabric contains functional groups of hydroxyl groups, which is the main functional group of cellulose. In addition, the dyeing cellulose-based fabrics were studied with 3 types of dyes: reactive dyes, direct dyes, and basic dyes. In all dyes, the main functional groups are amines, which are functional groups that can donate electrons to improve the functional group of cellulose-based fabrics. The characteristics of cellulose-based fabrics before and after dyeing were studied. The color fastness on cellulose-based fabrics was tested with a spectrophotometer. Morphology was studied by SEM and functional groups were studied by ATR-IR. The cellulose-based fabric was fabricated as a contact layer for the TENG device and studied the effect of the dye on the electrical output. Finally, cellulose-based fabric TENG could be used as pillowcase sensor to detect head position during sleep.

5.1 The result of the studying identity of cellulose-based fabric before dyeing

The results from the morphological characterization of the four cellulose-based fabrics by SEM showed long fiber strength densely stacked and porous all types of cellulose fabrics. The cellulose-based fabrics were different weaving structures. Plain weaving for cotton, linen, and rayon fabrics, and Tencel fabric is twill weaving. In addition, the characteristics and size of the fibers were significantly different. The rayon fibers have the smallest fiber with an average diameter of 18.8 ± 6 μm. The results of the study of the functional groups of the four cellulose fabrics before dyeing with FTIR in the wavenumber range from 4000-700 cm^{-1}. The absorption peak of all cellulose-based fabrics before dyeing was observed at 3335 cm^{-1}, consistent with the stretching vibration of the O-H bond (Hydroxyl group), which is the main functional group of cellulose.

5.2 The results of the study of cellulose-based fabric dyeing with 3 types of inorganic dyes

This research succeeds in dyeing cellulose-based fabrics with 3 types of dyes. Starting from preparing the fabric by weighing the fabric, desizing the fabric,

scouring the fabric, and dyeing the fabric. The dyeing process uses 6 reactive dyes, namely red, blue, yellow, orange, brown, and yellow. 5 direct dyes, namely blue, green, yellow, orange, and red, and dyes. 1 basic dye, namely red.

5.3 The result of the studying identity of cellulose-based fabric after dyeing

The result of cellulose-based fabric after dyeing showed that the functional peaks of the dye were not visible. When expanding the peak to the wavenumber range from 1800-1500 cm^{-1}, there is a shift to the left of the dyed cellulose-based fabric. Confirms that the cellulose-based fabric was dyed but the amount of dye concentration is too low. The peak of the dye is not clearly expressed and is covered by the peak of the cellulose-based fabric.

5.4 The results of the study and fabrication of the TENG device from cellulose-based fabric with comparing electrodes

In this research, two structures of cellulose-based fabric TENG were successfully fabricated by comparing the type of electrode. A vertical contact separation mode with dyed cellulose-based fabric and PTFE as the contact layer materials with the electrodes being an adhesive fabric coated with CNT. A single electrode mode consists of electrodes from CNT-coated adhesive fabric that is ironed onto cellulose-based fabric. Cellulose-based TENG with a single electrode structure was suitable for further application.

5.5 The study of the effect of dyes on the electrical output of TENG devices from cellulose-based fabric

Rayon fabric with basic red dye shows the best electrical output with the output voltage, output current, and output power at 46.6 V, 22.95 μA, and 110 μW, respectively. The output power is 2 times higher than that of undyed rayon fabric due to the structure of basic red dye having groups of amines with low EN values. Make it positively charged, which from the Inductive Effect phenomenon makes it capable of giving electrons. Resulting in the rayon dyed with basic red being enhanced to be more positively charged. When contact with a high negative charge of PTFE. This results in a higher difference ability to donate and gain electrons of the two contact layers. So, it can

be concluded that the functional group of the dye affects and is important in controlling the electrical output of rayon fabrics.

5.6 The result of the pillow sensor TENG application for detecting head position during sleep

In this research, rayon fabric based TENG can be applied. The fabrication is a pillow sensor TENG to detect the head position during sleep. The pillow sensor TENG used has a single-electrode structure because it is convenient to use and can be easily designed. The circuit of this application will consist of a triboelectric sensor from rayon fabric with basic red dye. Analog multiplexers are used to convert or amplify the signal received from sensors to an ADC and the signal was sent to an MCU. In this process, MCU will process the signal from the ADC to direct it to a memory card. The data in the memory card was saved in the data logger and can be analyzed signal on the Arduino program. The pillow sensor TENG was tested by using the dummy to change the position of the head in different positions on the sensor.

REFERENCES

Appendix

Journal of Metals, Materials and Minerals, 33(3), 1673, 2023

Cellulose-based fabrics triboelectric nanogenerator: Effect of fabric microstructure on its electrical output

Rawiwan KHWANMING[1], Satana PONGAMPAI[2], Naratip VITTAYAKORN[2] and Thitirat CHAROONSUK[1,*]

[1] *Department of Materials Science, Faculty of Science, Srinakharinwirot University, Sukhumvit 23, 10110, Watthana, Bangkok, Thailand.*
[2] *Advanced Material Research Unit, School of Science, King Mongkut's Institute of Technology Ladkrabang, 10520, Bangkok, Thailand.*

***Corresponding author e-mail:** thitiratc@g.swu.ac.th

Received date:
10 March 2023
Revised date
25 April 2023
Accepted date:
28 June 2023

Keywords:
Cellulose fabrics;
Fabric structure;
Triboelectric nanogenerator;
Textiles

Abstract

At present, fabric-based triboelectric nanogenerator (TENG) has been paid attention and developed for self-power generation systems with wearability for E-textiles, especially cotton. However, there are many commercial cellulose-based fabrics with different fiber characteristics and fabric structures that gain possibility to effect on TENG performance and has been underreported. This work presents the fabrication of the textile TENG by using four types of commercial cellulose-based fabrics as friction layer and compare the electrical output efficiency relating their molecular structure, fabric structure and surface morphology characteristics. As shown by the electrical output, though all fabrics can generate electricity for TENG device, nevertheless, the output signal is different because of their different total surface area of the fabric, affecting by different microstructure. The rayon fabric contains the smallest size fiber with highest surface area at the same woven structure. The obtained output voltage (V_{OC}) and current (Isc) of ~23 V and ~13 μA are ~1.8 times higher than most studied cotton fabric. This research demonstrated the importance of the microstructure and surface area of the fabrics that significantly affect TENG properties. The investigation in this work will useful and knowledgeable to select fabric materials before improving and using them for energy harvesting devices.

Cellulose-based fabrics triboelectric nanogenerator: Effect of fabric microstructure on its electrical output

1. Çelikel D. Smart E-Textile Materials. 2020.

2. Liu H, Lin X, Zhang S, Huan Y, Huang S, Cheng X. Enhanced performance of piezoelectric composite nanogenerator based on gradient porous PZT ceramic structure for energy harvesting. Journal of Materials Chemistry A. 2020;8(37):19631-40.

3. Lain MJ, Kendrick E. Understanding the limitations of lithium ion batteries at high rates. Journal of Power Sources. 2021;493:229690.

4. Tian R, Park S-H, King PJ, Cunningham G, Coelho J, Nicolosi V, et al. Quantifying the factors limiting rate performance in battery electrodes. Nature Communications. 2019;10(1):1933.

5. PavloviĆ B, IveziĆ D, ŽivkoviĆ M. A multi-criteria approach for assessing the potential of renewable energy sources for electricity generation: Case Serbia. Energy Reports. 2021(7):8624-32.

6. Okonkwo EC, Wole-Osho I, Bamisile O, Abid M, Al-Ansari T. Grid integration of renewable energy in Qatar: Potentials and limitations. Energy. 2021;235:121310.

7. Hansen JP, Narbel PA, Aksnes DL. Limits to growth in the renewable energy sector. Renewable and Sustainable Energy Reviews. 2017;70:769-74.

8. Behabtu HA, Messagie M, Coosemans T, Berecibar M, Anlay Fante K, Kebede AA, et al. A Review of Energy Storage Technologies' Application Potentials in Renewable Energy Sources Grid Integration. Sustainability. 2020;12(24):10511.

9. Fan F-R, Tian Z-Q, Lin Wang Z. Flexible triboelectric generator. Nano Energy. 2012;1(2):328-34.

10. Gunawardhana KRSD, Wanasekara ND, Dharmasena RDIG. Towards Truly Wearable Systems: Optimizing and Scaling Up Wearable Triboelectric Nanogenerators. iScience. 2020;23(8):101360.

11. Triboelectric Nanogenerators: A solution of the next energy [Internet]. Thaigovscholars. Available from: http://thaigovscholars.org/addon/PAPERS/154-167.pdf.

12. Yang C-R, Ko C-T, Chang S-F, Huang M-J. Study on fabric-based triboelectric nanogenerator using graphene oxide/porous PDMS as a compound friction layer. Nano Energy. 2022;92:106791.

13. Dzhardimalieva GI, Yadav BC, Lifintseva TyV, Uflyand IE. Polymer chemistry underpinning materials for triboelectric nanogenerators (TENGs): Recent trends. European Polymer Journal. 2021;142:110163.

14. Xiong J, Lin M-F, Wang J, Gaw SL, Parida K, Lee PS. Wearable All-Fabric-Based Triboelectric Generator for Water Energy Harvesting. Advanced Energy Materials. 2017;7(21):1701243.

15. Peng F, Liu D, Zhao W, Zheng G, Ji Y, Dai K, et al. Facile fabrication of triboelectric nanogenerator based on low-cost thermoplastic polymeric fabrics for large-area energy harvesting and self-powered sensing. Nano Energy. 2019;65:104068.

16. Niu Z, Cheng W, Cao M, Wang D, Wang Q, Han J, et al. Recent advances in cellulose-based flexible triboelectric nanogenerators. Nano Energy. 2021;87:106175.

17. Hsieh Y-L. Chemical structure and properties of cotton. 2007:3-34.

18. Vatankhah E, Tadayon M, Ramakrishna S. Boosted output performance of nanocellulose-based triboelectric nanogenerators via device engineering and surface functionalization. Carbohydrate Polymers. 2021;266:118120.

19. Yao C, Hernandez A, Yu Y, Cai Z, Wang X. Triboelectric nanogenerators and power-boards from cellulose nanofibrils and recycled materials. Nano Energy. 2016;30:103-8.

20. Felgueiras C, Azoia NG, Gonçalves C, Gama M, Dourado F. Trends on the Cellulose-Based Textiles: Raw Materials and Technologies. Frontiers in Bioengineering and Biotechnology. 2021;9.

21. Ansell MP, Mwaikambo LY. 2 - The structure of cotton and other plant fibres. In: Eichhorn SJ, Hearle JWS, Jaffe M, Kikutani T, editors. Handbook of Textile Fibre Structure. 2: Woodhead Publishing; 2009. p. 62-94.

22. Jeong J, Kwon J-H, Lim K, Biswas S, Tibaldi A, Lee S, et al. Comparative Study of Triboelectric Nanogenerators with Differently Woven Cotton Textiles for Wearable Electronics. Polymers. 2019;11(9):1443.

23. Mule AR, Dudem B, Patnam H, Graham SA, Yu JS. Wearable Single-Electrode-Mode Triboelectric Nanogenerator via Conductive Polymer-Coated Textiles for Self-Power Electronics. ACS Sustainable Chemistry & Engineering. 2019;7(19):16450-8.

24. Yao C, Yin X, Yu Y, Cai Z, Wang X. Chemically Functionalized Natural Cellulose Materials for Effective Triboelectric Nanogenerator Development. Advanced Functional Materials. 2017;27(30):1700794.

25. Zhang C, Lin X, Zhang N, Lu Y, Wu Z, Liu G, et al. Chemically functionalized cellulose nanofibrils-based gear-like triboelectric nanogenerator for energy harvesting and sensing. Nano Energy. 2019;66:104126.

26. Roy S, Ko H-U, Maji PK, Van Hai L, Kim J. Large amplification of triboelectric property by allicin to develop high performance cellulosic triboelectric nanogenerator. Chemical Engineering Journal. 2020;385:123723.

27. Nie S, Cai C, Lin X, Zhang C, Lu Y, Mo J, et al. Chemically Functionalized Cellulose Nanofibrils for Improving Triboelectric Charge Density of a Triboelectric Nanogenerator. ACS Sustainable Chemistry & Engineering. 2020;8(50):18678-85.

28. Nie S, Fu Q, Lin X, Zhang C, Lu Y, Wang S. Enhanced performance of a cellulose nanofibrils-based triboelectric nanogenerator by tuning the surface polarizability and hydrophobicity. Chemical Engineering Journal. 2021;404:126512.

29. Boonchai N, Mongkolthanaruk W, Harnchana V, Faungnawakij K, Pinitsoontorn S. Chemical functionalization of bacterial cellulose film for enhancing output performance of bio-triboelectric nanogenerator. Biointerface Research in Applied Chemistry. 2022;12:1587-600.

30. Zhang M, Li Y, Chang W, Zhu W, Zhang L, Jin R, et al. Negative inductive effect enhances charge transfer driving in sulfonic acid functionalized graphitic carbon nitride with efficient visible-light photocatalytic performance. Chinese Journal of Catalysis. 2022;43(2):526-35.

31. Gürses A, Açıkyıldız M, Güneş K, Gürses MS. Dyes and Pigments: Their Structure and Properties. Dyes and Pigments. Cham: Springer International Publishing; 2016. p. 13-29.

32. Opwis K, Schollmeyer E. Technical Textiles with Catalytic Properties2007.

33. Stoppa M, Chiolerio A. Wearable Electronics and Smart Textiles: A Critical Review. Sensors (Basel, Switzerland). 2014;14:11957-92.

34. Stoppa M, Chiolerio A. 4 - Testing and evaluation of wearable electronic textiles and assessment thereof. In: Wang L, editor. Performance Testing of Textiles: Woodhead Publishing; 2016. p. 65-101.

35. Tseghai GB, Malengier B, Fante KA, Nigusse AB, Van Langenhove L. Integration of Conductive Materials with Textile Structures, an Overview. Sensors. 2020;20(23):6910.

36. Saboor FH, Nguyen TA. Chapter Sixteen - Power Supplies for electronic textiles. Nanobatteries and Nanogenerators. 2021:435-45.

37. Avtar R, Sahu N, Aggarwal AK, Chakraborty S, Kharrazi A, Yunus AP, et al. Exploring Renewable Energy Resources Using Remote Sensing and GIS—A Review. Resources. 2019;8(3):149.

38. Pandey AK, R RK, Samykano M. Chapter 1 - Solar energy: direct and indirect methods to harvest usable energy. In: Pandey AK, Shahabuddin S, Ahmad MS, editors. Dye-Sensitized Solar Cells: Academic Press; 2022. p. 1-24.

39. Kanamura T, Homann L, Prokopczuk M. Pricing analysis of wind power derivatives for renewable energy risk management. Applied Energy. 2021;304:117827.

40. Wang F, Wang Z, Zhou Y, Fu C, Chen F, Zhang Y, et al. Windmill-inspired hybridized triboelectric nanogenerators integrated with power management circuit for harvesting wind and acoustic energy. Nano Energy. 2020;78:105244.

41. Bhatia SC. 14 - Geothermal power generation. In: Bhatia SC, editor. Advanced Renewable Energy Systems: Woodhead Publishing India; 2014. p. 334-88.

42. Hansen JP, Narbel PA, Aksnes DL. Limits to growth in the renewable energy sector. Renewable and Sustainable Energy Reviews. 2017;70:769-74.

43. Pablo Lopez D ´ ´ıez IG, Eduard Alarcon, Francesc Moll. Mechanical Energy Harvesting Taxonomy for Industrial Environments: Application to the Railway Industry.

IEEE International Symposium on Circuits & Systems Conference (ISCAS); Florence, Italy: Pablo Lopez D ´ ´ıez, Iosu Gabilondo, Eduard Alarcon, Francesc Moll; 2018.

44. Jiao P, Hasni H, Lajnef N, Alavi AH. Mechanical metamaterial piezoelectric nanogenerator (MM-PENG): Design principle, modeling and performance. Materials & Design. 2020;187:108214.

45. Tan Y, Yang K, Wang B, Li H, Wang L, Wang C. High-performance textile piezoelectric pressure sensor with novel structural hierarchy based on ZnO nanorods array for wearable application. Nano Research. 2021;14(11):3969-76.

46. Zhang Z, Chen Y, Guo J. ZnO nanorods patterned-textile using a novel hydrothermal method for sandwich structured-piezoelectric nanogenerator for human energy harvesting. Physica E: Low-dimensional Systems and Nanostructures. 2019;105:212-8.

47. Zhang X. Overview of Triboelectric Nanogenerators. Flexible and Stretchable Triboelectric Nanogenerator Devices2019. p. 1-18.

48. Khushboo, Azad P. Triboelectric nanogenerator based on vertical contact separation mode for energy harvesting. 2017 International Conference on Computing, Communication and Automation (ICCCA). 2017:1499-502.

49. Chen A, Zhang C, Zhu G, Wang Z. Polymer Materials for High-Performance Triboelectric Nanogenerators. Advanced Science. 2020;7.

50. Zou H, Zhang Y, Guo L, Wang P, He X, Dai G, et al. Quantifying the triboelectric series. Nature Communications. 2019;10(1):1427.

51. Kim YJ, Lee J, Park S, Park C, Park C, Choi H-J. Effect of the relative permittivity of oxides on the performance of triboelectric nanogenerators. RSC Advances. 2017;7(78):49368-73.

52. Kim H-J, Yim E-C, Kim J-H, Kim S-J, Park J-Y, Oh I-K. Bacterial Nano-Cellulose Triboelectric Nanogenerator. Nano Energy. 2017;33:130-7.

53. Zhou J, Wang H, Du C, Zhang D, Lin H, Chen Y, et al. Cellulose for Sustainable Triboelectric Nanogenerators. Advanced Energy and Sustainability Research. 2022;3(5):2100161.

54. Negm M, Sanad S. 1 - Cotton fibres, picking, ginning, spinning and weaving. In: Kozłowski RM, Mackiewicz-Talarczyk M, editors. Handbook of Natural Fibres (Second Edition): Woodhead Publishing; 2020. p. 3-48.

55. Zhang L, Yu Y, Eyer GP, Suo G, Kozik LA, Fairbanks M, et al. All-Textile Triboelectric Generator Compatible with Traditional Textile Process. Advanced Materials Technologies. 2016;1(9):1600147.

56. Wang S, Wang Z, Li J, Li L, Hu W. Surface-grafting polymers: from chemistry to organic electronics. Materials Chemistry Frontiers. 2020;4(3):692-714.

57. Fadillah G, Saputra OA, Saleh TA. Trends in polymers functionalized nanostructures for analysis of environmental pollutants. Trends in Environmental Analytical Chemistry. 2020;26:e00084.

58. Barret R. 2 - Importance and Evaluation of the pKa. In: Barret R, editor. Therapeutical Chemistry: Elsevier; 2018. p. 21-51.

59. 2 - Principles underlying the dyeing process. In: Shamey R, Zhao X, editors. Modelling, Simulation and Control of the Dyeing Process: Woodhead Publishing; 2014. p. 31-53.

60. Gan L, Guo H, Xiao Z, Jia Z, Yang H, Sheng D, et al. Dyeing and Characterization of Cellulose Powder Developed from Waste Cotton. Polymers. 2019;11(12):1982.

61. Baldrian P, Merhautová V, Gabriel J, Nerud F, Stopka P, Hruby M, et al. Decolorization of synthetic dyes by hydrogen peroxide with heterogeneous catalysis by mixed iron oxides. Applied Catalysis B: Environmental. 2006;66:258-64.

62. Stefan A, Dockery C, Nieuwland A, Roberson S, Baguley B, Hendrix J, et al. Forensic Analysis of Anthraquinone, Azo, and Metal Complex Acid Dyes from Nylon Fibers by Micro-extraction and Capillary Electrophoresis. Analytical and bioanalytical chemistry. 2009;394:2077-85.

63. Djilali Y, Elandaloussi EH, Aziz A, De Ménorval L. Alkaline treatment of timber sawdust: A straightforward route toward effective low-cost adsorbent for the enhanced

removal of basic dyes from aqueous solutions. Journal of Saudi Chemical Society. 2012;40.

64. Lozano-Alvarez J, Marañon V, Jauregui-Rincón J, Medina Ramirez I, Frausto-Reyes C, Salinas Gutiérrez R. Removal of Direct Dyes with Alginic Acid. Journal of the Mexican Chemical Society. 2015;59:215-28.

65. Habibah U, Ali S, Hussain T, Bhatti H, Asghar A. The Dyeing Process and the Environment: Enhanced Dye Fixation on Cellulosic Fabric Using Newly Synthesized Reactive Dye. Polish Journal of Environmental Studies. 2017;26.

66. Harugade A, Sherje AP, Pethe A. Chitosan: A review on properties, biological activities and recent progress in biomedical applications. Reactive and Functional Polymers. 2023;191:105634.

67. Jiang S, Zhang J, Yan S. Shear stress induced phase transitions of cubic Eu2O3 under non-hydrostatic pressures. AIP Advances. 2023;13(5):055308.

68. Kolodiazhnyi T, Sakurai H, Avdeev M, Charoonsuk T, Lamonova KV, Pashkevich YG, et al. Giant magnetocapacitance in cerium sesquioxide. Physical Review B. 2018;98(5):054423.

69. Önal A, Özbek O, Tombul KC, Nached S. Investigation of the dyeing properties of cotton fabrics and wool yarns using Prunus persica leaf extract. Journal of the Indian Chemical Society. 2021;98(7):100092.

70. Banna B, Mia R, Tanni K, Sultana N, Shamim A, Turzo R, et al. Effectiveness of dyeing with dye extracted from mango leaves on different fabrics by using various mordants. North. 2019;2:123-43.

71. Zuber M, Zia KM, Bhatti IA, Jamil T, Fazal ur R, Rizwan A. Modification of cellulosic fabric using polyvinyl alcohol, part-II: Colorfastness properties. Carbohydrate Polymers. 2012;87(4):2439-46.

72. Khwanming R, Pongampai S, Vittayakorn N, Charoonsuk T. Cellulose-based fabrics triboelectric nanogenerator: Effect of fabric microstructure on its electrical output. Journal of Metals, Materials and Minerals. 2023;33(3):1673.

73. Mathur K, Seyam A-F. Color and Weave Relationship in Woven Fabrics. 2011.

74. Rilda Y, Damara D, Putri Y, Refinel R, Agustien A, Pardi H. Pseudomonas aeruginosa antibacterial textile cotton fiber construction based on ZnO–TiO2 nanorods template. Heliyon. 2020;6:e03710.

75. Portella E, Romanzini D, Angrizani C, Amico S, Zattera A. Influence of Stacking Sequence on the Mechanical and Dynamic Mechanical Properties of Cotton/Glass Fiber Reinforced Polyester Composites. Materials Research. 2016;19.

76. Comnea-Stancu IR, Wieland K, Ramer G, Schwaighofer A, Lendl B. On the Identification of Rayon/Viscose as a Major Fraction of Microplastics in the Marine Environment: Discrimination between Natural and Manmade Cellulosic Fibers Using Fourier Transform Infrared Spectroscopy. Appl Spectrosc. 2017;71(5):939-50.

77. Titok V, Leontiev V, Yurenkova S, Nikitinskaya T, Barannikova T, Khotyleva L. Infrared Spectroscopy of Fiber Flax. Journal of Natural Fibers. 2010;7(1):61-9.

78. Korenberg C. The Effect of Ultraviolet-filtered Light on the Mechanical Strength of Fabrics. 2007;1:23-7.

79. Topalovic T, Nierstrasz VA, Bautista L, Jocic D, Navarro A, Warmoeskerken MMCG. Analysis of the effects of catalytic bleaching on cotton. Cellulose. 2007;14(4):385-400.

80. Duman O, Tunç S, Gürkan Polat T. Adsorptive removal of triarylmethane dye (Basic Red 9) from aqueous solution by sepiolite as effective and low-cost adsorbent. Microporous and Mesoporous Materials. 2015;210:176-84.

81. Khan Z, Jain K, Soni A, Madamwar D. Microaerophilic degradation of sulphonated azo dye – Reactive Red 195 by bacterial consortium AR1 through co-metabolism. International Biodeterioration & Biodegradation. 2014;94:167-75.

82. Wei Q, Zhang Y, Zhang K, Mwasiagi JI, Zhao X, Chow CWK, et al. Removal of direct dyes by coagulation: Adaptability and mechanism related to the molecular structure. Korean Journal of Chemical Engineering. 2022;39(7):1850-62.

83. Repon MR, Islam M, Mamun M, Abdur Rashid M. Comparative study on natural and reactive dye for cotton coloration. Journal of Applied Research and Technology. 2018;16:160-9.

84. Wang F, Zhang C, Wan X. Carbon Nanotubes-Coated Conductive Elastomer: Electrical and Near Infrared Light Dual-Stimulated Shape Memory, Self-Healing, and Wearable Sensing. Industrial & Engineering Chemistry Research. 2021;60(7):2954-61.

85. Costa R, Guedes A, Pereira A, Pereira C. Fabrication of all-solid-state textile supercapacitors based on industrial-grade multi-walled carbon nanotubes for enhanced energy storage. Journal of Materials Science. 2020;55.

86. Zhang R, Olin H. Material choices for triboelectric nanogenerators: A critical review. EcoMat. 2020;2(4):e12062.

87. Walden R, Aazem I, Babu A, Pillai SC. Textile-Triboelectric nanogenerators (T-TENGs) for wearable energy harvesting devices. Chemical Engineering Journal. 2023;451:138741.

88. Wu R, Ma L, Patil A, Meng Z, Liu S, Hou C, et al. Graphene decorated carbonized cellulose fabric for physiological signal monitoring and energy harvesting. Journal of Materials Chemistry A. 2020;8(25):12665-73.

89. Zhang Z, Cai J. High output triboelectric nanogenerator based on PTFE and cotton for energy harvester and human motion sensor. Current Applied Physics. 2021;22:1-5.

90. Tang Y, Zhou H, Sun X, Feng T, Zhao X, Wang Z, et al. Cotton-based naturally wearable power source for self-powered personal electronics. Journal of Materials Science. 2020;55:1-9.

91. Xia R, Zhang R, Jie Y, Zhao W, Cao X, Wang Z. Natural cotton-based triboelectric nanogenerator as a self-powered system for efficient use of water and wind energy. Nano Energy. 2022;92:106685.

92. He E, Sun Y, Wang X, Chen H, Sun B, Gu B, et al. 3D angle-interlock woven structural wearable triboelectric nanogenerator fabricated with silicone rubber coated graphene oxide/cotton composite yarn. Composites Part B: Engineering. 2020;200:108244.

93. Geng F, Huo X. A Self-Powered Sport Sensor Based on Triboelectric Nanogenerator for Fosbury Flop Training. Journal of Sensors. 2022;2022:3130928.

94. Bairagi S, Banerjee S, Chowdhury A, Ali W. Development of a Sustainable and Flexible Piezoelectric-cum-Triboelectric Energy Harvester Comprising a Simple Commodity Cotton Fabric. ACS Sustainable Chemistry & Engineering. 2021;9.

95. Feng P-Y, Xia Z, Sun B, Jing X, Li H, Tao X, et al. Enhancing the Performance of Fabric-Based Triboelectric Nanogenerators by Structural and Chemical Modification. ACS Applied Materials & Interfaces. 2021;13.

VITA